UNIVERSIDAD COMPLUTENSE DE MADRID
FACULTAD DE MEDICINA

TESIS DOCTORAL

Papel de p21/CDKN1A en la enfermedad hepática crónica

Role of p21/CDKN1A in chronic liver disease (CLD)

MEMORIA PARA OPTAR AL GRADO DE DOCTOR

PRESENTADA POR

Arantza Lamas Paz

Directores

Francisco Javier Cubero Palero
Yulia Nevzorova

Madrid

UNIVERSIDAD COMPLUTENSE DE MADRID

FACULTAD DE MEDICINA

TESIS DOCTORAL

Papel de p21/CDKN1A en la enfermedad hepática crónica
Role of p21/CDKN1A in chronic liver disease (CLD)

MEMORIA PARA OPTAR AL GRADO DE DOCTOR

PRESENTADA POR

Arantza Lamas Paz

DIRECTORES

Francisco Javier Cubero Palero
Yulia Nevzorova

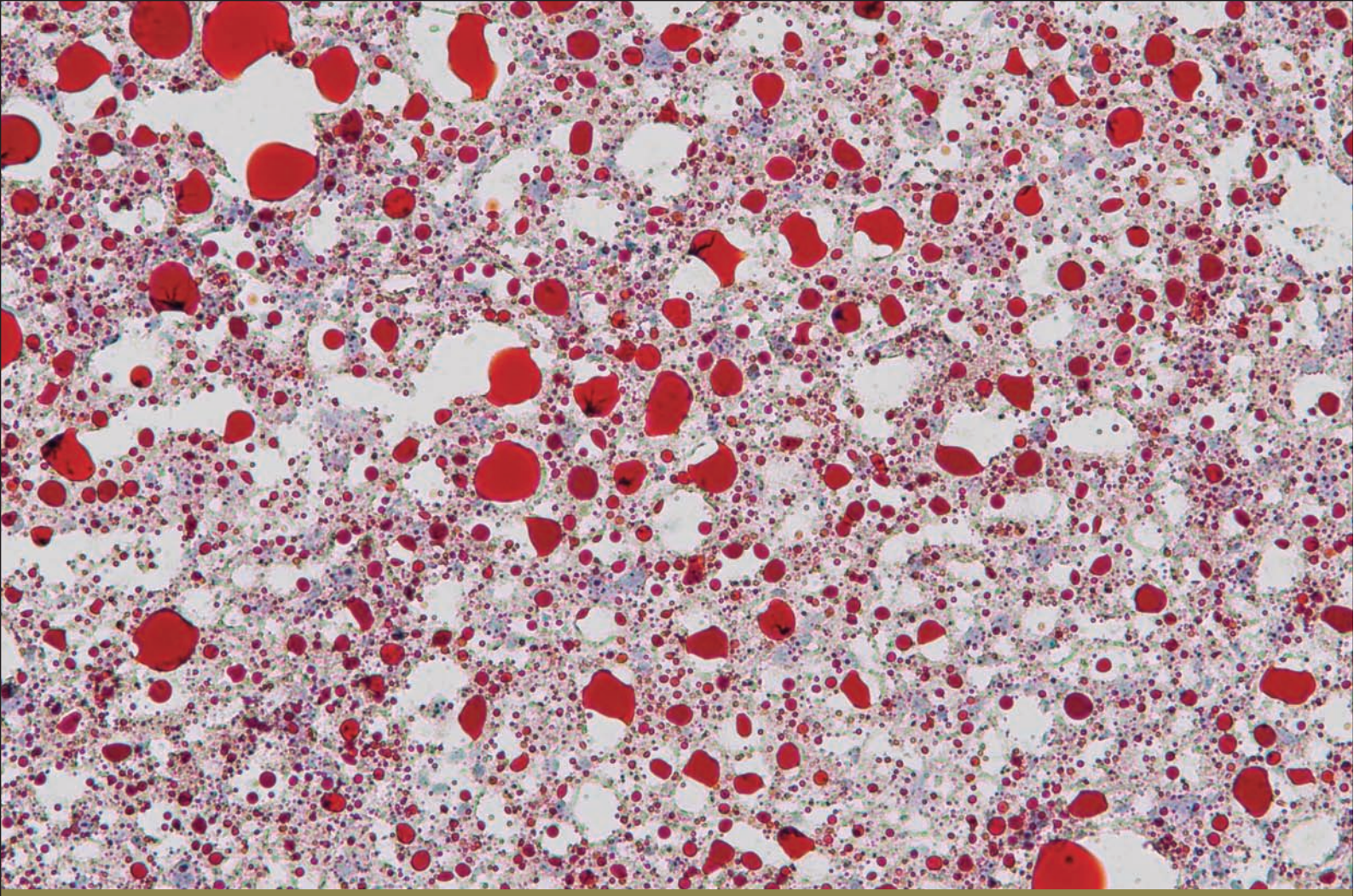

TESIS DOCTORAL

Papel de p21/CDKN1A en la enfermedad hepática crónica

Role of p21/CDKN1A in chronic liver disease (CLD)

ARANTZA LAMAS PAZ

Directores:
Francisco Javier Cubero Palero
Yulia Nevzorova

Facultad de Medicina
Universidad Complutense de Madrid

UNIVERSIDAD COMPLUTENSE DE MADRID

FACULTAD DE MEDICINA

TESIS DOCTORAL

Papel de p21/CDKN1A en la enfermedad hepática crónica

Role of p21/CDKN1A in chronic liver disease (CLD)

Doctorado en Investigación Biomédica

MEMORIA PARA OPTAR AL GRADO DE DOCTOR

PRESENTADA POR

Arantza Lamas Paz

DIRECTORES

Francisco Javier Cubero Palero

Yulia Nevzorova

AGRADECIMIENTOS
ACKNOWLEDGEMENTS

Agradecimientos / Acknowledgements

Ha llegado la hora de cubrir este apartado y eso significa que se acerca el final de esta etapa. Etapa en la que tengo mucho que agradecer.

Primeramente, a Javier Cubero por acogerme en los inicios de su laboratorio. Gracias por ofrecerme la oportunidad de realizar el trabajo de fin de Máster y posteriormente el Doctorado en este laboratorio. Javier se ha preocupado por mi futuro y formación, brindándome la oportunidad de asistir a congresos y seminarios, publicar artículos, así como poder realizar una estancia predoctoral en el extranjero. Ha insistido en que conociera en profundidad la carrera investigadora y todos los esfuerzos que ello conlleva; haciendo que mantenga la ilusión por seguir en ella. Gracias por darme la libertad de tomar decisiones en el proyecto y encauzarlas por el buen camino. Javier es un ejemplo de “persigue lo que quieres y lo conseguirás”. Tu rigurosidad, conocimiento y experiencia han hecho posible esta Tesis Doctoral.

I would like to really thanks the big labor from Yulia Nevzorova. Yulia always has good words and advice for everyone, she helps me a lot with professional and personal issues. She did not hesitate to come with me to the lab and show me how to perform experiments on the right way. Yulia has shared with me all her knowledge about laboratory and plant cares techniques. Her extensive experience in the area was essential for the development of this Doctoral Thesis, “спасибо”.

Gracias a Eduardo Martínez Naves por tutorizar esta Tesis Doctoral. Eduardo siempre ha dedicado tiempo para resolver problemas y dudas que me han surgido a lo largo de estos años, proponiendo soluciones con gran claridad y sencillez. Su profundo conocimiento de inmunología me ha hecho crecer en este campo.

It was a short period in his laboratory, but so grateful Prof. Puigserver introduced me to his group as a member. He gave me the opportunity to learn from his excellent group and all the brilliant techniques that they perform in the Dana-Farber Cancer Institute. Moreover, he has been interested in my project and help me to complete it with all the facilities that they have in the laboratory. Additionally, he gave me several advises for my future. I also would like to thank all the members of his group, they made me feel

at home, and specially thanks to Pedro and Beste that spent a lot of time teaching me. But I cannot forget Noa, Chris, Conor, Deyang and Jason.

José Ramón Regueiro, siempre dispuesto para ayudarnos y facilitarnos la labor a los predoctorales. Estoy enormemente agradecida por su dedicación y por haber compartido con todos nosotros su sabiduría.

Carlos ha llegado al laboratorio al final de mi estancia, aun así, su experiencia nos ha ayudado a resolver diferentes problemas, mejorando la organización del laboratorio. Sus consejos han sido de ayuda para mi formación en este campo.

My lab mates Nuria, Hui, Marker, Kang, Feifei and Fengjie. They have already left the laboratory, but they teach me and help me wherever I need it. Moreover, they have introduced me to the Chinese culture and food, “謝謝你”.

Olga, Raquel, Laura, Marina, Hanghang, Álex, Jose and Juanfran; altogether we constitute the actual Lovely Liver Lab. We all support each other, and specially you support me. We have shared professional and personal moments that have been part of this period, and I will not forget.

Especialmente, gracias a Olga porque juntas hemos recorrido esta etapa, desde del Grado hasta el Doctorado. Raquel, por acompañarnos mutuamente hasta horas no deseadas y por esas comidas 50%+2x1 de los findes en el lab. Laura, por haberme descontracturado la espalda en numerosas ocasiones. Marina, no ha faltado comida típica en ninguna fecha señalada, orden ni color morado. “Lindi leidis”. Nuria, Hanghang; por abrirme las puertas de vuestras casas. Gracias por vuestra amistad, habéis hecho que este periodo haya sido más ameno. “No pain, no gain”.

Bea, Marta y José Luis, gracias por formar esta pequeña familia en Boston. Ni uno más ni uno menos, los cuatro nos hemos complementado a la perfección. Para lo bueno y para lo malo. Repetiría la experiencia con vosotros sin dudarlo.

A los más veteranos que tanto me han enseñado: Ana V, Nacho, Alex, Agus, Anaïs. A los que hemos empezado a la vez: Irene, Laura Lucientes y Sergio; y a los que

posteriormente se han incorporado, pero no por ello menos importantes: Oscar, Bea A, Rebeca, Dany, Héctor, Ana Valle, Bárbara.

A todas y todos los miembros del Departamento de Inmunología por haberme acogido con tanto cariño, he aprendido mucho de vosotros.

Estoy muy agradecida por toda la ayuda que me han ofrecido Javier Vaquero, “Las Elenas” (Vázquez y Blázquez) e Iris Asensio. Gracias por proporcionarme vuestras instalaciones en el Hospital Universitario Gregorio Marañón y, gracias por enseñarme y por desempeñar diferentes técnicas que, sin vuestra ayuda, no hubiera sido posible llevar a cabo.

José Ramón Sañudo, Eva Maranillo y Teresa Vázquez por ofrecernos la oportunidad de asentarnos en su Departamento y por proporcionarnos toda la ayuda que hemos necesitado, así como un laboratorio completamente equipado.

A mis amigas, a mis amigos, por haber estado durante todo este tiempo, en Madrid y en Galicia. Han sido buenos momentos, y no tan buenos, pero habéis seguido ahí.

Gracias a la música y a la música en vivo, al deporte y a las plantas de mi balcón.

A mi familia, que siempre me esperan deseosos con los brazos abiertos “na terriña”. A los que están y los que ya se han ido, pero les hubiera gustado ver el resultado final.

A mi madre y mi padre, esto va por vosotros y sin vosotros no hubiera sido posible. Gracias. La filla os quiere mucho.

“Gracias, por tanto.
Por dulce o por amargo.
Gracias, por ser parte de mí.”

TABLE OF CONTENTS

Table of contents

RESUMEN

1. Resumen

Papel de p21/CDKN1A en la enfermedad hepática crónica

Introducción y objetivo

La creciente incidencia de la obesidad y la enfermedad del hígado graso no alcohólico (EHGNA/NASH) representa una seria amenaza para la salud mundial, pudiendo conducir a un aumento en el número de casos de enfermedad hepática avanzada, cirrosis y en última instancia derivar en carcinoma hepatocelular (CHC). El gen *p21/CDKN1A* es un regulador del ciclo celular que está involucrado en procesos celulares esenciales tales como: la detención del ciclo celular, la apoptosis, la diferenciación, la senescencia y la reparación del ADN. El objetivo principal de este estudio fue determinar el papel específico de p21/CDKN1A en la enfermedad hepática crónica.

Métodos

Se recopilaron datos del transcriptoma de tumores primarios y de tejido sano procedente de pacientes con CHC de la base de datos El Atlas del Genoma del Cáncer. Además, se recogieron biopsias de pacientes procedentes de mujeres y hombres de 20 años de edad o mayores que habían sido sometidos a una cirugía bariátrica debido a obesidad (con altos niveles de índice EHGNA), provenientes de la cohorte española del Hospital Universitario Arrixaca (Murcia, España).

Adicionalmente, ratones macho de entre 8 y 14 semanas de edad, B6;129S/J $p21^{+/+}$ (silvestres) y $p21^{-/-}$ (mutantes) fueron alimentados con dieta occidental (WD), dieta Lieber-DeCarli (LdC) con múltiples episodios de consumo agudo de alcohol o una dieta DUAL que combina la WD con el consumo crónico de alcohol; durante 14, 8 y 18 semanas, respectivamente. Además, se aislaron hepatocitos primarios de ratones silvestres y mutantes, y se realizaron ensayos funcionales de radioactividad con carbono 14 (^{14}C) con *sip21* y sus respectivos controles (*siCtrl*). Finalmente, se generaron ratones Alb-*Myc*^{tg}/$p21^{-/-}$ y se evaluó la progresión de la enfermedad hepática a las 52 semanas de edad.

Resultados

La expresión de *P21* se encuentra alterada en tumores de pacientes con CHC. Además, la expresión de *P21* se ve modificada en la clínica y en modelos múridos de EHGNA/NASH.

Los ratones mutantes $p21^{-/-}$ mostraron una disminución significativa en: (a) marcadores séricos de daño hepático (ALT y AST), (b) muerte celular (TUNEL, CC3/8, pRIPK1/3, pMLKL), (c) esteatosis hepática (triglicéridos, Oil Red O y en la oxidación de lípidos - *Pparα*, *Fxr1*- y reducción en la captación de ácidos grasos y lipogénesis *de novo* - *Pparγ*, *Cd36* y *Fas*), (d) inflamación (CD45, CD11b, *IL-6* y *Tnf-α*) y (e) marcadores de fibrosis (rojo de Sirio, vimentina, α-SMA y *Colágeno1α1*) comparados con ratones silvestres $p21^{+/+}$ en un modelo múrido de EHGNA (dieta DUAL y WD). Sin embargo, no se observaron diferencias significativas entre ratones $p21^{+/+}$ y $p21^{-/-}$ tras la dieta LdC con múltiples episodios de consumo agudo de alcohol. Además, ensayos de lipogénesis y oxidación de ácidos grasos con ^{14}C en hepatocitos primarios transfectados con *sip21* indicaron que p21 tiene un efecto muy significativo en la síntesis de lípidos en hepatocitos. Así mismo, la deleción de p21 en ratones transgénicos Alb-Myc^{tg}, incrementó la progresión de carcinoma hepatocelular.

Conclusiones

La expresión de *P21* se encuentra alterada en la clínica y la preclínica en casos de CHC y EHGNA/NASH. Los ratones $p21^{-/-}$ mostraron protección en modelos experimentales de EHGNA/NASH solos o en combinación con alcohol. Nuestros resultados indican que p21/CDKN1A juega un papel fundamental en el metabolismo lipídico del hepatocito, siendo una potencial diana terapéutica en el tratamiento de la enfermedad hepática crónica.

ABSTRACT

2. Abstract

Role of p21/CDKN1A in chronic liver disease (CLD)

Introduction and objective

The increasing incidence of obesity and non-alcoholic fatty liver disease (NAFLD/NASH) currently represents a serious threat to global health, potentially leading to an increase in the number of cases of advanced liver disease, cirrhosis and, ultimately, leading to hepatocellular carcinoma (HCC). The *p21/CDKN1A* gene is a cell cycle regulator that is involved in essential cellular processes such as: cell cycle arrest, apoptosis, differentiation, senescence, and DNA repair. The main aim of this study was to evaluate the specific role of p21/CDKN1A in chronic liver disease (CLD).

Methods

Transcriptome data from primary tumors and healthy tissue of HCC patients were collected from The Cancer Genome Atlas (TCGA) database. In addition, patients' biopsy from women and men aged 20 years old or older that underwent bariatric surgery due to obesity (high NAFLD activity score, NAS) were collected from the Spanish cohort from the University Hospital Arrixaca (Murcia, Spain).

Moreover, 8 to 14 weeks old B6;129S/J $p21^{-/-}$ (wild type) and $p21^{+/+}$ (mutant) male mice were fed with a Western diet (WD), a Lieber-DeCarli diet (LdC) with multiple ethanol (EtOH) binges or a DUAL diet that combines the WD with chronic EtOH consumption; during 14, 8 and 18 weeks, respectively. In addition, primary hepatocytes from mutant and wild type mice were isolated and radioactive carbon 14 (^{14}C) functional assays were performed with *sip21* and controls (*siCtrl*). Finally, Alb-*Myc*^{tg} /$p21^{-/-}$ mice were generated and evaluated the progression of liver disease at 52 weeks old.

Results

The expression of *P21* was altered in tumors of HCC patients. Additionally, *P21* expression was modified in clinic and in murine models of NAFLD/NASH.

The $p21^{-/-}$ mutant mice showed a significant decrease in: (a) serum markers of liver damage (ALT and AST), (b) cell death (TUNEL, CC3/8, pRIPK1/3, pMLKL), (c) hepatic steatosis (triglycerides, Oil Red O, and increase in lipid oxidation - *Pparα*, *Fxr1* - and a reduction in fatty acid uptake and *de novo* lipogenesis - *Pparγ*, *Cd36* y *Fas*), (d) inflammation (CD45, CD11b, *IL-6* and *Tnf-α*) and (e) fibrosis markers (Sirius red, vimentin, α-SMA and *Collagen1α1*) compared with $p21^{+/+}$ mice in a NAFLD murine model

(DUAL diet and WD). However, non-significant differences were observed between $p21^{+/+}$ and $p21^{-/-}$ mice after LdC diet plus multiple binges. Further to this, ^{14}C radioactive lipogenesis and fatty acid oxidation assays in primary hepatocytes transfected with *sip21* determined that the absence of p21 has a high significant effect in the synthesis of lipids in mouse hepatocytes. Furthermore, the deletion of p21 in Alb-*Myc*^{tg} transgenic mice increased the progression of tumorigenesis.

Conclusions

P21 expression was altered in clinical and in preclinical in HCC and NAFLD/NASH. $p21^{-/-}$ mice showed protection in murine models of NAFLD/NASH alone (WD) or in combination with EtOH (DUAL diet). Our results indicate that p21/CDKN1A plays a fundamental role in lipid metabolism of the hepatocyte, being a potential therapeutic target in the treatment of chronic liver disease (CLD).

ABBREVIATIONS

3. Abbreviations

^{14}C	Carbon-14
4-HNE	4-Hydroxynonenal
ACLD	Advanced chronic liver disease
ADH	Alcohol dehydrogenase
ALD	Alcohol-related liver disease
ALDH	Aldehyde dehydrogenase
ALT	Alanine aminotransferase
APCs	Antigen-presenting cells
APS	Ammonium persulfate;
ASH	Alcohol-related steatohepatitis
α-SMA	Alpha-smooth muscle actin
AST	Aspartate aminotransferase;
BEC	Biliary epithelial cells
BSA	Bovine serum albumin
BW	Body weight
CAT	Catalase endoplasmic reticulum
CC-3	Cleaved caspase-3
CC-8	Cleaved caspase-8
CCL2	C-C motif chemokine ligand 2
CD11b	Cluster of differentiation 11b
CD36	Cluster of differentiation 36
CD45	Cluster of differentiation 45
CDKs	Cyclin dependent kinases
CDKNs	Cyclin dependent kinase inhibitors
cDNA	Complementary DNA
ChREBP	Carbohydrate response element binding protein
Ck19	Cytokeratine 19
CLD	Chronic liver disease
c-Myc	Myelocytomatosis oncogene cellular homologous
CRN	Clinical research network
CT	Threshold cycle
Cyc	Cyclin
CYP2E1	Cytochrome P450 2E1
dH_2O	Distillate H_2O
DMSO	Dimethyl sulfoxide

DNL	*De novo* lipogenesis
DPM	Decompositions per minute
DTT	Dithiothreitol
ECM	Extracellular matrix
EDTA	Ethylenediaminetetraacetic acid
EHGNA	Enfermedad del hígado graso no alcohólico
ER	Endoplasmic reticulum
EtOH	Ethanol
eWAT	Epididymal white adipose tissue
FAO	Fatty acid oxidation
FBS	Fetal bovine serum
FELASA	Federation for Laboratory Animal Science Associations
FFAs	Free fatty acids
FXR	Farnesoid X receptor
GAPDH	Glyceraldehyde-3-phosphate dehydrogenase
GS	Glutamine synthetase
GTT	Glucose test tolerance
H2AX	Histone 2AX
HCC	Hepatocellular carcinoma
HBSS	Hanks' balanced salt solution
HSCs	Hepatic stellate cells
H&E	Hematoxylin and eosin
IF	Immunofluorescence
IHC	Immunohistochemistry
IL-1	iInterleukin 1
IL-6	Interleukin 6
IP	Intraperitoneal
KCs	Kupffer cells
LPS	Lipopolysaccharide
LdC	Lieber-DeCarli
LDH	Lactate dehydrogenase
LSECs	Liver sinusoidal endothelial cells
LW	Liver weight
MetS	Metabolic syndrome
MetOH	Methanol
MLKL	Mixed linage kinase domain-like protein

mPck1	Mitochondrial phosphoenolpyruvate carboxykinase 1
mRNA	Messenger RNA
NAFLD	Non-alcoholic fatty liver disease
NAS	NAFLD activity score
NASH	Non-alcoholic steatohepatitis
NK	Natural killer
NKT	Natural killer-T-cells
NP40	Nonidet P-40
NPC	Non-parenchymal cells
OD	Optical density
ORO	Oil red O
PBS	Phosphate buffered saline
PCNA	Proliferating cell nuclear antigen
PC	Pyruvate carboxylase
PCR	Polymerase chain reaction
Pepck	Phosphoenolpyruvate carboxykinase
PPAR	Peroxisome proliferation-active receptor
PUFAs	Polyunsaturated fatty acids
qRT-PCR	Quantitative real-time polymerase chain reaction
RB	Retinoblastoma proteins
RIPK	Receptor-interacting serine/threonine-protein kinase
RNAi	RNA interference
ROS	Reactive oxygen species
RT	Room temperature
SD	Standard deviation
SDS	Sodium dodecyl sulfate
siRNA	Small interfering RNAs
SR	Sirius red
SREBP1c	Sterol regulatory element-binding protein-1c
TBS	Tris-buffered saline
TCGA	The Cancer Genome Atlas
TLRs	Toll-like receptors
TMED	Tetramethylethylenediamide
TNF-α	Tumor necrosis factor alpha
TUNEL	Terminal deoxynucleotidyl transferase dUTP nick end labeling
UV	Ultraviolet

VLDL	Very low-density lipoprotein
WB	Western blot
WD	Western diet
WHO	World Health Organization

INTRODUCTION

4. Introduction

4.1 Liver anatomy and functions

The liver is the largest internal organ and gland of the human body, conventionally divided into left and right lobes. The liver comprises around 2% of a healthy adult's body weight (1.2 to 1.6 kg); whereas, in mice, represents 4.5% of the total body weight [1]. The liver is covered by a visceral peritoneum and a connective tissue layer, and it is located in the right upper quarter of the body, under the lower ribs, closed to the gall bladder, the stomach, the spleen and the gut [2-4].

The liver is the unique organ with a dual blood supply: the hepatic artery (left and right) that supplies approximately 25% of the blood to the liver and brings oxygenated blood from the aorta; and the portal vein, that supplies the 75% of the blood and brings the nutrients and harmful substances from the gut, spleen and stomach - the oxygenated blood from the aorta supplies the spleen, stomach and intestine and the deoxygenated blood with nutrients goes towards the liver through the portal vein. Blood leaves the liver and returns towards the heart through the right, middle and left hepatic veins that run into the inferior vena cava. The gallbladder is connected to the liver by the bile ducts and stores bile, an important fluid for the appropriate absorption of lipids from the digestion.

The liver is composed of several types of cells that develop different roles and together regulate the hepatic function. The 80% of the total cell population in the liver corresponds to parenchymal cells that include the hepatocytes and cholangiocytes (biliary epithelial cells, BEC). However, only the 20% corresponds to non-parenchymal cells (NPC), including: hepatic stellate cells (HSCs), Kupffer cells (KCs), lymphocytes and liver sinusoidal endothelial cells (LSECs). In the liver, cells and blood vessels (central vein and portal triad - portal vein, bile duct and hepatic artery) are structured around a functional unit, the lobule [5]. (**Figure 1**).

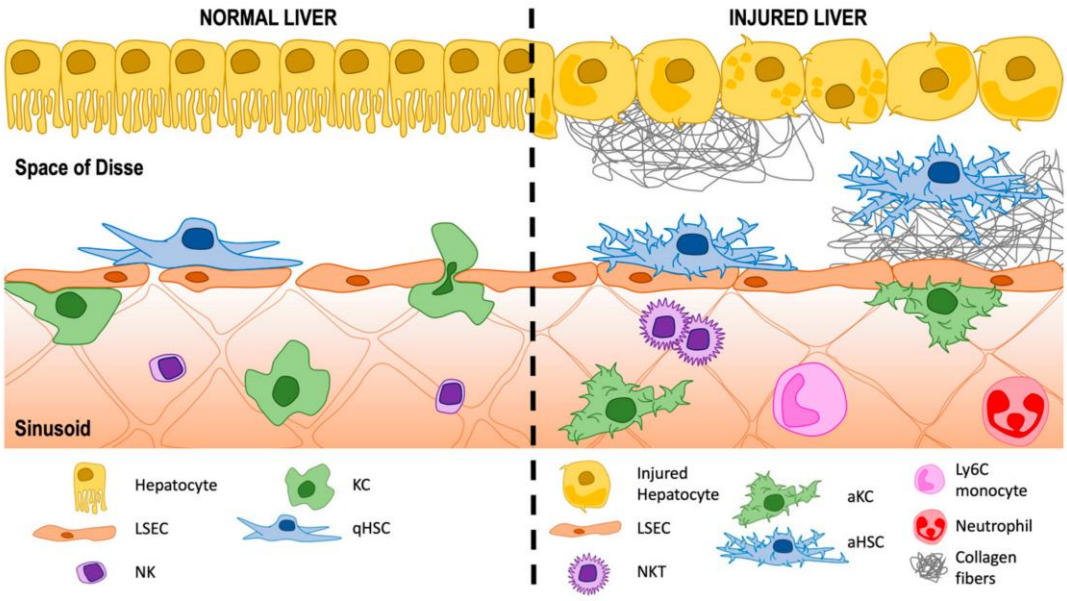

Figure 1. Schematic representation of parenchymal and non-parenchymal liver cells in normal conditions (normal liver) and in an injured liver. In a healthy liver, hepatocytes, natural killers (NK) and LSECs maintain their structure and function. In the injured liver, the architecture changes associated with the activation of KCs and HSCs, producing an infiltration of immune cells (neutrophils and monocytes) that recruit natural killer-T-cells (NKT). Moreover, hepatocytes lose their structure and function, associated with the increased extracellular matrix deposition (ECM) from HSCs. HSCs, hepatic stellate cells; KCs, Kupffer cells; LSECs, liver sinusoidal epithelial cells; NK, natural killers; NKT, natural killer-T-cells. Courtesy of Sanz-García *et al.* [6].

4.2 Parenchymal and non-parenchymal liver cells

4.2.1 Hepatocytes

Hepatocytes are the most abundant cell population of the liver, they are radially located in the liver lobule and separated from the blood by an endothelial wall, leaving open the space of Disse. These cells present a polygonal shape with a microvillous surface at the sinusoidal exposure [5]. Hepatocytes possess endocrine and exocrine functions, playing a crucial role in the synthesis, accumulation, detoxification, and transport of substances. Hepatocytes harbor an extensive endoplasmic network adjacent to numerous mitochondria and Golgi apparatuses, reflecting their high metabolic activity including: β-oxidation, lipogenesis, glucose release and utilization, amino acid uptake and ammonia detoxification, bile and cholesterol formation, and synthesis of certain plasma proteins such as albumin and fibrinogen [5, 7].

4.2.2 Cholangiocytes

Cholangiocytes are biliary epithelial cells situated in the extrahepatic and intrahepatic bile ducts, they are heterogeneous in size and functions and contribute to bile composition by solute transport process and bile flow. They are responsible for up to 30% of total bile flow in humans, however the contribution in rodents is probably lower [8]. The primary function of these cells is to fluidize and alkalinize canalicular bile, a process that involves a number of secretory and absorptive functions [9]. Thus, the bile duct epithelium can reabsorb water, glucose, glutathione, bile acids and electrolytes [10].

Immature cholangiocytes are considered progenitor cells that participle in epithelium renewal and tissue regeneration. However, cholangiocytes differentiate along the biliary tree in terms of cell polarity, expression of receptors and transporters, and response to hormones [11-15]. Differentiated cholangiocytes have distinct basolateral and apical plasma membranes, the latter containing microvilli that provide a fivefold increase in cell surface area [16-18] and a single primary cilium able to detect and transmit bile signals and regulate cell functions (differentiation, proliferation and secretion) [18, 19].

4.2.3 Hepatic stellate cells (HSCs)

Hepatic stellate cells (HSCs) are located in the space of Disse and separated from the sinusoidal lumen by the LSECs [20]. HSCs are a dynamic cell population that can be found in quiescent state, containing lipid droplets that store vitamin A [21]. These cells show a well-developed rough endoplasmic reticulum, resembling that of fibroblasts. The activation of these cells leads to the transition from a quiescent vitamin A-storing cell to a proliferative fibrogenic myofibroblast-like phenotype synthesizing a variety of extracellular matrix (ECM) components (collagen types I, III and IV, fibronectin, laminin and hyaluronic acid) [22], which constitutes a central event in acute and chronic liver injury [23]. Additionally, these cells also synthesize and secrete ECM-degrading metalloproteinases, cytokines, growth factors and express different receptors [22].

4.2.4 Kupffer cells (KCs)

Kupffer cells (KCs) are resident macrophages in the liver that are antigen-presenting cells (APCs) strategically located within the liver sinusoidal vasculature. These cells present a surface with many cytoplasmic extensions (filipodia, lamellipodia and pseudopodia) and a cytoplasm with numerous lysosomes and cellular inclusions [24]. Due to these characteristics; they possess a high pinocytic, phagocytic and digestive

capacity, having the task to clear the portal blood from a variety of foreign or undesirable material (aged erythrocytes, coagulation products, thrombocytes aggregates, parasites, bacteria, viruses, endotoxins and cancer cells) [25]. Specially, KCs actively migrate to their target and injury site upon activation and secrete a cocktail of cytokines that results in the recruitment of white bloods cells and NK cells contributing to the local healing process [26].

4.2.5 Liver sinusoidal epithelial cells (LSECs)

Liver sinusoidal epithelial cells (LSECs) have fenestrae and are located at the sinusoidal lumen, maintaining barrier functions [27]. These cells possess numerous bristle-coated endocytic vesicles and many lysosomes in their cell body, indicating a high endocytic activity of macromolecular complex by receptor-mediated endocytosis. It is well known that LSECs are effective scavenger cells of waste products from the blood circulation [28]. This capacity, together with the presence of fenestrae that facilitate free bidirectional transcellular transport, makes these cells different from any other type of endothelial cells in the body and critical for sensing changes in portal blood pressure [29].

4.3 Cell cycle

Eukaryotic cell cycle is divided in two main periods: the interphase, the longest period, and a shorter period called mitosis, or M phase. The interphase is divided into four different phases: G1 phase, where cells decide to growth or to enter a quiescent state (G0 phase); S phase, where DNA synthesis occurs; and G2 phase, where cells prepare to M phase. In M phase, cells divide the genetic material and cytokinesis occurs. Quiescent cells exit the G0 phase after mitogen stimulation, necessary to trigger a cascade of events that converge in the release of E2F transcription factors, responsible for the release of genes involved in the initiation of S phase [30].

In the mammalian cell cycle, the transition through the different phases is controlled by the cyclins, the serine/threonine cyclin-dependent kinases (CDKs), the CDK inhibitors (CDKNs) and the family of retinoblastoma proteins (RB) [31]. Cell cycle progression is ensured by the synchronized activate or inactivate status of the CDKs when associated with cyclins or CDKNs.

CDK1, 2, 4 and 6 play major roles in the regulation of cell cycle progression [32]. Growth factors, such as estrogen and epidermal growth factor, promote CyclinD protein expression that interacts and activates CDK4 and CDK6 leading to G1 progression. CDK4 or CDK6 phosphorylate and inactivate the retinoblastoma protein (pRB).

pRB is a tumor suppressor protein that negatively regulates the progression of the cell cycle. When pRB is unphosphorylated, it represses the E2F transcription factors. When CyclinD-CDK4/6 complex phosphorylates and inactivates pRB [33], EF2 starts to transcribe important genes for G1/S phase transition, such as DNA polymerase-α and CyclinE and A [34]. CyclinE-CDK2 complexes become active and continue to hyperphosphorylate pRB creating a positive feedback loop that allows the release of E2Fs and their dimeric partners to fully activate the expression of genes that guarantee cell cycle progression [35, 36]. After this point, called the restriction point, the subsequent phases of the cell cycle are no longer responsive to extrinsic factors. Subsequently, CyclinA activates CDK2, driving the cell into the S phase. Lastly, CyclinB1 and B2 activate CDK1 to ensure the progression through G2 and the entry into M phase by phosphorylating several proteins that participate in DNA replication, centrosome and chromosome function and organization of structures required for cytokinesis [37].

In addition, the progression of the cell cycle is controlled by the negative regulators, the Inhibitors of CDK4 (INK4) and the Cip/kip protein families which can inhibit CDK activities because of anti-mitogenic signals (starvation or differentiation signals). The binding of the INK4 protein family to CDK4/6 produces an allosteric change that interferes with the binding of these kinases to CyclinD, thus maintaining pRB in a hyperphosphorylated state and ultimately promoting cell cycle arrest. The INK4 family includes $p16^{INK4a}$ (CDKN2A), $p15^{INK4b}$ (CDKN2B), $p18^{INK4c}$ (CDKN2C), and $p19^{INKd}$ (CDKN2D) [9]. CyclinD-, E-, A- and B-dependent kinase complexes- are targeted by the Cip/Kip protein family consisting of p21 (CDKN1A), p27 (CDKN1B), and p57 (CDKN1C) [9]. The Cip/Kip inhibitors target the already formed Cyclin-CDK complexes and obstruct their interaction with their substrates [38]. Cip/Kip inhibitors are induced by different stimuli. For example, p21 can be induced by DNA damage and restricts Cyclin-CDK complexes to promote cell cycle progression until DNA damage repair has occurred [38]. (**Figure 2**).

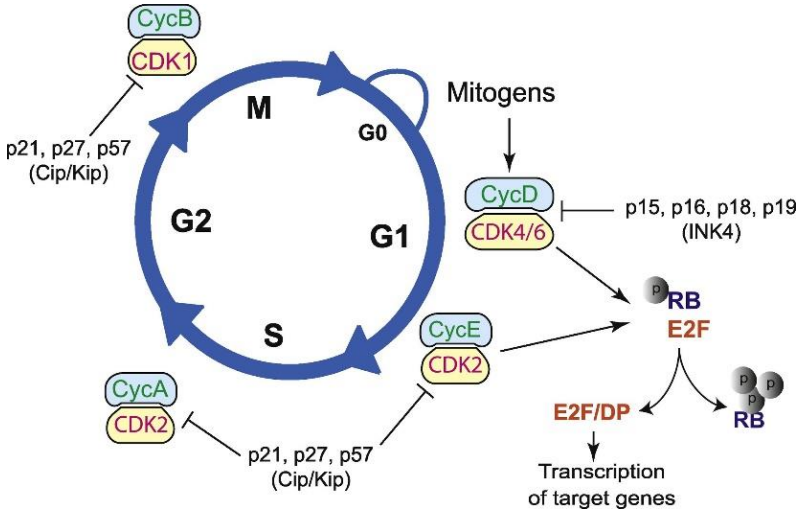

Figure 2. Scheme of the cell cycle progression. The cell cycle includes the G1, S, G2 and M phases. These phases are controlled by cell cycle regulators. Quiescent cells exit G0 phase after mitogen stimulation (CyclinD transcription, translation and assembly with their CDK partner). CyclinD and CDK4/6 complex accumulate during G1 phase and phosphorylate and inactivate pRB. Hyperphosphorylated pRB releases E2F transcription factors and trigger the transcription of the target genes necessary for S phase progression, including CyclinE. In the transition from S to G2, CDK2 is activated by CyclinA. Finally, to enter in M phase, CyclinB activates CDK1. During the whole cycle, the activation and function of the different Cyclin-CDKs complexes are negatively regulated by CDKNs protein families (INK4 and Cip/Kip). CDK, cyclin dependent kinase; CDKNs, cyclin dependent kinase inhibitors; Cyc, Cyclin. Courtesy of Leal-Esteban *et al.* [30].

4.4 p21/CDKN1A

p21$^{Walf1/Cip1/Sdi1}$ is a member of the cyclin dependent kinase inhibitors (CDKN) of the Cip/Kip family; specifically, p21 is the CDKN1A [39]. It has been reported that p21 is involved in multifaceted and heterogeneous cellular functions, the encoded protein binds to and inhibits the activity of Cyclin-CDK4 or Cyclin-CDK2, required for the RB phosphorylation with the consequent release and activation of E2F1-dependent gene expression. Thus, p21 regulates the progression through the G1 phase of the cell cycle and inhibition of DNA synthesis. Additionally, p21 could target CDK1 in some tissues, leading to growth arrest in the G2 phase of the cell cycle [38, 40]. p21 also inhibits proliferation competing with proliferating cell nuclear antigen (PCNA) [41] or indirectly at the transcriptional level [42, 43]. Microarray-based studies suggest that p21 expression

positively correlates with the suppression of genes involved in cell cycle progression and the induction of genes of senescence [44].

Since it has been described, it is known that is a transcriptional target of the tumor suppressor p53 [45], through which this protein mediates the p53-dependent cell cycle G1 phase arrest in response to a variety of stress stimuli. Furthermore, p21 has additionally key roles in apoptosis, differentiation, reprogramming of induced pluripotent stem cells, DNA repair, transcription and cell migration [39]. Interestingly, myelocytomatosis oncogene cellular homolog (*c-Myc*) has been shown to inhibit *p21* gene expression [46] and is capable of interacting with p21, disrupting its interaction with PCNA, leading to a decrease in the inhibition of DNA [47].

4.5 Pathophysiology of chronic liver disease (CLD)

Chronic liver disease (CLD) is the 10th cause of death worldwide, with 2 million individuals dying of liver disease each year [48, 49], representing a major health problem [50].

CLD is defined as the progressive deterioration of liver functions with a continuous process of inflammation, destruction, and regeneration of liver parenchyma, which leads to fibrosis and in end-stage cirrhosis and hepatocellular carcinoma (HCC). The spectrum of etiologies is broad for CLD and includes non-alcoholic fatty liver disease (NAFLD) and alcohol-related liver disease (ALD). NAFLD and ALD are hepatic insults that range from pure fatty liver and simple steatosis through non-alcoholic (NASH) and alcohol-related (ASH) steatohepatitis, to advanced chronic liver disease (ACLD). ACLD encompasses different stages such as: fibrosis, progression to cirrhosis, and end-stage complications such as primary liver cancer. Cirrhosis is a final stage of CLD that results in the disruption of liver architecture, the formation of widespread nodules, vascular reorganization, neo-angiogenesis, and deposition of an extracellular matrix. Cirrhosis from any aetiology is the strongest risk factor for HCC [51, 52], which is the major cause of death in patients with cirrhosis and represents the 1-6% annual incidence [53].

4.5.1 Non-alcoholic fatty liver disease/non-alcoholic steatohepatitis (NAFLD/NASH)

Following the global epidemic of obesity, the prevalence of NAFLD has risen, making it a major cause of liver disease worldwide [54]. The term NAFLD encompasses a board spectrum of conditions from simple fat accumulation to NASH, fibrosis, cirrhosis

and HCC. NAFLD has been defined as the exclusion of secondary causes of steatosis and excessive alcohol consumption, however it has been proved that NAFLD can coexist with other liver pathologies, resulting in more severe injury [55].

NAFLD is linked to metabolic syndrome (MetS) and, nowadays, it is known that there is a strong interlink between NAFLD and MetS components: abdominal obesity [56], dyslipidemia [57, 58] hypertension [59] and impaired metabolism [60]. This relationship is complex and has a bi-directional component: the development of NAFLD is linked to MetS and NAFLD can promote type 2 diabetes and hypertension and increase the risk of cardiovascular events [61-63]. The pathogenesis of NAFLD has not been fully established yet. The two-hit hypothesis assumes that the first hit involves lipid accumulation in the hepatocyte, being insulin the key pathogenic factor for the development of hepatic steatosis. The first hit increases the susceptibility of hepatocytes to secondary injuries or insults that constitute the second hit, such as oxidative stress, mitochondrial dysfunction, overproduction and the release of pro-inflammatory cytokines and the endotoxin-mediated activation of the innate immune response; promoting hepatic injury, inflammation, and fibrosis. [64, 65]. This theory has now been replaced by a more complex, multiple-hit hypothesis. It states that not only diet and lifestyle but also genetic factors lead to dyslipidemia, insulin resistance, and adipocyte dysfunction, resulting in endoplasmic reticulum (ER) stress, oxidative stress, release of proinflammatory cytokines and mitochondrial dysfunction, thus promoting inflammation and fibrosis [66].

Lipotoxicity is one of the most investigated mechanisms in the pathogenesis of NAFLD. However, simple steatosis is considered an early state and NASH is associated with higher risk of cirrhosis and HCC development [67]. Evolution from simple steatosis to NASH results from a complex interplay that involves either, liver cell population (parenchymal and no parenchymal) and pathological signals coming from other organs, (fat tissue and gut). Moreover, it has also been clear that intestinal dysbiosis plays a pivotal role in disease progression. [68]. (**Figure 3**).

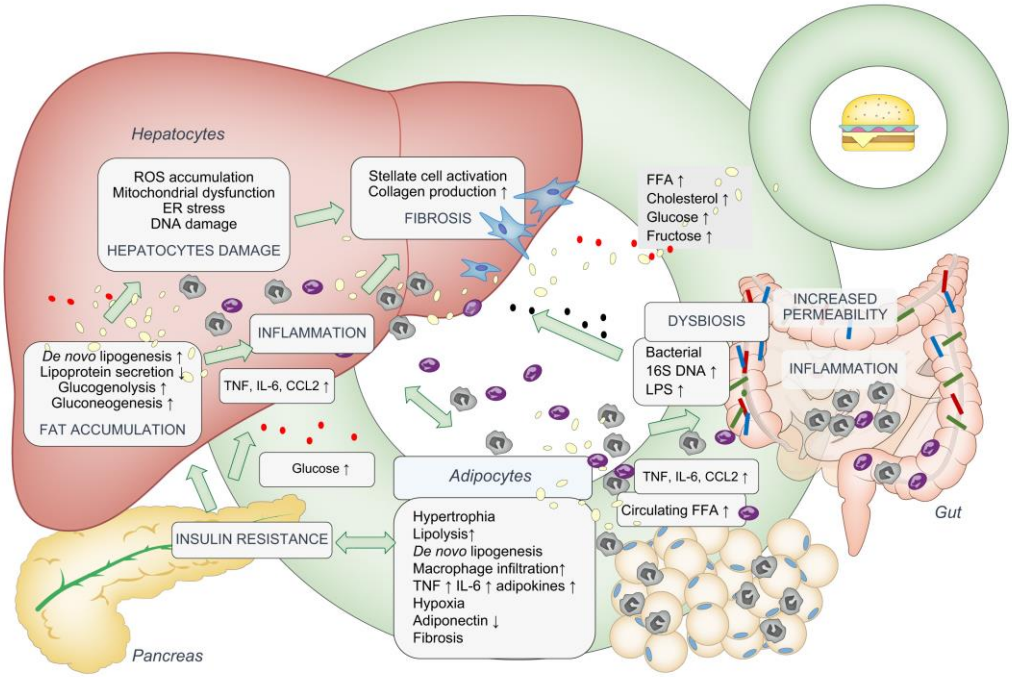

Figure 3. Pathophysiology of NAFLD/NASH. The most common risk factors of NAFLD/NASAH are diet-induced obesity and insulin resistance that trigger macrovesicular steatosis, lobular inflammation, hepatocellular ballooning, activation of HSCs and fibrosis. Moreover, key cellular pathways are activated, such as ER stress, lipotoxicity and *de novo* lipogenesis, oxidative stress, apoptosis and fibrogenic pathways. Additionally, intestinal dysbiosis plays a pivotal role in disease progression. CCL2, C-C motif chemokine ligand 2; ER, endoplasmic reticulum; FFAs, free fatty acids; IL-6, interleukin 6; LPS, lipopolysaccharide; ROS, reactive oxygen species; TNF, tumor necrosis factor. Courtesy of Nevzorova *et al.* [69].

4.5.2 Alcohol-related liver disease (ALD)

Global alcohol consumption has decreased in the past few decades, whereas the consumption remains high, with values of 10 L of pure alcohol consumed per adult each year in Europe [70]. ALD can range from simple fatty liver to ASH, fibrosis and leading to cirrhosis and HCC [71]. Although many individuals consuming more than 60 g of alcohol per day (e.g., 1/2 a bottle of wine or more than 1 L of beer) develop steatosis, only a minority of the patients with steatosis progress to ASH and 10–20% eventually develop cirrhosis [72, 73]. Genetic and nongenetic factors modify both the individual susceptibility and the clinical course of ALD. The mechanisms of ALD are not completely understood. A recent metanalysis found increased risks of mortality from liver cirrhosis

among men and women drinking 12–24 g of ethanol (EtOH) per day [30]. Indeed, among women, a significant increase was also seen for those drinking up to 12 g/day [74].

EtOH could be metabolized by three systems: (1) the hepatocyte cytoplasmic alcohol dehydrogenase (ADH) system, (2) the cytochrome P450 2E1 (CYP2E1) enzymes and (3) the catalase endoplasmic reticulum (CAT) system, a peroxisomal enzyme that also catalyzes the removal of reactive oxygen species (ROS) [75, 76]. Acetaldehyde is further metabolized to acetate by the action of the aldehyde dehydrogenase (ALDH). As a result, EtOH metabolism brings about gut dysbiosis, inflammation and increased permeability causing increased circulating free fatty acids and bacterial-derived products such as lipopolysaccharides (LPS), that are recognized by pathogen-recognition receptors, including Toll-like receptors (TLRs) and activates KCs. Thus, KCs resulting in the activation of proinflammatory cytokines (TNF-α, IL-1 and IL-6) that activates HSCs and leads to accumulation of ECM proteins in the liver tissue with synergistic effects on hepatic damage, fibrosis development and cirrhosis. [69, 77, 78]. (**Figure 4**).

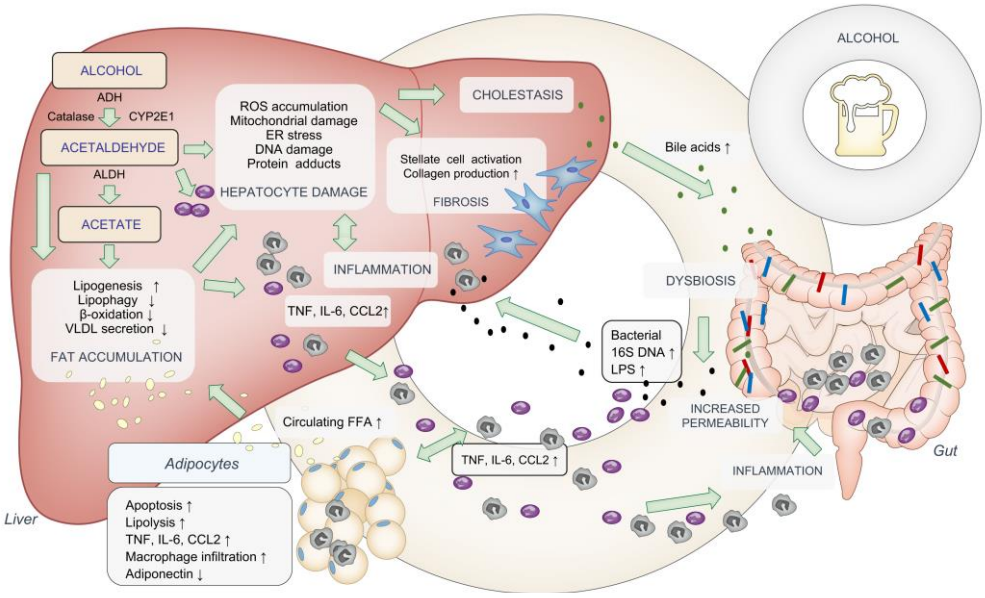

Figure 4. Pathophysiology of ALD. EtOH is metabolized into acetaldehyde by ADH, CYP2E1 and by the catalase (a peroxisomal enzyme that catalyzes the removal of ROS). Acetaldehyde is metabolized to acetate by the ALDH. As a result, EtOH metabolism leads to gut dysbiosis, inflammation and increased permeability that affects lipid accumulation (caused by increased circulating free fatty acids), hepatic immune cell infiltration, hepatocyte damage, cholestasis, and fibrosis. ADH, alcohol dehydrogenase;

ALDH, acetaldehyde dehydrogenase; CCL2, C-C motif chemokine ligand 2; CYP2E1, EtOH: ethanol; cytochrome P450 isoenzyme 2E1; ER, endoplasmic reticulum; FFAs, free fatty acids; IL-6, interleukin 6; LPS, lipopolysaccharide; ROS, reactive oxygen species; TNF, tumor necrosis factor; VLDL, very low-density lipoprotein. Courtesy of Nevzorova *et al.* [69].

OBJECTIVES

5. Objectives

In the present study, we aimed to evaluate the specific role of p21 in chronic liver disease (CLD), especially in the development of CLD, ranging from NAFLD/NASH to ALD-derived cirrhosis and end-stage hepatocellular carcinoma (HCC).

Specific Aims:

In the current project, the following specific aims will be addressed:

1. To evaluate the presence of p21 expression in clinical and preclinical chronic liver disease (CLD).

2. To analyze the role of p21 in a dual setting of Western diet (WD) and alcohol intake (NAFLD/ALD).

3. To understand the role of p21 in non-alcoholic fatty liver disease/non-alcoholic steatohepatitis (NAFLD/NASH).

4. To evaluate the role of p21 in alcohol-related liver disease (ALD).

5. To decipher the molecular events underlying the role of p21 in the initiation and progression of chronic liver disease (CLD).

6. To study the impact of p21 in a mouse model of low latency hepatocellular carcinoma (HCC).

MATERIALS AND METHODS

6. Materials and methods

6.1 Materials

6.1.1 Chemicals

Reagent	Manufacturer
[1-^{14}C] palmitic acid	PerkinElmer, Boston, USA
20% glucose solution	Braun GmbH, Krönberg, Germany
2,2,2-tribromoethanol ($Br_3C{-}CH_2OH$)	Sigma-Aldrich, Madrid, Spain
2-methyl-2-butanol ($CH_3CH_2C(CH_3)_2OH$)	Sigma-Aldrich, Madrid, Spain
30% acrylamide/bis solution	Bio-Rad, Madrid, Spain
4X Laemmli buffer	Bio-Rad, Madrid, Spain
Acetic acid (glacial) 100% (CH_3COOH)	AppliChem, Barcelona, Spain
AEBSF hydrochloride	Thermo Fisher Scientific, Madrid, Spain
Agarose D1 low EEO	Condalab, Madrid, Spain
Ammonium persulfate (APS, $(NH_4)_2S_2O_8$)	Bio-Rad, Madrid, Spain
Bovine serum albumin, lyophilized powder, ≥96% (BSA)	Sigma-Aldrich, Madrid, Spain
Calcium chloride ($CaCl_2$)	Sigma-Aldrich, Madrid, Spain
Cdkn1a mouse siRNA oligo duplex	Origene, Rockville, USA
Chloroform ($CHCl_3$)	AppliChem, Barcelona, Spain/Themo Fisher Scientific, Boston, USA
Collagen from rat tail	Sigma-Aldrich, Madrid, Spain
Complete mini	Roche, Madrid, Spain
D (+)-glucose ($C_6H_{12}O_6$)	Sigma-Aldrich, Madrid, Spain
D (+)-sucrose ($C_{12}H_{22}O_{11}$)	AppliChem, Barcelona, Spain
D-[^{14}C(U)] glucose	PerkinElmer, Boston, MA
Dako faramount aqueous mounting medium	Dako, Agilent, Madrid, Spain
DEPC water	AppliChem, Barcelona, Spain
Dexamethasone ($C_{22}H_{29}FO_5$)	Sigma-Aldrich, St. Louis, USA
Direct red 80 (Sirius red)	Sigma-Aldrich, Madrid, Spain
Di-sodium hydrogen phosphate 7-hydrate for analysis ($Na_2HPO_4 \cdot 7H_2O$)	AppliChem, Barcelona, Spain
DMEM with high glucose, without L-glutamine, with sodium pyruvate	GE Healthcare, Logan, USA

DMEM with L-Glutamine, without D-glucose, without sodium pyruvate	Thermo Fisher Scientific, Boston, USA
Dimethyl sulfoxide (DMSO, $(CH_3)_2SO$)	Sigma-Aldrich, Madrid, Spain
Dithiothreitol (DTT)	Thermo Fisher Scientific, Madrid, Spain
DNA ladder (50 bp)	Thermo Fisher Scientific, Madrid, Spain
Dodecyl sulphate sodium salt (SDS for analysis, $C_{12}H_{25}NaO_4S$)	AppliChem, Barcelona, Spain
ECL prime western blotting detection reagents	GE Healthcare, Madrid, Spain
Eosin Y	Sigma-Aldrich, Madrid, Spain
Ethanol absolute for analysis (CH_3CH_2OH)	AppliChem, Barcelona, Spain
Ethidium bromide ($C_{21}H_{20}BrN_3$)	Thermo Fisher Scientific, Invitrogen, Madrid, Spain
Ethylenediamine-tetra acetic acid (EDTA, $(HO_2CHH_2)_2NCH_2CH_2N(CH_2CO_2H)_2$)	Sigma-Aldrich, Madrid, Spain
Ethylenediamine-tetra acetic acid sodium salt solution (EDTA, 0.5 M)	Corning Inc., NY, USA
Fetal bovine serum (FBS)	Thermo Fisher Scientific, Boston, USA
Formaldehyde solution 4% (CH_2O)	AppliChem, Barcelona, Spain
Gelatin from bovine skin, Type B	Sigma-Aldrich, Madrid, Spain
Glucagon ($C_{153}H_{225}N_{43}O_{49}S$)	Sigma-Aldrich, St. Louis, USA
Goat serum	Thermo Fisher Scientific, Gibco, Madrid, Spain
Hanks' balanced salt solution (HBSS 1x)	Corning Inc., NY, USA
HyClone L glutamine	GE healthcare life sciences, Logan, USA
Hydrochloric acid technical grade 37% (HCl)	AppliChem, Barcelona, Spain
Hydrogen peroxide 30% (H_2O_2)	AppliChem, Barcelona, Spain
ImmPACT DAB HRP Substrate	Vector Laboratories, Petersburg, UK
Insulin	Sigma-Aldrich, St. Louis, USA
Isoflurane	Solvet, Segovia, Spain
Isopropanol	AppliChem, Barcelona, Spain
L-[^{14}C(U)] lactic acid	PerkinElmer, Boston, USA
Lipofectamine RNAi max	Thermo Fisher Scientific, Boston, USA
Liver digestion buffer	Thermo Fisher Scientific, Boston, USA

Magnesium chloride hexahydrate ($Cl_2H_{12}MgO_6$)	Sigma-Aldrich, Madrid, Spain
Mayer's hematoxylin	AppliChem, Barcelona, Spain
Methanol (MetOH) BioChemica	AppliChem, Barcelona, Spain
Midori green advance	Nippon genetics, Düren, Germany
Non-fat dried milk powder	AppliChem, Barcelona, Spain
Nonidet P-40 (NP40)	AppliChem, Barcelona, Spain
Novex sharp protein standard	Thermo Fisher Scientific, Invitrogen, Madrid, Spain
Oil red O	Sigma-Aldrich, Madrid, Spain
Opti-MEM	Sigma-Aldrich, St. Louis, USA
Penicillin streptomycin (10,000 units/mL penicillin and 10,000 µg/mL streptomycin)	Gibco, Paisley, UK
Perchloric acid ($HClO_4$)	Sigma-Aldrich, St. Louis, USA
Percoll (pH 8.5-9.5)	Sigma-Aldrich, St. Louis, USA
PhosSTOP	Roche, Madrid, Spain
Picric acid saturated aqueous solution	Sigma-Aldrich, Madrid, Spain
Precision plus protein standards	Bio-Rad, Madrid, Spain
Ponceau S solution	Sigma-Aldrich, Madrid, Spain
Potassium chloride> 99.0% (KCl)	Merck, Madrid, Spain
Restore western blot stripping buffer 500 mL	Thermo Fisher Scientific, Madrid, Spain
Roti®-Histokitt	Carl Roth, Karlsruhe, Germany
ROTISZINT®eco plus, 5 L, plastic (Scintillation fluid)	PerkinElmer, Boston, USA
Sodium bicarbonate ($NaHCO_3$)	Sigma-Aldrich, Madrid, Spain
Sodium chloride for molecular biology (NaCl)	AppliChem, Barcelona, Spain
Sodium deoxycholate ($C_{24}H_{39}NaO_4$)	Sigma-Aldrich, Madrid, Spain
Sodium dihydrogen phosphate monohydrate ($NaH_2PO_4 \cdot H_2O$)	AppliChem, Barcelona, Spain
Sodium fluoride (NaF)	Sigma-Aldrich, Madrid, Spain
Sodium hydroxide (NaOH)	AppliChem, Barcelona, Spain
Sodium pyruvate solution (100 mM, $C_3H_3NaO_3$)	Gibco, Paisley, UK

Tetramethylethylenediamine (TEMED)	Bio-Rad, Madrid, Spain
Tissue-Tek® O.C.T.™ compound	Sakura, Barcelona, Spain
Tris/glycine buffer 10x	Bio-Rad, Madrid, Spain
Tri-sodium citrate 2-hydrate ($HOC(COONa)(CH_2COONa)_2 \cdot 2H_2O$)	AppliChem, Barcelona, Spain
Tris ($C_4H_{11}NO_3$)	AppliChem, Barcelona, Spain
Triton X-100	AppliChem, Barcelona, Spain
Trizol reagent	Thermo Fisher Scientific, Madrid, Spain
Tween-20	Sigma-Aldrich, Madrid, Spain
Vectashield mounting medium with DAPI	Vector Laboratories, Petersburg, UK
Xylene (C_6H_{10})	Carl Roth, Karlsruhe, Germany
Xylene cyanol FF	Sigma-Aldrich, Madrid, Spain

6.1.2 Standard buffer and media

NID buffer	Volume/Quality	Final concentration	PH value
KCl	3.73 g	0.05 M	pH = 8.3
Tris	10 mL	0.01 M	
$MgCl_2$	0.41 g	2 mM	
Gelatin type B	0.1 g	0.1 mg/mL	
NP-40	4.5 mL	0.45 %	
Tween-20	4.5 mL	0.45 %	

NID buffer should store at 4ºC and in dark.

10x Phosphate-buffered saline (PBS)	Volume/Quantity
NaCl	78.80 g
KCl	3.50 g
Na_2HPO_4	26.80 g
NaH_2PO_4	2.76 g
Distilled H_2O (dH_2O)	1 L
1x PBS	**Volume**
10x PBS	100 mL
dH_2O	1 L

Hepatic triglycerides homogenization buffer	Volume/Quantity	PH value
Tri-sodium citrate 2-hydrate	390.00 g	pH = 7.5
EDTA	110.00 mg	
D (+)-sucrose	21.35 mg	
dH_2O	250 mL	

Hepatic triglycerides homogenization buffer should be prepared in advance and store at 4ºC to use.

Picro-Sirius red (SR) solution	Volume/Quantity
Direct Red 80	0.25 g
Picric acid saturated aqueous solution*	250 mL

*Picric acid is an explosive product in contact with the oxygen

Acidified water	Volume
Acetic acid	1.5 mL
dH_2O	300 mL

Oil red O (ORO) stock solution	Volume/Quantity
ORO powder	0.5 g
Isopropanol	100 mL
Oil red O (ORO) working solution	**Volume**
ORO stock solution	48 mL
dH_2O	32 mL

ORO stock solution should be prepared in advanced and perfectly mixed during 2 h warming it. Working solution should be filtered three times with Whatman paper to avoid solid particles. Both solutions must be kept in dark.

150 mM Na-citrate solution (TUNEL)	Volume/Quantity	PH value
150 mM Na-citrate	8.8 g	pH = 6.0
Triton-X-100	0.2 mL	
1x PBS	200 mL	

RIPA buffer	Volume	Final concentration
SDS 10%	1.0 mL	0.1 %
Sodium deoxycholate	0.5 g	0.5 %
NP40	0.5 mL	0.5 %
NaCl 5M	3.0 mL	150 mM
Tris-HCl 1 M, pH = 7,8	5.0 mL	50 mM
EDTA	2.0 mL	250 mM
dH_2O	100.0 mL	

RIPA buffer complete	Volume/Quantity
PhosSTOP	1 tablet
Complete Mini	1 tablet
DTT	20 µL
AEBSF hydrochloride (100 mM)	100 µL
RIPA buffer	10 mL

RIPA buffer and RIPA buffer complete should be keep at 4ºC.

1x SDS-running buffer	Volume/Quantity
Tris/glycine buffer	100 mL
10% SDS	10 mL
dH_2O	1 L

1x Transfer buffer	Volume
Tris/glycine buffer	100 mL
MetOH	200 mL
dH_2O	1 L

Transfer buffer should be stored at 4ºC to use.

10x Tris-buffered saline (TBS)	Volume/Quantity
Tris	24.2 g
NaCl	80.0 g
dH_2O	1 L

1x TBS	Volume
10x TBS	100 mL
Tween-20	0.5 mL

dH_2O	1 L

40x avertin solution (anesthesia)	**Volume/Quantity**
2,2,2-tribromoethanol	1 g
2-metil-2-butanol	630 µL
1x PBS	1 mL

Perfusion buffer	**Volume/Quantity**	**pH value**
HBSS 1x	500 mL	pH = 7.2
0.5 M EDTA	685 µL	
Sodium bicarbonate	0.7 g	

Perfusion buffer should be warmed at 42ºC, filtered and checked the pH every time before use.

Plating medium	**Volume/Quantity**
DMEM high glucose	1 L
FBS	100 mL
Sodium pyruvate (100 mM)	20 mL
Penicillin streptomycin	10 mL
1 mM dexamethasone	1 mL
1 mM Insulin	100 µL

Plating medium should be prepared fresh and filtered and sterilized before use.

Maintenance medium	**Volume/Quantity**
DMEM No glucose	500 mL
BSA	10 g
Sodium pyruvate (100 mM)	10 mL
Penicillin streptomycin	5 mL
1 mM dexamethasone	50 µL
1 mM Insulin	0.5 µL
5 mM glucose	2.5 mL

Maintenance medium should be prepared fresh, filtered and sterilized before use.

Starvation medium	Volume/Quantity
DMEM No glucose	500 mL
BSA	10 g
Sodium pyruvate (100 mM)	10 mL
Penicillin streptomycin	5 mL

Starvation medium should be prepared fresh, filtered and sterilized before use.

6.1.3 Immunoblotting gels

Stacking gel (5%)	Volume
dH_2O	4.5 mL
30% acrylamide/bis solution	1.3 mL
10% APS	80 µL
10% SDS	80 µL
Tris/HCl pH = 6.8	2.0 mL
TEMED	8.0 µL
Total volume	8.0 mL

Separating gel	8%	10%	12%	15%
dH_2O	9.3 mL	7.9 mL	6.6 mL	4.6 mL
30% acrylamide/bis solution	5.3 mL	6.7 mL	8.0 mL	10.0 mL
10% APS	200 µL	200 µL	200 µL	200 µL
10 SDS	200 µL	200 µL	200 µL	200 µL
Tris/HCl pH = 8.8	5.0 mL	5.0 mL	5.0 mL	5.0 mL
TEMED	12.0 µL	8.0 µL	8.0 µL	8.0 µL
Total volume	20 mL	20 mL	20 mL	20 mL

6.1.4 Standard kits and enzymes

Kit/Assay	Manufacturer
High capacity cDNA reverse transcription kit	Thermo Fisher Scientific, Madrid, Spain
In situ cell death detection kit, fluorescein	Roche, Madrid, Spain

Normal horse serum blocking solution, 2.5%	Vector Laboratories, Petersburg, UK
Pierce BCA protein assay kit (Reagent A: contains sodium carbonate, sodium bicarbonate, pierce BCA detection reagent in 0.1 N sodium hydroxide. Reagent B: bright blue clear solution free of particulate matter)	Thermo Fisher Scientific, Madrid, Spain/Boston, USA
Triglycerides liquicolor mono kit	RAL, Barcelona, Spain

Enzyme	Manufacturer
BLOXALL® endogenous blocking solution, peroxidase and alkaline phosphatase	Vector Laboratories, Petersburg, UK
Hotstart-taq master mix	Quiagen, Madrid, Spain
Proteinase K-solution	AppliChem, Barcelona, Spain
Ready mix™ redtaq™ PCR reaction mix with $MgCl_2$	Sigma-Aldrich, Madrid, Spain
SYBR GreenERTM qPCR super mix	Thermo Fisher Scientific, Invitrogen, Madrid, Spain

6.1.5 Murine diets

Diet	Manufacturer
Chow diet	Altromin LASQC diet Rod18-H, Germany
Western diet (D18121807)	Research Diets, New Brunswick, NJ
Lieber-DeCarli'82, shake and pour, ethanol (F1258sp)	Steriltech, Bio-Serv, Madrid, Spain
Lieber-DeCarli'82, shake and pour, control (F1259SP)	Steriltech, Bio-Serv, Madrid, Spain

6.1.6 Immunostaining and immunoblotting antibodies

6.1.6.1 Primary antibodies

Product	Manufacturer	Reference	Dilution
4-hydroxynonenal (4-HNE)	Abcam	ab46545	1:100 (IHC)

Alpha-smooth muscle actin (α-SMA)	Merck	A 2547	1:800 (WB)
Beta-actin (β-ACTIN)	Cell Signaling Technology	4967	1:1000 (WB)
Cluster of differentiation 11b (CD11b)	BD	550282	1:500 (IF)
Cluster of differentiation 45 (CD45)	BD	550539	1:100 (IF)
Cleaved caspase-3 (CC-3)	Cell Signaling Technology	9661	1:1000 (WB)
Cleaved caspase-8 (CC-8)	Cell Signaling Technology	8592	1:1000 (WB)
Cytochrome P450 (CYP2E1)	Abcam	ab28146	1:1000 (WB)
Cytokeratin 19 (CK19)	Abcam	ab15463	1:100 (IHC)
Gliceraldehyde-3-phosphate dehydrogenase (GAPDH)	Bio-Rad	MCA4739	1:5000 (WB)
Glutamine Synthetase (GS)	Abcam	ab73593	1:1000 (IHC)
Ki67	Abcam	ab16667	1:100 (IHC)
P21	Santa Cruz	sc-6246	1:1000 (WB)
Phosphorylated mixed linage kinase domain-like protein (pMLKL (S345))	Abcam	ab196436	1:1000 (WB)
Phosphorylated receptor-interacting serine/threonine-protein kinase 1 (pRIPK1 (S166))	Cell Signaling Technology	31122	1:1000 (WB)
Phosphorylated receptor-interacting serine/threonine-protein kinase 1 (pRIPK3 (T231/S232))	Cell Signaling Technology	57220	1:1000 (WB)
Vimentin	Cell Signaling Technology	5741	1:100 (IHC)

6.1.6.2 Secondary antibodies

Product	Manufacturer	Reference	Dilution
Anti-mouse HRP	Bio-Rad	STAR207P	1:5000 (WB)
Anti-mouse biotinylated	Vector Laboratories	BA-9200	(IHC)
Anti-rabbit HRP	Cell Signaling Technology	70745	1:3000 (WB)
Anti-rabbit biotinylated	Vector Laboratories	BA-1000	(IHC)
Anti-rat Alexa Fluor 488	Invitrogen	A11006	1:1000 (IF)

6.1.7 Primer sequences used for qRT-PCR

Primers were designed and checked for specificity with Primer Blast tool from NCBI and purchased from Sigma-Aldrich (Madrid, Spain).

6.1.7.1 Human primers:

Gene	Forward (5'-3')	Reverse (5'-3')
GAPDH	ACAACTTTGGTATCGTGGAAGG	GCCATCACGCCACAGTTTC
P21	TGTCCGTCAGAACCCATGC	AAAGTCGAAGTTCCATCGCTC
P27	AACGTGCGAGTGTCTAACGG	CCCTCTAGGGGTTTGTGATTCT

6.1.7.2 Mouse primers:

Gene	Forward (5'-3')	Reverse (5'-3')
α-Sma	CCCCTGAAGAGCATCGGACA	TGGCGGGACATTGAAGGT
Cd36	CAAATGCAAAGAAGGAAAGCC	AATGGTCCCAGTCTCATTTAGC
Chrebp	GTCCGATATCTCCGACACACTCTT	CATTGCCAACATAAGCATCTTCTG
Collagen-1α1	TGTGTGCGATGACGTGCAAT	GGGTCCCTCGACTCCTAC
CyclinA2	TGATGCTTGTCAAATGCTCAGC	AGGTCCTCCTGTACTGCTCAT
CyclinD1	GCGTACCCTGACACCAATCTC	ACTTGAAGTAAGATACGGAGGGC
CyclinE1	GAAAAGCGAGGATAGCAGTCAG	CCCAATTCAAGACGGGAAGTG

Fas	GGCTGTGAACACTGTGTTCGC	GGATGGTCAACAACCATAGGCG
Ggapdh	TGTTGAAGTCACAGGAGACAACCT	AACCTGCCAAGTATGATGACATCA
IL-6	GCTACCAAACTGGATATAATCAGGA	CCAGGTAGCTATGGTACTCCAGAA
P21	TTGCACTCTGGTGTCTGAGC	TCTGCGCTTGGAGTGATAGA
P53	TGCTCACCCTGGCTAAAGTT	AATGTCTCCTGGCTCAGAGG
Pparα	ATTCGGCTGAAGCTGGTGTAC	CTGGCATTTGTTCCGGTTCT
Pparγ	CACAATGCCATCAGGTTTGG	GCTGGTCGATATCACTGGAGATC
Srebp1c	GGAGCCATGGATTGCACATT	GGCCCGGGAAGTCACTGT
Tnf-α	CCTCTTCTCATTCCTGCTTGTGG	GAGAAGATGATCTGAGTGTGAGG

6.1.8 Primer sequences for genotyping PCR

Gene	Forward (5'-3')	Reverse (5'-3')
c-Myc	CTTCCTCGTCGCAGATGAA	GGCAAACATACGCAAGGG
P21 38031 (Common)	CAGCAAAGCCTTGATTCTGA	
P21 38032 (*wild type* Reverse)	GCCCTGGACTTTGGGATACT	
P21 38033 (Mutant Reverse)	TCATTCCTCCCACTCATGATCT	

6.1.9 Instrument and equipment

Instrument/Equipment	Manufacturer
ACCU-CHECK glucometer	Roche Madrid, Spain
Amersham Imager 600	GE Healthcare, Amersham, UK
Antigen 2100-Retriever	Aptum Biologics, Hants, UK
Centrifuge 5415 D	Eppendorf AG, Madrid, Spain
Centrifuge Z233M-2 and refrigerated	Hermle Labor Technik GmbH, Wehingen, Germany
Class II bio II advance plus microbiological safety cabinet	Azbil Telstar Technologies Slu, Barcelona, Spain

Cryostat CM1950	Leica Biosystems, Madrid, Spain
Digital microscope camera Moticam 2500	Ryf AG, Bettlachstrasse, Switzerland
DISKUS Z16 APO	Leica Biosystems, Madrid, Spain
Drying and sterilizing ovens natural convection	J.P. selecta, Barcelona, Spain
Eclipse Ci optical microscope	Nikon, Madrid, Spain
FastPrep-24^{TM}5G	MP Biomedicals, Illkirch-Graffenstaden, France
Gel chamber MINI-Protein	Bio-Rad, Madrid, Spain
Gel Doc 2000 system	Bio-Rad, Madrid, Spain
Glass homogenizers	Omni International, Inc. Kennesaw, GA, USA
Leica EG1160 embedding center, dispenser + hot plate	Leica Biosystems, Madrid, Spain
Leica MZ16 stereomicroscope with Leica DFC480 digital camera	Leica Biosystems, Madrid, Spain
LI-COR Odyssey	LI-COR, Madrid, Spain
Manual microtome RM2125 RTS	Leica Biosystems, Madrid, Spain
Microcentrifuge IR 220 VAC	Carl Roth, Karlsruhe, Germany
NanoDrop^{TM} One Microvolume UV-Vis spectrophotometer	Thermo Fisher Scientific, Madrid, Spain
Potter-Elvehjem tissue grinder and drill	PRO Scientific, Oxford, UK
Retriever (2100)	Aptum Biologics, Hants, UK
SPECTROstar^{Nano} spectrophotometer	BMG LABTECH, Ortenberg, Germany
T100 Thermal Cycler	Bio-Rad, Madrid, Spain
Thermomixer	Eppendorf, Madrid, Spain
Thermo Scientific Forma Steri-Cycle i250 CO_2 incubator	Thermo Fisher Scientific, Madrid, Spain
Unipower ultraviolet (UV)-transilluminator	Cultek, Madrid, Spain
Vertical laminar flow workbench, mini-V/PCR	Azbil Telstar Technologies Slu, Barcelona, Spain
Vortex Reax 200	Dismalab, Madrid, Spain
Water bath HI1210	Leica, Madrid, Spain
Water bath (STANDARD of 12877)	DILABO, Torralba de Calatrava, Spain

ZEISS Axio Lab.A1 microscope	Carl Zeiss Microscopy GmbH, Jena, Germany

6.1.10 Software

Software	Manufacturer
Adobe Photoshop CS6 13.0*32	Adobe Systems, San Jose, USA
Applied Biosystems 7300 Real-Time PCR System software	Thermo Fisher Scientific, Madrid, Spain
AxioVision SE64. Rel.4.9	Carl Zeiss Microscopy GmbH, Madrid, Spain
BioRender	BioRender.com (2022)
GraphPad Prism version 8.0	San Diego, CA
ImageJ Version 1.52u	LOCI, University of Wisconsin, USA
Microsoft Office	Microsoft, Madrid, Spain
Video copy processor P90E	Mitsubishi, Madrid, Spain

6.1.11 Others

Product	Manufacturer
1.1 mL serum-gel polypropylene microtubes	Sarstedt Inc, Barcelona, Spain
Cell culture plate sterile, 96 Well, flat-bottom with lid	Greiner Bio-One, Madrid, Spain
Cell scrapers	Thermo Fisher Scientific, Boston, USA
CellStar® cell culture multiwell plates (6-wells, 12-wells)	Greiner Bio-One, Madrid, Spain
Coverslips	Dismalab, Hirschmann, Madrid, Spain
Cryogenic tubes	Thermo Fisher Scientific, Madrid, Spain
Easypet 3 electronic pipetting	Eppendorf, Madrid, Spain
Eppendorf reference 2G single-channel, fixed, volume (10 µL, 100 µL, 1000 µL)	Eppendorf, Madrid, Spain
Eppendorf tubes (1.5 mL, 2.0 mL)	Thermo Fisher Scientific, Madrid, Spain
Falcon tissue culture treated flasks (50 mL, 250 mL)	Thermo Fisher Scientific, Madrid, Spain
Falcon tube (15 mL, 50 mL)	Labbox, Barcelona, Spain
Gavage needle	Kent Scientific, Torrington, USA

Glass feeding tubes with screw caps (50 mL)	Steriltech, Bio-Serv, Madrid, Spain
Graduated filter tip (sterile) 10 µl	Dismalab, Madrid, Spain
Histology cassettes	Dismalab, Madrid, Spain
Holders for tubes, short, #9015	Dismalab, Madrid, Spain
MicroAmp fast optical 96 well reaction plate, 0.1mL	Thermo Fisher Scientific, Madrid, Spain
MicroAmp optical adhesive film	Thermo Fisher Scientific, Madrid, Spain
MicroAmp optical 8-tube strip with attached optical caps	Thermo Fisher Scientific, Madrid, Spain
Micropipete tips (100 µL, 200 µL and 1 mL)	Grenier Bio One, Dismalab, Madrid, Spain
Mini Trans-Blot® electrophoretic transfer cell	Bio-Rad, Madrid, Spain
Nitrocelulose blotting membrane, 0.2 µm	Amersham, Dornstadt, Germany
Nitrocelulose blotting membrane, 0.45 µm	Amersham, Dornstadt, Germany
Pipettes (5 mL, 10 mL, 25 mL)	Greiner Bio-One, Dismalab, Madrid, Spain
Polyvinylidene difluoride (PVDF) membrane (0.45 µm or 0.22 µm)	Bio-Rad, Madrid, Spain
Reactive strips (Ref: 06916686001)	Roche, Madrid, Spain
Screw caps for Lieber-DeCarli feeding tubes	Steriltech, Bio-Serv, Madrid, Spain
Scintillation vial	Thermo Fisher Scientific, Boston, USA
Slides	Dismalab, Madrid, Spain
Syringes 1 mL Luer	BD Plastipak, Madrid, Spain
Syringe 1 mL with 27 x 13 needle	BD Plastipak, Madrid, Spain
Tri-Carb 2900 TR liquid scintillation counter (Packard)	PerkinElmer, Boston, USA
Whatman® paper	Bio-Rad, Madrid, Spain

6.2 Methods

6.2.1 Patients

All patients' biopsy (n = 83) from women and men aged ≥ 20 years old that underwent bariatric surgery due to obesity (high NAFLD activity score, NAS) were recruited from the Spanish cohort from the University Hospital Arrixaca (Murcia, Spain). Patients were divided according to the NAS score in the following groups: Healthy patients with NAS = 0, NAS ≤ 2 and NAS ≥ 3 score patients. Standard clinical data related to liver injury or liver specific function was collected from all the patients; serum biochemical (alanine aminotransferase - ALT - and aspartate aminotransferase - ALT) and NAS score.

6.2.2 Mice maintenance

All mice strains were maintained in the animal facility of the Faculty of Biology at Complutense University of Madrid (UCM) in a temperature-controlled room with 12 h light/dark cycle and as free access to food and water, according to the guidelines of the Federation for Laboratory Animal Science Associations (FELASA). All animal procedures were carried out according to Spanish legal requirements and animal protection law and approved by the authority of environment conservation and consumer protection of the Regional Government of Madrid (PROEX- 125.1/20, 397.2/21).

6.2.3 Mice strain

For our study, we used 8 to 14 weeks old male constitutive p21 knockout ($p21^{-/-}$) mice (B6;129S2-Cdkn1atm1Tyj/J, Jackson labs, Barcelona, Spain) and wild type ($p21^{+/+}$) mice (B6;129SF2/J, Jackson labs), as controls. Moreover, male transgenic mice carrying a *c-Myc* transgene under the control of the hepatocyte-specific albumin promoter (Alb-Myc^{tg}) as previously described [79] and Alb-Myc^{tg}/$p21^{-/-}$ mouse strain, generated crossing Alb-Myc^{tg} transgenic mice with $p21^{-/-}$ mice, both were maintained with a chow diet for 52 weeks.

6.2.4 Genotyping of transgenic mice

The correct genotype of mice was verified by polymerase chain reaction (PCR) analysis. DNA was extracted from fresh mouse tails and digested shaking overnight at 56ºC with proteinase K (AppliChem, Barcelona, Spain) in NID buffer (1:100). Enzymatic

activity of proteinase K was stopped at 95ºC during 10 min. Tails were centrifuged at 12000 rpm for 10 min and 2 µL of the supernatant was used for PCR reaction.

PCR reactions were performed in a T100 thermal cycler (Bio-Rad, Madrid, Spain) as follows:

a. p21 wild type genotyping:

Reagent	**Volume**
DNA	2.0 µL
Primer *P21* 38031	1.0 µL
Primer *P21* 38032	1.0 µL
Hotstart-taq master mix	12.5 µL
DEPC H_2O	8.5 µL
Total volume	25.0 µL

b. p21 knockout genotyping:

Reagent	**Volume**
DNA	2.0 µL
Primer *P21* 38031	1.0 µL
Primer *P21* 38033	1.0 µL
Hotstart-taq master mix	12.5 µL
DEPC H_2O	8.5 µL
Total volume	2.50 µL

Xylene cyanol (Sigma-Aldrich) was used as a loading buffer to facilitate the observation of the sample during gel loading and electrophoresis in p21 genotyping.

c. *Alb-Myc*^{tg} genotyping:

Reagent	**Volume**
DNA	2.0 µL
Primer *c-Myc f*orward	1.0 µL
Primer *c-Myc* reverse	1.0 µL
Ready mix™ redtaq™ PCR reaction mix with $MgCl_2$	12.5 µL
DEPC H_2O	8.5 µL
Total volume	25.0 µL

PCR cycle programs were as follows:

a. p21 wild type genotyping:

PCR program	Temperature	Time (h:min:sec)	Cycles
Initial denaturing	98 ºC	00:02:00	
Denaturing	98 ºC	00:00:20	x 10 (Touchdown)
Annealing	63 ºC (-0.5 ºC per cycle)	00:00:15	
Elongation	68 ºC	00:00:10	
Denaturing	94 ºC	00:00:15	x 28
Annealing	60 ºC	00:00:15	
Elongation	72 ºC	00:00:10	
Final elongation	72 ºC	00:00:02	
Conservation	10 ºC	Hold	

b. p21 knockout genotyping:

PCR program	Temperature	Time (h:min:sec)	Cycles
Initial denaturing	98 ºC	00:03:00	
Denaturing	98 ºC	00:00:30	x 35 cycles
Annealing	60 ºC	00:01:00	
Elongation	72 ºC	00:01:00	
Final elongation	72 ºC	00:02:00	
Conservation	10 ºC	Hold	

c. Alb-*Myc*^{tg} genotyping:

PCR program	Temperature	Time (h:min:sec)	Cycles
Initial denaturing	98 ºC	00:02:00	
Denaturing	95 ºC	00:00:15	x 34 cycles
Annealing	56 ºC	00:30:00	

Elongation	72 ºC	00:01:00
Final elongation	72 ºC	00:05:00
Conservation	4 ºC	Hold

6.2.5 Gel electrophoresis

PCR products were separated by 2% (w/v) agarose gels. The specific amount of agarose was perfectly diluted in TAE-buffer (1x) in a microwave. Mixture was cooled to room temperature (RT) for 5-10 min and 2 µL ethidium bromide (Thermo Fisher Scientific, Invitrogen, Madrid, Spain) or 3 µL of Midori green advance (Nippon genetics, Düren, Germany) was added to visualize DNA. An amount of 20 µL per sample was run in 1x TAE-buffer at 120 V during 45 min. DNA ladder (50 bp; Thermo Fisher Scientific, Invitrogen) was used to determine the specific size of fragments. Results were visualized in an Unipower UV-transilluminator (Cultek, Madrid, Spain) or in a GelDoc Go Imagining system (Bio-Rad) and printed or saved as a .tiff document, respectively.

6.2.6 Development of preclinical models:

a. DUAL diet

A DUAL diet was performed for 18 weeks as a model of NAFLD/NASH plus ALD, as previously described [80]. Test group was treated with a DUAL diet composed by a Western diet (WD; D18121807; Research Diets, Inc. New Jersey, USA) and 10% absolute EtOH (AppliChem) in drinking sweetened water (6.75% D (+)-glucose; Sigma-Aldrich). WD is enriched in fat and cholesterol. Regular rodent chow diet (Altromin LASQCdiet Rod18-H, Germany) and filtered tap water was used as corresponding control diet (**Figure 5**).

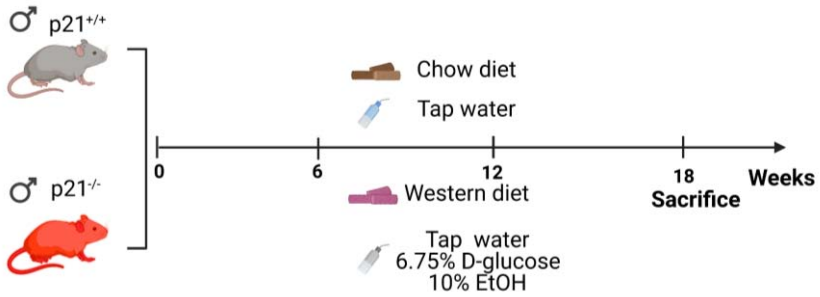

Figure 5. A schematic description of the DUAL model. $p21^{+/+}$ and $p21^{-/-}$ male mice were fed with a DUAL diet (WD plus 10% EtOH in sweetened water) for 18 weeks. Controls were fed with normal chow diet plus filtered tap water. WD, Western diet.

b. Western diet (WD)

A model of NAFLD was performed feeding mice with a WD (D18121807; Research Diets, Inc. New Jersey, USA) and filtered tap water for 14 weeks as previously described [81]. Controls were fed with normal chow diet (Altromin LASQCdiet Rod18-H) and filtered tap water (**Figure 6**).

Figure 6. A schematic description of the WD model. $p21^{+/+}$ and $p21^{-/-}$ male mice were fed with a WD for 14 weeks. Controls were fed with normal chow diet. Both groups of mice were free allowed to filtered tap water. WD, Western diet.

c. Lieber-DeCarli (LdC) diet plus multiple binges

As a model for experimental ALD, mice were treated with a chronic EtOH diet, the Lieber-DeCarli liquid diet (LdC; Steriltech, Bio-Serv, Madrid, Spain) for 8 weeks, with a previous adaptation week, plus a dose of 30% EtOH - gavage of 6 g/kg body weight (BW) - every two weeks using a gavage needle (Kent Scientific, Torrington, USA). PBS gavage was used for controls [82]. (**Figure 7**). The basic formula of the LdC control diet is presented in the **Table 1** and contains 15.1 % of total energy (kcal) as protein and 35.9% as fat. The remainder of the energy is provided as carbohydrates which, in the EtOH formula, were isocalorically replaced by EtOH (35.5% of total kcal in the up-to-date commercially available diets). Liquid food was freshly prepared every day in glass feeding tubes with screw caps (Steriltech, Bio-Serv) and changed in the early afternoon. Oral gavage was administrated in the early morning the same day every two weeks. [83].

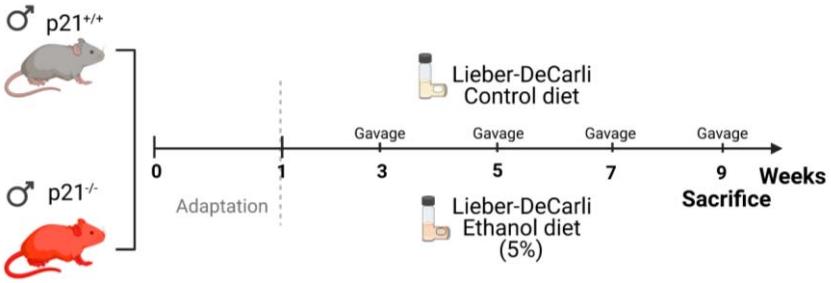

Figure 7. A schematic description of the LdC model. p21$^{+/+}$ and p21$^{-/-}$ male mice were fed with a LdC EtOH and control diet for 8 weeks, with a previous adaptation week, plus multiple oral gavage (one oral gavage every two weeks). EtOH, ethanol; LdC, Lieber-DeCarli.

Nutrients	LdC control	LdC EtOH
Protein	15.1	15.1
Fat	35.9	35.9
Carbohydrates	49.0	13.5
EtOH	-	35.5

Table 1: LdC control and EtOH diet nutrient composition expressed as % of total kcal as fat, carbohydrates and EtOH. EtOH, ethanol; LdC, Lieber-DeCarli. [83].

d. Hepatocellular carcinoma (HCC) murine model

As a model of low latency liver cancer, Alb-*Myc*^{tg} transgenic mice [84] (that overexpress *c-Myc* in hepatocytes) and Alb-*Myc*^{tg}/p21$^{-/-}$ mouse strain (generated crossing Alb-*Myc*^{tg} transgenic mice with p21$^{-/-}$ mice) were maintained with chow diet (Altromin LASQCdiet Rod18-H) for 52 weeks (**Figure 8**).

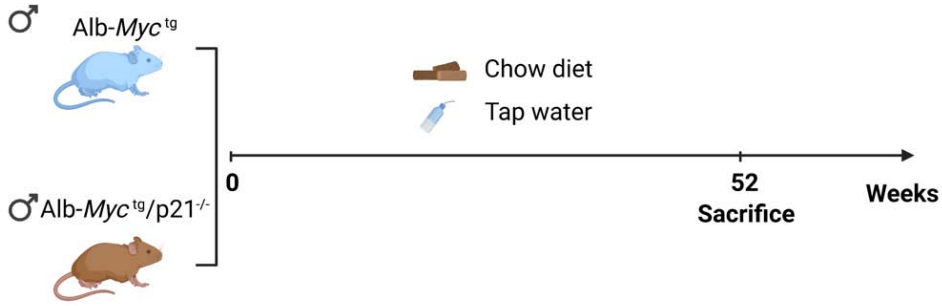

Figure 8. A schematic description of the experimental model chosen to understand the role of p21 in liver carcinogenesis. Alb-*Myc*^{tg} mice, a mouse model of low latency HCC, and the double mutant, Alb-*Myc*^{tg}/p21$^{-/-}$ mice, were kept for 52 weeks old with a chow diet.

6.2.7 Glucose tolerance test (GTT)

At the end of the treatment, glucose levels in blood were measured in 6 h fasted mice by glucose tolerance test (GTT). An amount of 7.5 g/kg body mass of 20% glucose solution (Braun GmbH, Krönberg, Germany) was gently administrated by intraperitoneal (IP) injection. Glucose levels were measured using an Accu-Check glucometer (Roche,

Madrid, Spain) and reactive strips (Roche, REF:06916686001) at 0, 5, 30, 60, 90 and 120 minutes using established protocols [85].

For the IP injection, the area of the injection was disinfected with 70% EtOH, and 1 mL syringe (27G needle) was introduced in the lower right quadrant of the abdomen - to avoid the damage to the urinary bladder, caecum and other abdominal organs - towards the head at a 40º angle to horizontal (in fat animals almost the entire length of the needle length may need to be inserted, but in smaller mice, only about half of the needle length may need to be inserted) and pulled back on the plunger to ensure negative pressure prior to injecting. The total volume injected per mouse was calculated according to the body weight. The maximum volume of administration allowed per mice is < 10 mL/kg. [85].

6.2.8 Weekly food/water intake and body weight measurement

Food and water intake were measured once per week, usually on Fridays in the early morning. Food was weighted (g) and water volume was measured (mL) and recorded. Total kcal ingested were calculated according to the energetic value of food and drinking water. The equivalences were: chow diet = 3 kcal/g, WD = 4.5 kcal/g, D-glucose = 4 kcal/g and EtOH = 7 kcal/g.

Moreover, to monitor and control the body weight of the mice, we have weighed them every week, on the same day and at approximately the same time in the morning.

6.2.9 Mice dissection

Twelve-hours fasted mice were sacrificed by an overdose of isoflurane (Solvet, Segovia, Spain), chloroform (Thermo Fisher Scientific, Boston, USA) or avertin solution (20 µL/g), and body weight (BW) was measured. After that, mice were opened at the abdomen along the *linea alba* and blood, and organs were collected.

a. Blood

Blood was taken from the vena cava inferior with a 1 mL syringe (27G needle) for serum analysis. Serum was separated in 1.1 mL Serum-Gel Polypropylene microtubes (Sarstedt Inc, Barcelona, Spain) by centrifugation at 12000 rpm, 10 min, 4ºC, collected and stored at -80ºC for subsequent determination of aminotransferase activities and triglycerides content.

b. Organs

First, liver and epididymal white adipose tissue (eWAT) were removed and weighed. After that, liver was extracted and washed with cold 1x PBS. Liver images were taken in a MZ16 Stereo microscope with a Leica DFC480 digital camera by means of the DISKUS Z16 APO (Leica, Madrid, Spain). Organs were cut in small pieces and frozen in cryotubes (Thermo Fisher Scientific) in liquid nitrogen and stored at -80ºC for RNA and protein isolation. Moreover, tissue was stored in plastic cassettes, fixed in 4% formaldehyde (AppliChem) and embedded in paraffin to perform hematoxylin and eosin (H&E), Sirius red (SR) and immunohistochemistry (IHC) staining. Otherwise, small pieces of liver were preserved in Tissue-Tek O.C.T.™ (Sakura, Barcelona, Spain) compound and kept in -80°C for ORO and immunofluorescence (IF) staining. In the present project, we focused on the study of the liver.

6.2.10 Transaminases and triglycerides in serum

Serum was diluted 1:5 for measuring serologic markers such as: alanine aminotransferase (ALT), aspartate aminotransferase (AST), lactate dehydrogenase (LDH), triglycerides (mg/dL) in the Gregorio Marañón Research Health Institute at Madrid (iISGM) and in the Central Laboratory Facility at the University Hospital RWTH of Aachen in Germany, using automated analyzers.

6.2.11 Primary hepatocytes assays

6.2.11.1 Primary hepatocytes isolation

Mouse primary hepatocytes were isolated from 6 to 10 weeks old male $p21^{+/+}$ (C57BL6/J - Jackson labs, Boston, USA - and B6;129S/J - Jackson labs, Barcelona, Spain) and $p21^{-/-}$ (Jackson labs) mice following standard protocols [86].

First, the pump was washed with 70% EtOH and the tubing was primed with previously warmed (42ºC) perfusion buffer (pump speed 3 mL/min). A 27G needle was connected to the end of the tubing. Two 50 mL falcon were prepared with perfusion buffer and digestion buffer. The recipe was previously described in **6.1.2 standard buffer and media** section.

Mice were scarified with an overdose of chloroform or 1x avertin solution (20 µL/g). For perfusion procedure, mice were opened making an “U”-shaped incision in the abdomen and secure the skin near the head using a needle, gut was moved away, and

liver lobe was shift to the left-up part to reveal the portal vein and vena cava. The vena cava is cannulated, the edge of the needle should be rest on the vena cava in a flat angle (parallel to the vein), the needle bevel should be facing upwards, and the portal vein was cut. The liver was perfused to wash out blood and circulating cells from the liver, as well as to eliminate calcium via EDTA. Warm perfusion buffer was running during 2 min. In 1 min it should immediately turn a tan color. After that, pump was stopped and quickly transferred the inlet tubing from perfusion buffer to the pre-warmed liver digestion buffer tube and quickly turned the pump back on. The liver digestion buffer was running for 10 min. Liver was gently dissected out, shortly washed in PBS and gently scraped off with razor; connective tissue and gall bladder were removed. Subsequently, it was washed and resuspended with 10 mL plating medium through 70 µm and kept on ice until every mouse is finished. Finally, hepatocytes were density separated by Percoll (Sigma-Aldrich) gradient centrifugation.

Isolated cells were seeded into at different densities (10^6 cells/12-well dishes and 2×10^6 cells/6-well dishes) in plating medium. After overnight treatment, cells were switched to maintenance medium (containing 10% fetal bovine serum, 2 mM sodium pyruvate, 2% penicillin/streptomycin, 0.1 µM dexamethasone, and 1 nM insulin). Primary hepatocytes were used for ^{14}C functional assays (*de novo* lipogenesis, fatty acids and glucagon oxidation) after *sip21*/*siCtrl* transfection and for ORO staining. (**Figure 9**).

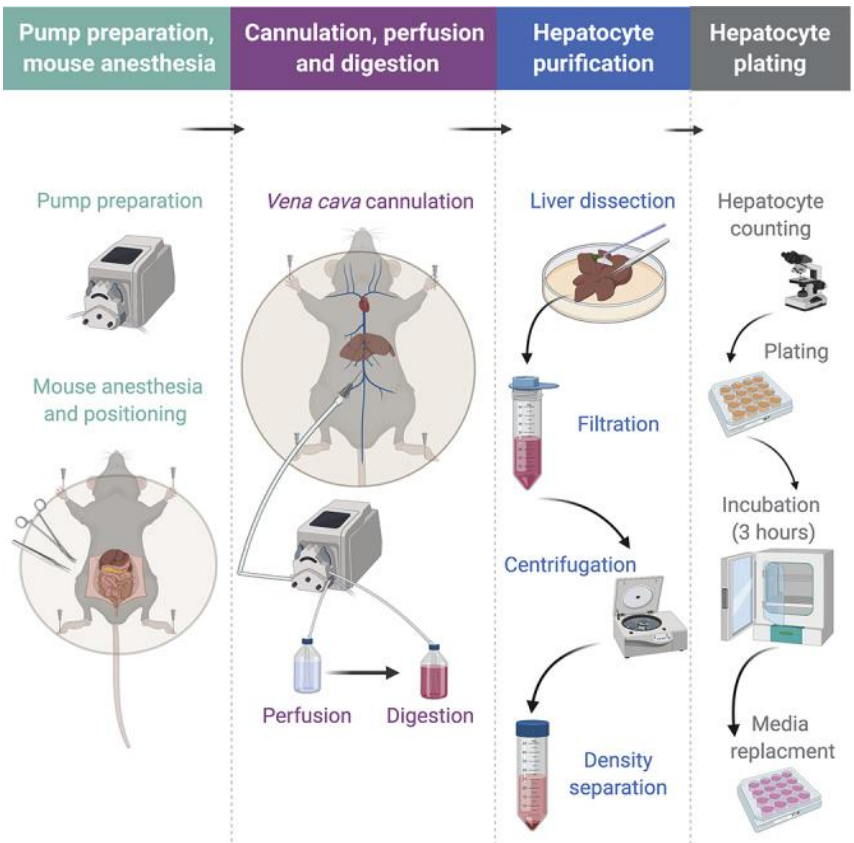

Figure 9. A schematic description of the isolation of primary hepatocytes from mice. Pump preparation for the procedure. Mouse sacrifice and positioning for the dissection. Vena cava cannulation and administration of perfusion and digestion buffers. Liver dissection and hepatocytes purification. Hepatocytes plating and media replacement. Courtesy of Charni-Natan *et al*. [86].

6.2.11.2 siRNA transfection

In mammalian cells, RNA interference (RNAi) can be triggered by small interfering RNAs (siRNAs) that cause strong, yet transient inhibition of gene expression on specific genes. In the present study, reverse *siRNA* transfection was performed with lipofectamine RNAi max (Thermo Fisher Scientific) following the manufacturer's protocol. In brief, 0.1 µM of control or *p21* RNA duplex (CDKN1a mouse siRNA oligo duplex; Origene, Rockville, USA) and 3 µL lipofectamine RNAi max were gently mixed in 100 µL Opti-MEM (Sigma-Aldrich), incubated for 10 min at RT and added before plating 10^6 hepatocytes/mL.

6.2.12 Hepatic triglycerides content

Hepatic triglycerides concentrations from liver were measured following the manual guide of triglycerides liquicolor mono kit (RAL, Barcelona, Spain).

An amount of 21-23 mg of liver tissue was homogenized on ice with a manual glass homogenizer in 1 mL homogenization buffer (**6.1.2 standard buffer and media**) previously prepared and cooled. The exact amount of liver (mg) was recorded to calculate the total amount of triglycerides.

The homogenate solution was centrifuged for 5 min at 1200 rpm, 4ºC and the upper two layers were gently mixed and transferred to a new tube. Samples were dilute in homogenization buffer (1:3) and 2 µL were mixed with 200 µL kit reagent in a 96-well flat bottom plate (Grenier Bio One, Dismalab, Madrid, Spain). After an incubation of 45 min at RT, absorbance was measured at 450 nm in a spectrophotometer (BMG LABTECH, Ortenberg, Germany). A standard curve was prepared diluting standard solution in dH_2O at 50 mg/dL, 75 mg/dL, 100 mg/dL, 150 mg/dL,175 mg/dL; dH_2O was used as a blank control. Liver triglycerides content were calculated according to the absorbance of the standard curve and the grams of liver used.

6.2.13 Histological analysis

6.2.13.1 Tissue processing and embedding

Two pieces of tissue per cassette were fixed in 4% formaldehyde (AppliChem), washed in 1x PBS (3 x 10 min) and stored at 4ºC. For tissues, paraffin embedding samples were washed in tap water for 0.5-1 h and the next protocol was followed:

- Dehydration: samples were dehydratase in 50% EtOH tank for 30 min and subsequently in 70%, 85%, 95% EtOH tanks for 1 h/tank. Tissues were kept in a fresh 95% EtOH tank for overnight. Next day, tissue cassettes were transferred into a 100% EtOH tank for 30 min, twice.
- Cleaning: tissue pieces were kept in EtOH absolute:xylene (1:1) for 30 min and, after that, two times in xylene for 30 min.
- Wax infiltration: three tanks of wax previously warmed at 70ºC in the water bath were used for the wax infiltration. Samples were kept in each tank for 1 h.
- Embedding: small pieces of tissue were embedded into paraffin blocks with an embedding Leica EG1160 embedding center, dispenser + hot plate machine (Leica, Madrid, Spain).

Paraffin sections of liver were cut to a thickness of 5 µm using a manual microtome (Leica) and a water bath (Leica). Slices were dry at 60ºC for 1 h in the oven and kept at RT.

6.2.13.2 Hematoxylin and eosin (H&E) staining

Hematoxylin and eosin (H&E) staining was performed in paraffin sections of liver tissue. Deparaffinization and rehydration of the samples were performed as follow: 3 x 5 min xylene, 2 x 5 min 100% EtOH, 2 x 5 min 95% EtOH, 2 x 5 min 70% EtOH, 2 x 5 min dH_2O. For nuclei staining, slides were immersed in hematoxylin for 2 min, rinsed in tap water for 10 min and 2 x 5 min in dH_2O. Followed by eosin staining and dehydration: 3 min eosin, 2 x 10 sec 95% EtOH, 2 x 10 sec 100% EtOH, 3 x 5 min xylene. Finally, the stained paraffin sections were mounted with a coverslip using Roti®-Histokitt. Pictures were acquired in a 20x magnification with an Eclipse Ci optical microscope (Nikon, Madrid, Spain).

6.2.13.3 Sirius red (SR) staining

In order to determinate collagen deposition, Sirius red (SR) staining was performed. First, paraffin sections were deparaffinized by incubation in 60ºC for 30 min,

followed by 2 x 5 min xylene and rehydrated using a descending percentage of EtOH series (2 x 2 min 100% EtOH, 2 min 95% EtOH, 2 min 80% EtOH and 2 min dH_2O). Subsequently, slides were incubated for 1 h in Picro-Sirius red solution. Afterwards, staining was fixed by 4 min incubation in acidified water. Picro-Sirius red solution and acidified water are described in section **6.1.2 standard buffer and media**. Then, sections were dehydrated in 100% EtOH (2 x 30 seconds) and cleared in xylene (2 x 5 min). Roti®-Histokitt was used for mounting stained paraffin sections. Pictures were taken in a 20x magnification using an Eclipse Ci optical microscope (Nikon).

Collagen deposition was showed as red fibers in the liver and positive area was quantified via Image J© software (National Institutes of Health, Bethesda, MD).

6.2.13.4 Immunohistochemistry (IHC) staining

Paraffin sections cut to a thickness of 5 µm were preheated at 60ºC for 30 min in the oven and subsequently deparaffinized and rehydrated with xylene and serial EtOH solutions (from 100% to 70%), respectively. After that, antigen unmasking was performed by boiling sections in 10 mM sodium citrate buffer (citrate/PBS-T, pH = 6.0) using a pressure-cooker Antigen 2100-Retriever (Aptum Biologics, Hants, UK). When a cycle of the pressure-cooker is completed, slides were washed in dH_2O 3 x 5 min and treated with BLOXALL® endogenous blocking solution (Vector Laboratories, Petersburg, UK) during 10 min to inactivates endogenous peroxidase. Including this step and from now, samples were surrounded with a hydrophobic solution to individually stain each section and all the procedures were performed in a humid chamber to avoid dehydration of the sections.

After removing the blocking solution, samples were washed 2 x 5 min dH_2O plus 1 x 5 min PBS. To avoid nonspecific binding of immunoglobulins in the tissue, samples were blocked with 50 µL 2.5% normal horse serum blocking solution (Vector Laboratories) for 30 min at RT. After that, sections were incubated with primary antibody diluted in PBS with 1% BSA and 0.3% Triton (antibodies dilution are provided in **6.1.6 Immunostaining and immunoblotting** section) for overnight at 4ºC.

The next morning, slides were washed 3 x 5 min with PBS and incubated with biotinylated secondary antibodies (Vector Laboratories) during 1 h at RT. To eliminate the excess of secondary antibody, slices were washed 3 x 5 min in PBS and signals were developed with DAB (Vector Laboratories). The incubation with DAB ranges from 30 sec to 3 min depending on the antigen to analyze. Positive areas/cells stain in brown

when the DAB reacts with the biotinylated secondary antibodies. After that, sections were submerged in dH_2O and counterstained with hematoxylin for 40 sec. Dehydrating was performed in increasing percentages of EtOH and then in xylene. Slices were mounted with Roti®-Histokitt and pictures were taken using an optical microscope (Nikon). Image J© software (National Institutes of Health) was used to quantify positive cells.

6.2.13.5 Oil Red O (ORO) staining

To detect neutral lipids and triglycerides in liver tissue and in primary hepatocytes, ORO staining was performed in 8 µm frozen liver sections previously cut in a cryostat (Leica) or in cells growth in round coverslips. Samples were fixed in 4% formaldehyde for 25 min (frozen sections were previously air-dried for 40 min) and washed 3 x 5 min in dH_2O. Subsequently, samples were stained for 40 min with ORO working solution and counterstained with hematoxylin (the nuclei will be stained by the hematoxylin). After ORO working solution and hematoxylin, slides were shortly washed with dH_2O and rinsed with tap water until water runs clear. Slides were mounted with a ready to use Dako faramount aqueous mounting medium (Dako, Agilent, Madrid, Spain). Pictures were taken with an optical microscope (Nikon), immediately after staining. Lipid content was showed as red droplets and Image J© software (National Institutes of Health) was used to quantify the positive area.

6.2.13.6 Immunofluorescence (IF) staining

Immunofluorescence (IF) staining were performed in 5 µm frozen liver sections. Sections were air-dried for 20 min, fixed in 4% formaldehyde (AppliChem) and washed with PBS 3 x 5 min. PBS containing 5% goat serum and 0.3% Triton was used for blocking step (1 h, RT) followed by incubation with primary antibody in blocking solution at optimized dilutions at 4°C overnight. List of primary antibodies are provided in **6.1.6 Immunostaining and immunoblotting antibodies** section. On the second day, slides were washed with PBS 3 x 10 min and incubated with anti-rat secondary antibody labelled with Alexa Fluor 488 (Thermo Fisher Scientific, Invitrogen) for 1 h at RT. Then, slides were washed 3 x 10 min in PBS. Nuclei were counterstained with Vectashield mounting medium containing DAPI (Vector Laboratories, Petersburg, UK). A humidity box was used to keep the slides wet and prevent them from drying out. Microscopy and image acquisition were performed using an Axio Imager A1 microscope (Carl Zeiss Microscopy GmbH, Jena, Germany) and AxioVision software. Image J© software (National Institutes of Health) was used to quantify positive cells.

6.2.13.7 Terminal deoxynucleotidyl transferase dUTP nick end labelling (TUNEL) staining

Cell death was determined with terminal deoxynucleotidyl transferase dUTP nick end labelling (TUNEL) staining. During late stages of programmed cell death, or apoptosis, DNA becomes highly fragmented. This fragmentation provides an opportunity to attach a modified dUTP to the 3'-OH ends of the damaged DNA using the enzyme terminal deoxynucleotidyl transferase dUTP nick end labeling (TUNEL) reaction. The modified dUTP, such as BrdUTP or EdUTP, can then be detected. Freshly 5 µm cryosections from mouse liver were dried in air for 30 min, fixed in 4% formaldehyde at RT for 20 min, followed by 3 x 10 min wash in PBS. After that, slides were incubated in 30% hydrogen peroxide diluted in Methanol (MetOH), (20 mL 30% H_2O_2 + 180 mL MetOH), followed by incubated in PBS for another 10 min. To have access to the DNA, the nuclei were permeabilized in 150 mM Na-citrate solution prepared as shown before (**6.1.2 standard buffer and media** section).

The permeabilization solution was removed by washing twice in PBS solution for 10 min. Next, slides were incubated with labelling solution (per sample: 0.5 µL enzyme solution, 5 µL 10x TUNEL diluted buffer, 44.5 µL TUNEL labelling solution) overnight at 4ºC.

On the second day, the slides were washed with 4 x 10 min PBS and mounted with DAPI for nuclear counterstaining. Microscopy and image acquisition were performed using an Axio Imager A1 microscope (Carl Zeiss Microscopy GmbH). Positive cells were quantified by Image J© software (National Institutes of Health).

6.2.13.8 Imaging and staining analysis

Mounted samples were observed in the microscope (optical - Nikon - and fluorescent - Carl Zeiss Microscopy GmbH - microscopes) and pictures were taken for subsequent image analysis.

Pictures were randomly taken at 20x and 40x magnification and were analyzed in Image J© software (National Institutes of Health). Area was quantified for SR, ORO, vimentin, 4-HNE and positive cells were counted for TUNEL, Ki67, CD45, CD11b staining. Data were represented as % area or % positive cells, respectively.

6.2.14 RNA isolation and analysis

6.2.14.1 RNA isolation and determination of RNA concentration

RNA from liver tissue (patients and mice) and cells were isolated with Trizol (Thermo Fisher Scientific) reagent following the manufacturer's recommendations. The place to work with RNA should be perfectly cleaned with 70% EtOH, contamination and RNAses are frequently problems in this technique.

For tissue, 50-60 mg of liver tissue was homogenized in a FastPrep-24^{TM}5G (MP Biomedicals, Illkirch-Graffenstaden, France) with Trizol. Whereas, for primary hepatocytes, 1 mL of Trizol was added into 6-well plates. Samples were kept in Trizol for 10 min at RT to allow complete dissociation of the proteins complex and 200 µL of chloroform were added and mixed shaking. After 20 min incubation, samples were centrifuged 10 min, 12000 rcf at 4ºC and the mixture separates into a lower red phenol-chloroform, an interphase and a colorless upper aqueous phase. Then, 400 µL from the aqueous phase containing the RNA were transferred to a new tube, angling the tube 45º and pipetting the solution out.

To precipitate the RNA, samples were incubated for 15 min with 400 µL of isopropanol (AppliChem) at 4ºC and centrifuged for 10 min at 12000 rcf at 4ºC. Total RNA precipitate forms a white gel-like pellet at the bottom of the tube, and supernatant was discarded with a micropipette.

For the washing of the RNA, pellet was resuspended in 1 mL 70% EtOH and centrifuged 10 min, 12000 rcf at 4ºC, this process was repeated twice. Supernatant was discarded with a micropipette and pellet was dry at RT.

Finally, to solubilize the RNA, the pellet was diluted with DEPC water and vortexed 20-30 sec at 65ºC, maximum speed in the thermomixer (Eppendorf, Madrid, Spain). Samples were stored at -80ºC.

6.2.14.2 Complementary DNA (cDNA) synthesis

For the complementary DNA (cDNA) synthesis, RNA concentration of each sample was measured in a Nanodrop (Thermo Fisher Scientific) using an optical density (OD) of 260 nm and the purity of the sample was determined according to the E260/E280 ratio; a protein free nuclei acid solution typically has a 1.8-2.0 ratio.

Reverse transcription is a process to transcribe single-stranded RNA to cDNA. According to the RNA concentration measurements, each RNA sample was standardized into a 1 µg/µL dilution. Reverse transcription was performed using an Applied Biosystems™ high-capacity cDNA reverse transcription kit (Thermo Fisher Scientific) following the manufacturer's protocol:

Reagent	Volume
RNA (1 µg/µL)	10 µL
DEPC water	4.2 µL
10x buffer RT	2 µL
25x dNTPs	0.8 µL
10x random primer	2 µL
Enzyme Reverse transcriptase	1 µL
Total volume	20 µL

Reactions were incubated in a PCR thermocycler (T100 thermal cycler, Bio-Rad) following the next protocol:

Temperature	Time (h:min:sec)
25 ºC	00:10:00
37 ºC	02:00:00
85 ºC	00:05:00
4 ºC	Hold

6.2.14.3 Quantitative Real-Time Polymerase Chain Reaction (qRT-PCR)

Quantitative real-time PCR (qRT-PCR) is a method used for the amplification and quantification of DNA products. The DNA amplification is monitored at each cycle of the PCR and is based on fluorescent detection. The fluorescent signal increases with increasing PCR cycles. The point at which the fluorescence becomes measurable is called the threshold cycle (CT). A lower CT values denote for higer amounts of the gene of interest. qRT-PCR was performed in 20 µL reaction volume using SYBR Green Master Mix (Thermo Fisher Scientific, Invitrogen) and a 7300 real time PCR system by the Genomics and Proteomics Facility (Faculty of Biology, UCM). At the end of the PCR,

baselines and threshold values were established using AB7300 Real-Time PCR System software (Thermo Fisher Scientific), and the CT values were exported to Microsoft Excel to calculate relative messenger RNA (mRNA) expression according to the ΔΔCT method [87], which determinate the relative quantification of a target gene in comparison to a housekeeping gene (*Gapdh*). The list of primers used is provided in the **6.1.7 Primer sequences used for qRT-PCR** section.

To perform the qRT-PCR analysis, the reaction mix and program was used as follows:

qRT-PCR reaction mix	**Volume**
Primer forward	1 µL
Primer reverse	1 µL
SYBR GreenERTM qPCR super mix	10 µL
cDNA	5 µL
DEPC water	3 µL
Total volume	20 µL

PCR program	**Temperature**	**Time (h:min:sec)**	**Cycles**
Activation	95 ºC	00:00:10	
Denaturing	95 ºC	00:00:15	x 40
Annealing/Elongation	60 ºC	00:01:00	
Conservation	4ºC	hold	

To perform the dissociation curve, the following steps were added to the PCR program:

Temperature	**Time (h:min:sec)**
95 ºC	00:00:15
60ºC	00:01:00
95 ºC	00:00:15

6.2.15 Protein isolation and analysis

6.2.15.1 Protein extraction and quantification

Frozen liver tissue protein extraction from mice, approximately, 50 mg frozen liver tissue was homogenized on ice with 500 µL RIPA complete buffer (**6.1.2 standard buffer and media**). For primary hepatocytes, 50 µL of RIPA complete buffer was used. Liver

tissue was homogenized on ice using a manual glass homogenizer (Omni International, Inc. Kennesaw, GA, USA) and cells were collected using scrapers (Thermo Fisher Scientific). This step was followed by an incubation of 30 min on ice and a centrifugation of 10 min, 12000 rpm at 4ºC. The upper layer was transferred to a new tube and protein quantification was calculated using the Pierce BCA Protein Assay Kit (Thermo Fisher Scientific), based on a colorimetric detection. For the protein quantification, 5 µL of protein was mixed with working reagent (50:1, reagent A:B) in a 96-well plate and incubated during 30 min at 37ºC. The plate was read in a spectrophotometer (BMG LABTECH) set to 562 nm. Protein concentration was calculated according to the OD_{562} of the standard curve of BSA (2000 µg/mL, 15000 µg/mL, 1000 µg/mL, 750 µg/mL, 500 µg/mL, 250 µg/mL, 125 µg/mL, 25 µg/mL). RIPA complete buffer was used as a blank. The final concentration of the samples was adjusted to 4 µg/µL for liver samples and 1-2 µg/µL for primary hepatocytes containing 4X Laemmli buffer. Liver and cell samples were desaturated 10 min at 95ºC shaking in the thermomixer and stored at -80ºC.

6.2.15.2 Immunoblotting assay

Protein expression was detected performing immunoblotting technique. Liver and cell samples were defrosted, homogenized by vortex and a short spin. Handmade gels containing 5% polyacrylamide stacking gel and separating gel that range from 8 to 15% according to the molecular weight of the proteins were used. An amount of 80 µg of liver tissue and 20 µg of cells were loaded and separated at 80-150 V in running buffer. After the electrophoresis, the separated proteins were transferred from the gel onto a PVDF membrane (0.45 µm or 0.22 µm pore) making a sandwich with Whatman paper in a wet chamber for 2h at 300 mA on ice following the standard protocols [88]. Running and transfer buffers were prepared as is indicated in materials section (**6.1.2 standard buffer and media**). To confirm the correct transference of the proteins, Ponceau S solution (Sigma-Aldrich) was used. Then, the membranes were incubated in 5% non-fat dry milk or BSA diluted in 0.1% TBS-Tween (TBS-T) to block non-specific binding sites. After 1 h, membranes were incubated with the optimized dilution of primary antibody in 2.5% non-fat dry milk or BSA shaking overnight at 4ºC. The next morning, to get rid of non-bound antibody, the membranes were washed 3 x 10 min in TBS-T and incubated with the horseradish peroxidase (HRP-)-conjugated secondary antibody diluted in 2.5% non-fat dry milk or BSA. Subsequently, membranes were washed 3 x 10 min in TBS-T. Target bands were visualized incubating the membrane in Amersham ECL Prime (GE Healthcare, Amersham, UK) for 2 min and exposing it to an odyssey Fc Imaging system (LI-COR, Madrid, Spain) or Amersham Imager 600 (GE Healthcare) until specific signals

were detectable. Primary and secondary antibodies' dilution are provided in **6.1.6 Immunostaining and immunoblotting antibodies** section**.**

6.2.16 Functional studies in primary hepatocytes

6.2.16.1 *De novo* lipogenesis (DNL) assay

Primary hepatocytes were plated at 2 x 10^6 per well in 6 well plates. After overnight starvation medium containing 5 mM glucose, hepatocytes were rinsed with PBS and overnight spiked with 0.25µCi/mL of D-[^{14}C(U)] glucose (PerkinElmer, Boston, USA) in starvation medium containing 20 mM unlabeled glucose (**6.1.2 standard buffer and media** section). Cells were washed twice with PBS and then harvested in 200 µL of 0.5% Triton in PBS, and 500 µL of 2:1 chloroform:MetOH was added to 150 µL before vortexing at high speed for 20-30 sec and incubating overnight at 4 ºC. The remaining protein lysate was used for protein quantification and normalization. Before vortexing, 125 µL of dH_2O was added and centrifuged for 15 min at 1000 rpm at 4 ºC. The bottom phase was transferred to a large 20 mL scintillation vial containing 3 mL of scintillation fluid (PerkinElmer). Incorporation of ^{14}C carbons into lipid fraction was measured using a Tri-Carb 2900 TR liquid scintillation counter (PerkinElmer), and all reads in DPM1 (decompositions per minute) were normalized to protein content calculated with Pierce BCA Protein Assay Kit (Thermo Fisher Scientific). Each experiment was performed in triplicates in the presence or absence of 20 nM insulin (Sigma-Aldrich, St. Louis, USA).

6.2.16.2 Fatty acid and lactate oxidation assays

Cellular palmitic and lactate acid rates were determined in isolated primary hepatocytes using protocols previously described [89]. A density of 10^6 cells/well of primary hepatocytes were cultured in 12-well plates. Hepatocytes were overnight incubated with a starvation medium (glucose-deprived DMEM, 0.1% BSA, 2 mM sodium pyruvate, 2% penicillin/streptomycin) containing 5 mM glucose. Next morning cells were pretreated with glucagon (Sigma-Aldrich) treatment in starvation medium for 2 h, rinsed with PBS and incubated with [1-^{14}C] palmitic acid (0.4µCi/mL) or L-[^{14}C(U)] lactic acid (0.2µCi/mL) (PerkinElmer) for fatty acid and lactate oxidation assays, respectively. The oxidation reactions were terminated, and CO_2 was released from the media by the addition of 1 M $HClO_4$. Whatman filter paper saturated with 2 M NaOH was placed in the cup of the tube to capture CO_2. Following a 3 h incubation at 25°C, $^{14}CO_2$ resulting from oxidized lactate or fatty acid was quantified by scintillation counting (DPM1) of the filter paper. Each experiment was performed in quadruplicates in the presence or absence of glucagon (Sigma-Aldrich).

6.2.17 Data collection (TCGA analysis)

Transcriptome data of HCC patients was obtained from The Cancer Genome Atlas (TCGA) database (https://www.cancer.gov/). The mRNA expression data of 371 primary tumors and 50 normal tissues were collected. The differential expression of *P21* gene in HCC and control samples were evaluated using GraphPad Prism version 8.0 (San Diego, CA).

Data from the TCGA of survival probability in HCC patients was collected and correlated with *P21* expression. A total number of 365 patients were evaluated.

6.2.18 Statistical analysis

Data are expressed as mean ± SD. GraphPad Prism version 8.0 (San Diego, CA) was used to perform statistical analysis and graphs design. To evaluate the statistical differences between patients, $p21^{-/-}$ and $p21^{+/+}$ mice and *siCtrl* and *sip21* primary hepatocytes in functional assays, one-way ANOVA followed by Turkey post-hoc test was used. Statistical significance between Alb-*Myc*^{tg} and Alb-*Myc*^{tg}/$p21^{-/-}$ mice and, *siCtrl* and *sip21* primary hepatocytes in qRT-PCR assays was determined by t-test. P-values for significance are indicated as follows: * p=0.05; ** p<0.01; *** p<0.001, **** p<0.0001. * symbol represents the differences between treated groups *vs* control, # was used to indicate differences between mice genotypes and between *sip21* and *siCtrl* primary hepatocytes.

RESULTS

7. Results

7.1 p21 expression is altered in clinical and preclinical chronic liver disease (CLD)

It has been reported that the expression of p21 is related with the development of CLD [90]. Thus, we first focused on the analysis of the expression of p21 in HCC in TCGA database. Results showed that the expression of *P21* in primary tumor is significantly diminished compared to normal tissue (**Figure 10A**). However, the survival probability in HCC patients did not correlate with the expression of *P21*. There were no significant differences in terms of survival between patients with high and low/medium expression levels of *P21* (**Figure 10B**).

Moreover, we studied a cohort of Spanish patients from the University Hospital Arrixaca (Murcia, Spain) that underwent bariatric surgery due to obesity (high NAFLD activity score, NAS). Serum levels of ALT and AST correlates with the NAS score, being significantly higher in patients with NAS score ≥ 3 (**Figure 10C, D**). Nevertheless, *P21* and *P27* - cell cycle inhibitors - mRNA expression tested by qPCR in these patients determined a significant reduction in the expression in individuals with advanced stages of liver injury, NAS score ≥ 3, compared to patients with NAS ≤ 2 score (**Figure 10E, F**).

Additionally, we checked mRNA transcripts for *P21* and P21 levels measured by immunoblotting assay in different mouse models of CLD in wild type mice: a DUAL diet model that synergistically combines the effects of alcohol and western diet (WD), a WD model and an acute-on-chronic EtOH model that combines the Lieber-DeCarli (LdC) diet plus multiples EtOH binges. The *P21* mRNA expression was upregulated after a DUAL and a WD. Moreover, there is an overexpression of P21 protein checked by immunoblotting assay in wild type mice, especially after a DUAL diet (model of NAFLD with ALD background), whereas no differences in EtOH feeding groups (**Figure 10G, H**).

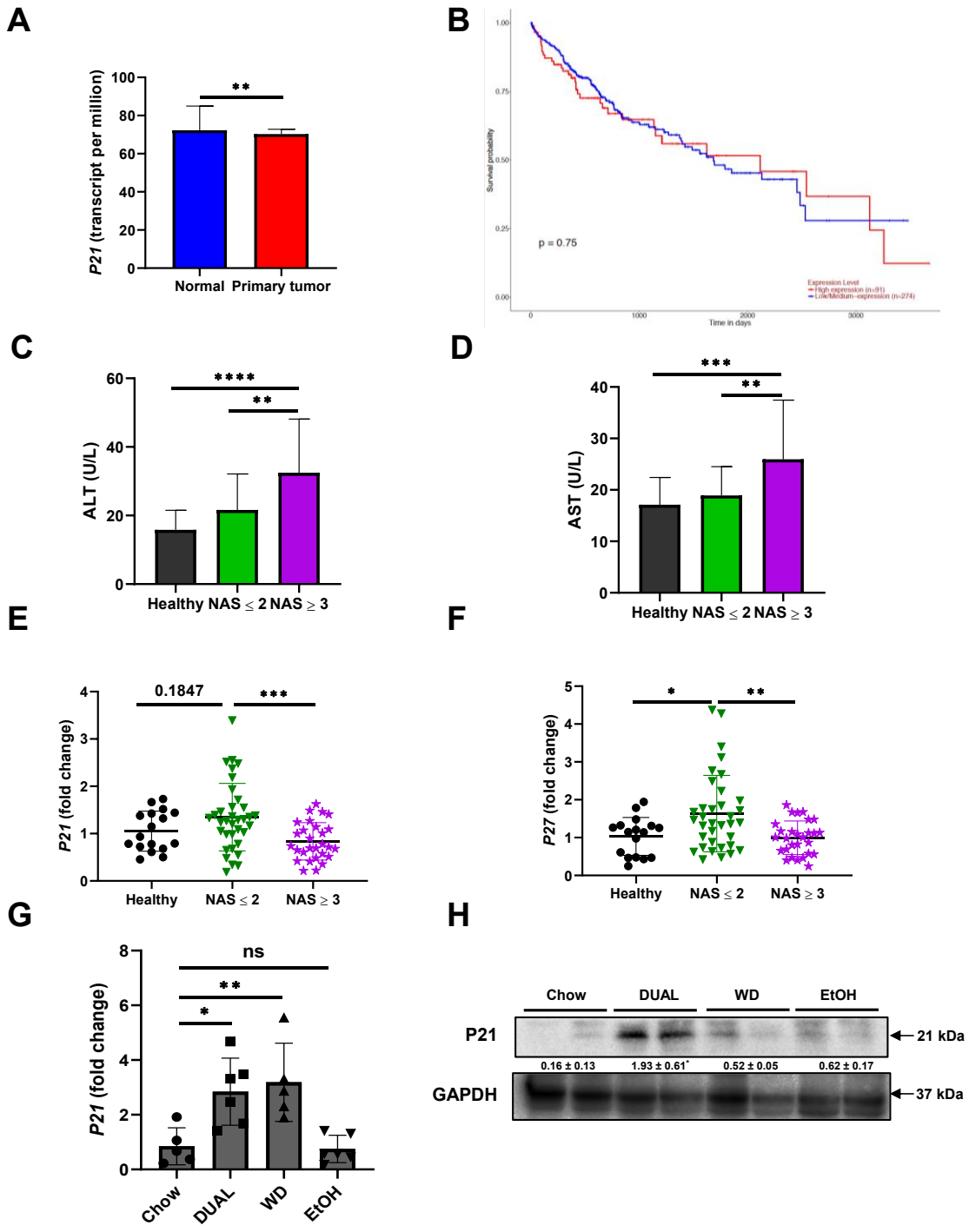

Figure 10. p21 expression in patients and in preclinical models. (**A**) Expression of *P21* in HCC TCGA sample types (n = 421). (**B**) Effect of *P21* expression level on HCC patient's survival (n = 365). (**C**) ALT and (**D**) AST serum levels measured in a cohort of Spanish patients from the University Hospital Arrixaca (Murcia, Spain). (**E**) *P21* and (**F**) *P27* mRNA expression in a cohort of Spanish patients from the University Hospital Arrixaca (Murcia, Spain) (n = 83). (**G**) *P21* mRNA relative expression to *Gapdh* tested in liver of B6;129S/J wild type mice ($p21^{+/+}$) after different murine models of CLD (DUAL

diet, WD, EtOH diet) and controls (chow diet). (n = 6-7) (**H**) Representative immunoblotting analysis of P21 in liver samples of $p21^{+/+}$ mice after a DUAL, WD and EtOH diets and controls. Ratio between P21 and GAPDH was calculated. Two individuals' samples from each group are shown as a representative of the group. (n = 4). Data are expressed as the mean ± SD. Values with distinct superscripts are significantly different from each other (*P < 0.05, **P < 0.01, ***P < 0.001; ****P < 0.0001), assessed by one-way ANOVA.

7.2 Generation of transgenic $p21^{+/+}$ and $p21^{-/-}$ mice

To further study the role of p21 in CLD, constitutive p21 knockout mice ($p21^{-/-}$) were included in the present study and wild type $p21^{+/+}$ mice were used as controls; both in a B6;129S/J background. In order to confirm the correct genotype of mice, a PCR analysis was performed using the DNA previously extracted from the tail of 4 weeks old mice. The *P21*$^{+}$ allele was detected in agarose gel electrophoresis as a 208 bp DNA fragment, whereas the *P21*$^{-}$ allele was shown as 317 bp DNA fragment (**Figure 11A**). Moreover, the *P21* expression tested by qRT-PCR in the liver of both groups of mice revealed a significantly downregulation in the $p21^{-/-}$ mice compared to $p21^{+/+}$ mice (**Figure 11B**).

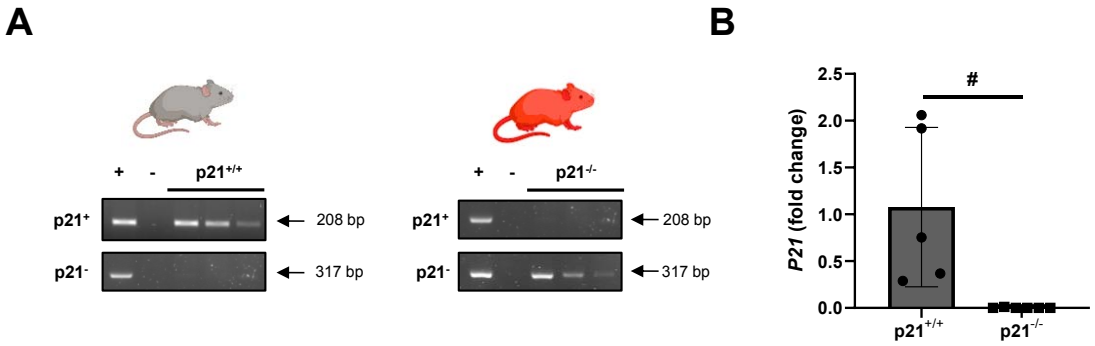

Figure 11. Confirmation of *P21* deletion in $p21^{-/-}$ mice. (**A**) 2% agarose gel showing the genotyping PCR result from mice tails of $p21^{+/+}$ and $p21^{-/-}$ mice. *P21*$^{+}$ band appears at 208 bp, whereas *P21*$^{-}$ is shown at 317 bp. Positive and negative controls were included in the gel. (**B**) *P21* mRNA expression measured in liver of $p21^{+/+}$ and $p21^{-/-}$ mice relative to *Gapdh*. (n = 6). Data are expressed as the mean ± SD. Values with distinct superscripts are significantly different from each other assessed by t-test, # shows intergroup differences. (n = 6, #P < 0.05).

7.3 The absence of p21 protects mice from liver injury and steatosis after a DUAL diet

According to our results and due to the significant increase of p21 expression after a DUAL diet, a model that synergistically combines the effects of a Western diet (WD) and alcohol, we focused the study in $p21^{+/+}$ and $p21^{-/-}$ mice after 18 weeks of treatment (**Figure 5**).

During the treatment period, food and water intake were recorded once a week and daily kcal intake were calculated. Food and water kcal intake determine a higher daily caloric consumption in DUAL-fed mice compared to controls, whereas no differences were observed between $p21^{+/+}$ and $p21^{-/-}$ mice after the treatment (**Figure 12A**). Indicating that the possible differences between genotypes of mice were not because of different amounts of food intake.

Additionally, body weight (BW) increased steadily in all treated groups throughout the experimental period. Even soon, there is a significant reduction in the BW increase during and after the treatment in $p21^{-/-}$ mice after a DUAL diet (**Figure 12B**).

Obesity and ALD are associated with changes in the function of adipose tissue, which has important systemic and hepatic consequences [91]. There was a significantly increase in eWAT weight (g) after treatment in both genotypes of mice, but we could not find significant differences in the amount of eWAT between both genotypes of mice, as well as in the eWAT weight/BW ratio (**Figure 12C**).

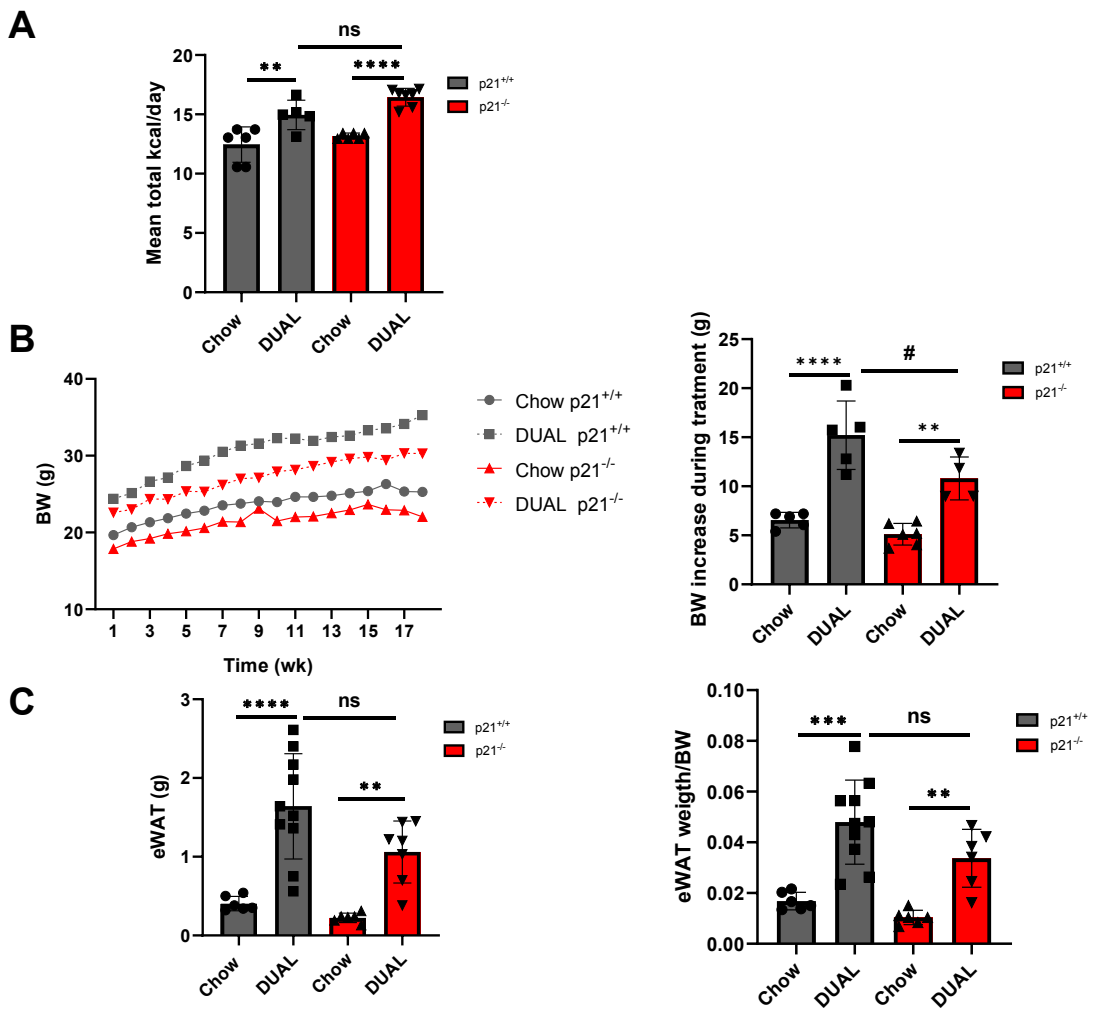

Figure 12. Body weight increase is reduced in p21$^{-/-}$ mice during the DUAL diet treatment, but no changes in eWAT were detected. (**A**) Mean of total kcal/day consumed by p21$^{+/+}$ and p21$^{-/-}$ mice after a DUAL diet and a chow diet for 5 weeks period of the treatment. (**B**) Body weight (BW) curve during the feeding period and BW increase after the treatment expressed in grams. (**C**) eWAT weight (g) and eWAT weight to BW ratio after treatment. Data are expressed as the mean ± SD. Values with distinct superscripts are significantly different from each other assessed by one-way ANOVA, * shows intragroup differences and # intergroup differences. (n = 6-10, **P < 0.01, ***P<0.001, ****P<0.0001, #P < 0.05).

It has been reported that a DUAL diet causes changes in liver of C57BL6/J mice in terms of liver damage, hepatomegaly, hepatocyte enlargement, ballooning and steatosis [80], so we further examined the livers.

In the present study, mice exhibit enlarged and pale livers, a sign of fat accumulation, after a DUAL diet compared to controls, showed by macroscopic pictures of the liver (**Figure 13A**). As previously reported by us [80], a DUAL diet causes a significant increase in the liver weight (LW), body weight (BW) and liver weight to body weight ratio (LW/BW) in mice, indicating a pathology [80]. Here, both genotypes of mice showed a significantly increase in these three parameters compared to controls (LW, BW and LW/BW ratio); however, the increase in LW and LW/BW ratio was significantly reduced in $p21^{-/-}$ mice compared to controls ($p21^{+/+}$). (**Figure 13B**). Additionally, serum markers of liver damage were evaluated. ALT was significantly increased, and AST and LDH showed a tendency to increase in $p21^{+/+}$ mice after a DUAL diet compared with controls. However, $p21^{-/-}$ mice were protected from liver injury (**Figure 13C**).

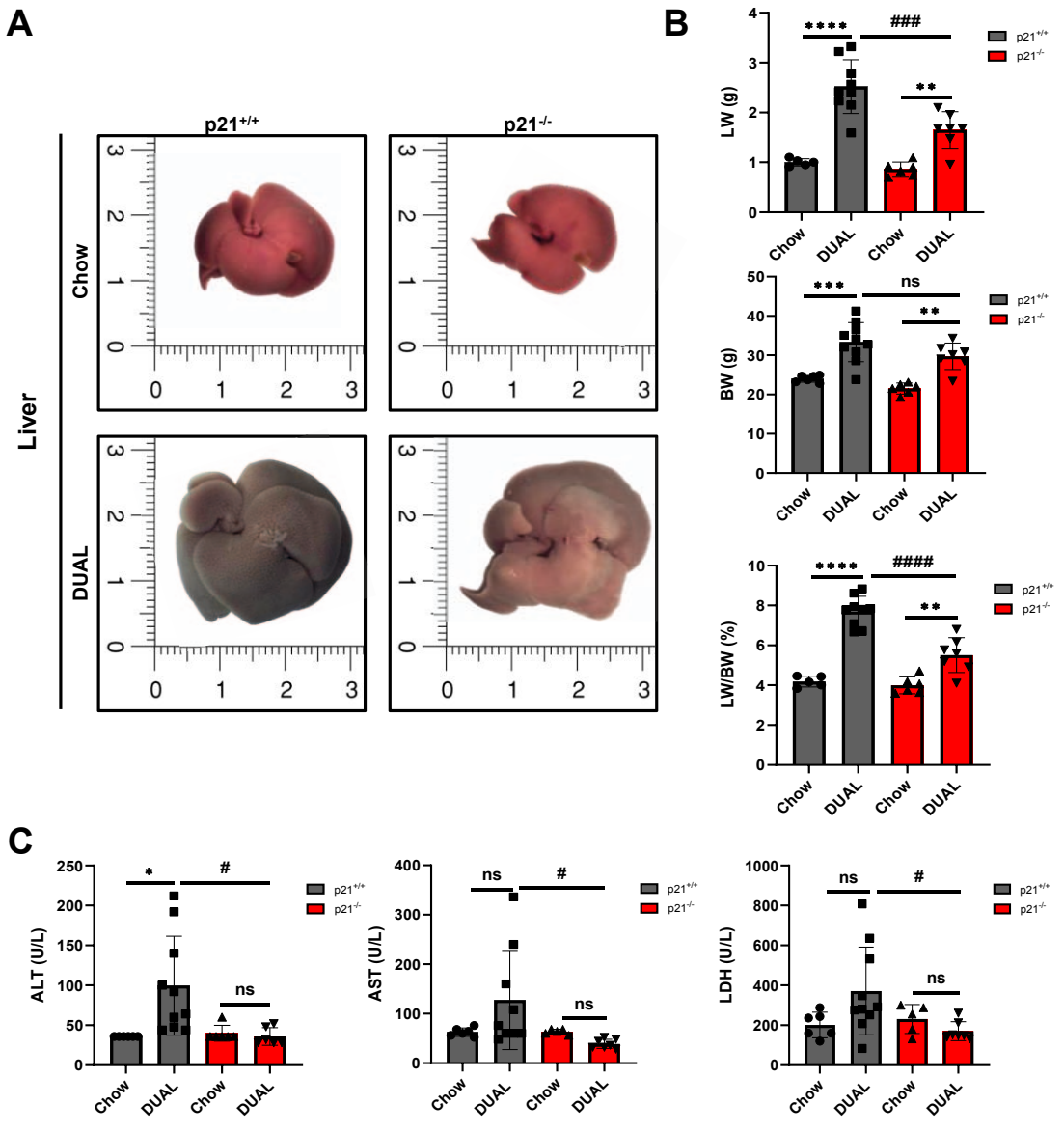

Figure 13. $p21^{-/-}$ mice display protection against liver damage after a DUAL diet. (**A**) Liver pictures of wild type and mutant mice after a DUAL diet. Pictures were taken with a Stereo microscope and the scale bar was represented in cm. (n = 6-10). (**B**) Liver weight (LW), Body weight (BW) and BW/LW ratio expressed in grams of $p21^{+/+}$ and $p21^{-/-}$ mice after a DUAL diet. (n = 5-9). (**C**) ALT, AST and LDH measurements (U/L) in serum of $p21^{+/+}$ and $p21^{-/-}$ mice after a DUAL diet (n = 6-10). Data are expressed as the mean ± SD. Values with distinct superscripts are significantly different from each other assessed by one-way ANOVA, * shows intragroup differences and # intergroup differences. (*P < 0.05, **P < 0.01, ***P<0.001, ****P<0.0001, #P < 0.05, ###P < 0.001, ####P < 0.0001).

Additionally, data from hepatic triglycerides content and lipid accumulation measured by ORO staining showed a significant increase in $p21^{+/+}$ DUAL-fed mice, while $p21^{-/-}$ mice exhibited a significant reduction compared with wild type $p21^{+/+}$ mice after a DUAL diet treatment (**Figure 14A-C**). Moreover, levels of triglycerides in serum are significant diminished in $p21^{+/+}$ DUAL-fed mice compared with chow diet, whereas no significant changes were observed in $p21^{-/-}$ mice related to controls (**Figure 14D**). These data indicate that wild type mice are incorporating a higher quantity of triglycerides from serum to the liver.

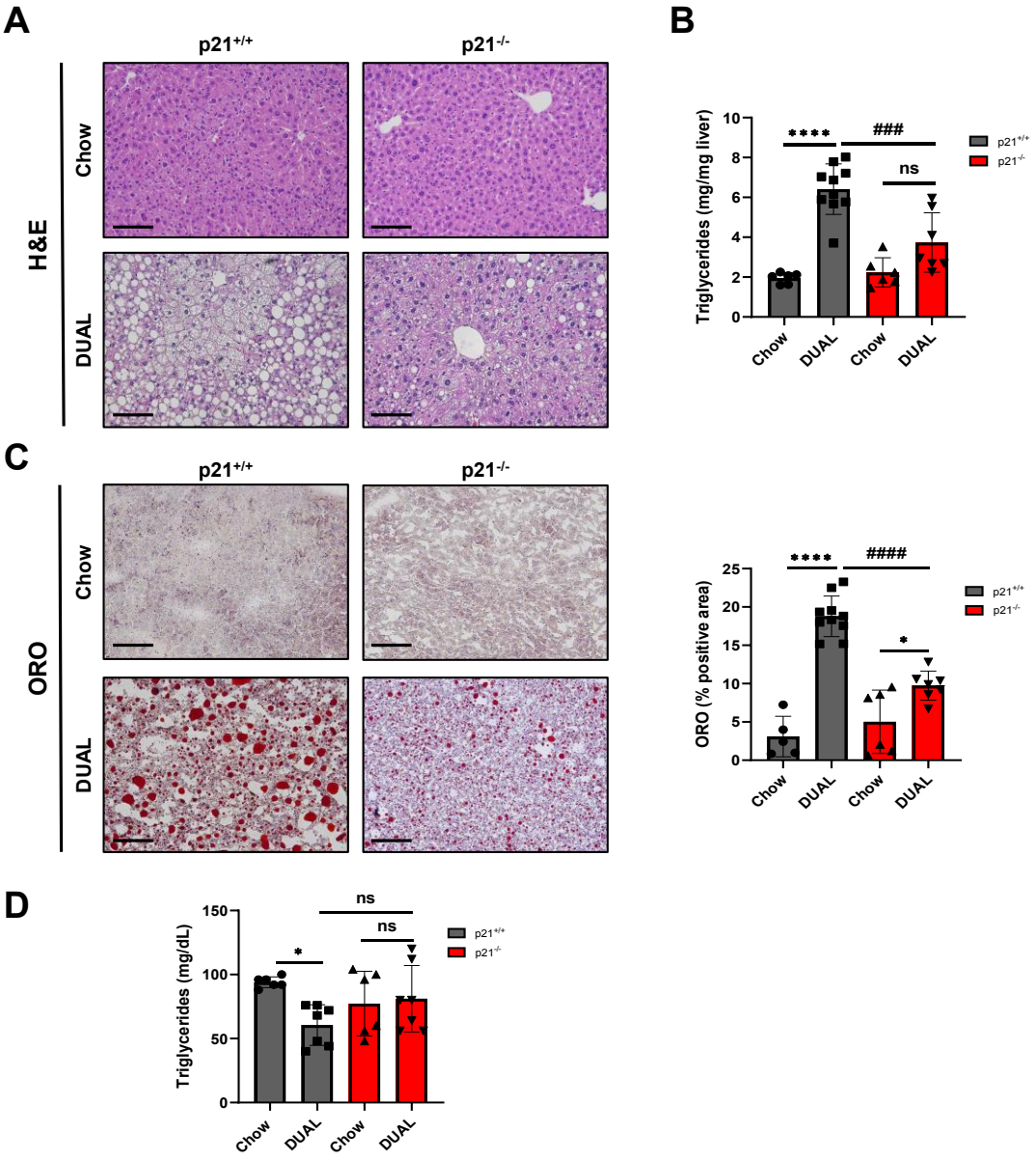

Figure 14. Lipid accumulation is significantly reduced in liver after a DUAL diet in p21$^{-/-}$ mice. (**A**) Representative H&E staining in p21$^{+/+}$ and p21$^{-/-}$ mice after a DUAL diet and controls. (n = 6-10). Scale bar = 100 µm. (**B**) Quantification of hepatic triglycerides after a DUAL diet (mg/mg liver). (n = 6-10). (**C**) ORO staining performed in liver cryosection and each quantification (% positive area). Scale bar = 100 µm. (n = 6-10). (**D**) Serum triglycerides levels after a DUAL diet and controls (mg/dL) (n = 6-7). Data are expressed as the mean ± SD. Values with distinct superscripts are significantly different from each other assessed by one-way ANOVA, * shows intragroup differences and # intergroup differences (*P < 0.05, ****P<0.000, ###P < 0.001, ####P < 0.0001).

Since lipid metabolism was affected by p21 deletion, we further explored genes and enzymes that play a pivotal role. A DUAL diet triggered a decreased level of lipid and free fatty acid (FFA) oxidation genes, including *Pparα* and *Fxr1* (**Figure 15A, B**). Moreover, an induction of *Pparγ*, *Cd36* and *Fas* genes related to the FA uptake and *de novo* lipogenesis was observed (**Figure 15C-E**). However, in $p21^{-/-}$ mice after a DUAL diet, the expression of *Pparα* and *Fxr1* were significantly increased and *Pparγ*, *Cd36* and *Fas* statistically reduced, in contrast to $p21^{+/+}$ mice (**Figure 15A-E**).

Nevertheless, glucose metabolism was unaltered since the mRNA transcripts of *Phosphoenolpyruvate carboxykinase* (*Pepck) cytosolic* and *Pyruvate carboxylase (PC)* expression, showed no significant differences between the experimental groups (**Figure 15F, G**).

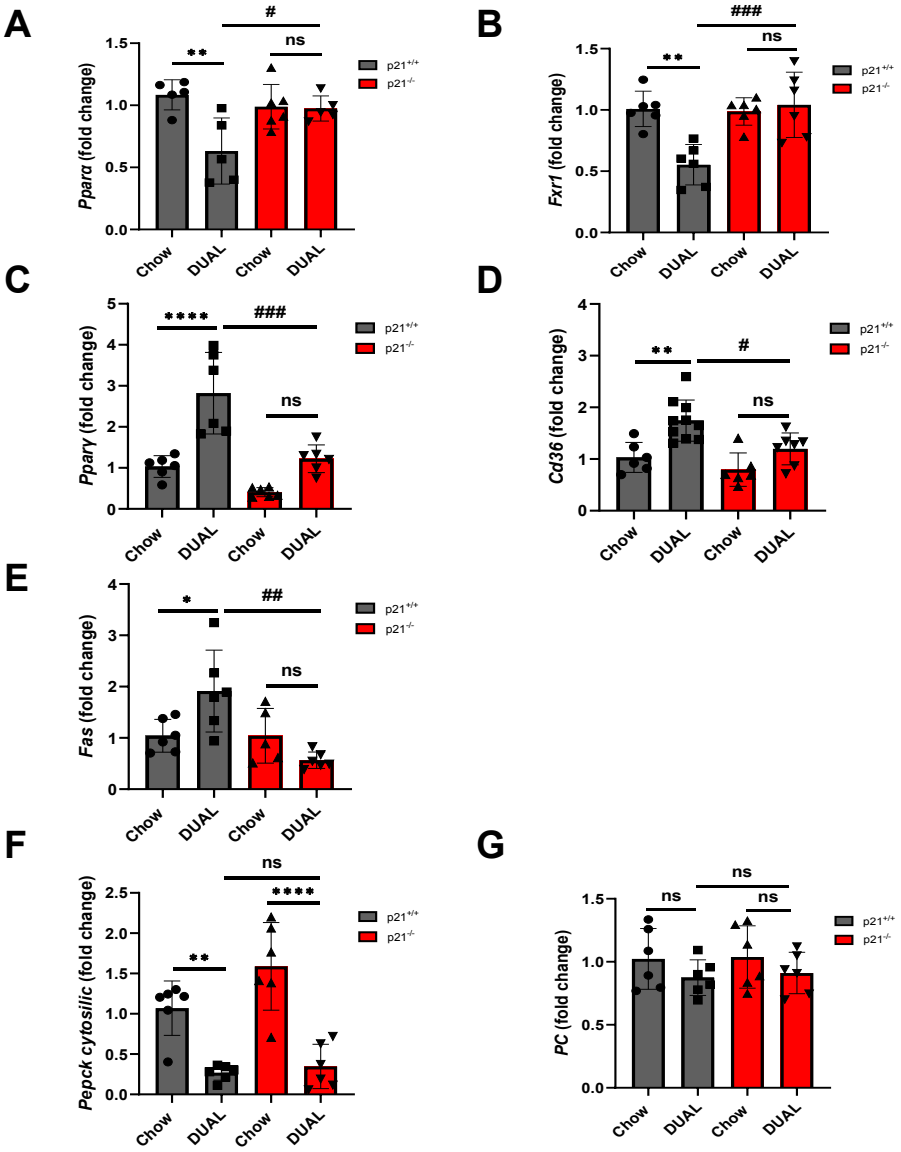

Figure 15. Lipid balance is deregulated in p21$^{-/-}$ mice after a DUAL diet. (**A**) *Pparα*, (**B**) *Fxr1* (**C**) *Pparγ* (**D**) *Cd36* and (**E**) *Fas* mRNA expression determined by qRT-PCR and normalized to the amount of *Gapdh* in liver of wild type and mutant mice. (**F**) *Pepck cytosolic* and (**G**) *Pyruvate carboxylase (PC)* mRNA relative expression to *Gapdh* in p21$^{+/+}$ and p21$^{-/-}$ livers. Data are expressed as the mean ± SD. Values with distinct superscripts are significantly different from each other assessed by one-way ANOVA, * shows intragroup differences and # intergroup differences (n = 6-10, *P < 0.05, **P < 0.01, ****P<0.0001, #P < 0.05, ##P < 0.01, ###P < 0.001).

7.4 Lipid peroxidation and DNA damage are reduced in p21$^{-/-}$ mice after a DUAL diet

Extensive fat accumulation in the liver tissue together with alcohol consumption exacerbates the generation of oxidative stress, a key event that accelerates and worsen steatosis and initiate progression to steatohepatitis and fibrosis [92]. Although both genotypes of mice induced the same expression of cytochrome P450 (CYP2E1) after a DUAL diet (**Figure 16A**), 4-HNE – a lipid peroxidation product – revealed less 4-HNE positivity in p21$^{-/-}$ mice after a DUAL diet (**Figure 16B**). Lipid peroxidation products leads to DNA damage, which represents an important component of the physiologic process during oxidative stress. Additionally, DNA damage response leads to double stand breaks formation and rapidly phosphorylation of the histone H2AX [93]. Thus, immunohistochemistry staining of γ-H2AX in liver sections showed a significant increase in the number of γ-H2AX positive cells in p21$^{+/+}$ mice, while there is a significant reduction in p21$^{-/-}$ mice compared to wild type mice in the DUAL-fed group (**Figure 16C**). These findings indicated that the absence of p21 after a diet rich in fat and cholesterol combined with chronic EtOH consumption reduces lipid peroxidation and DNA damage in the liver.

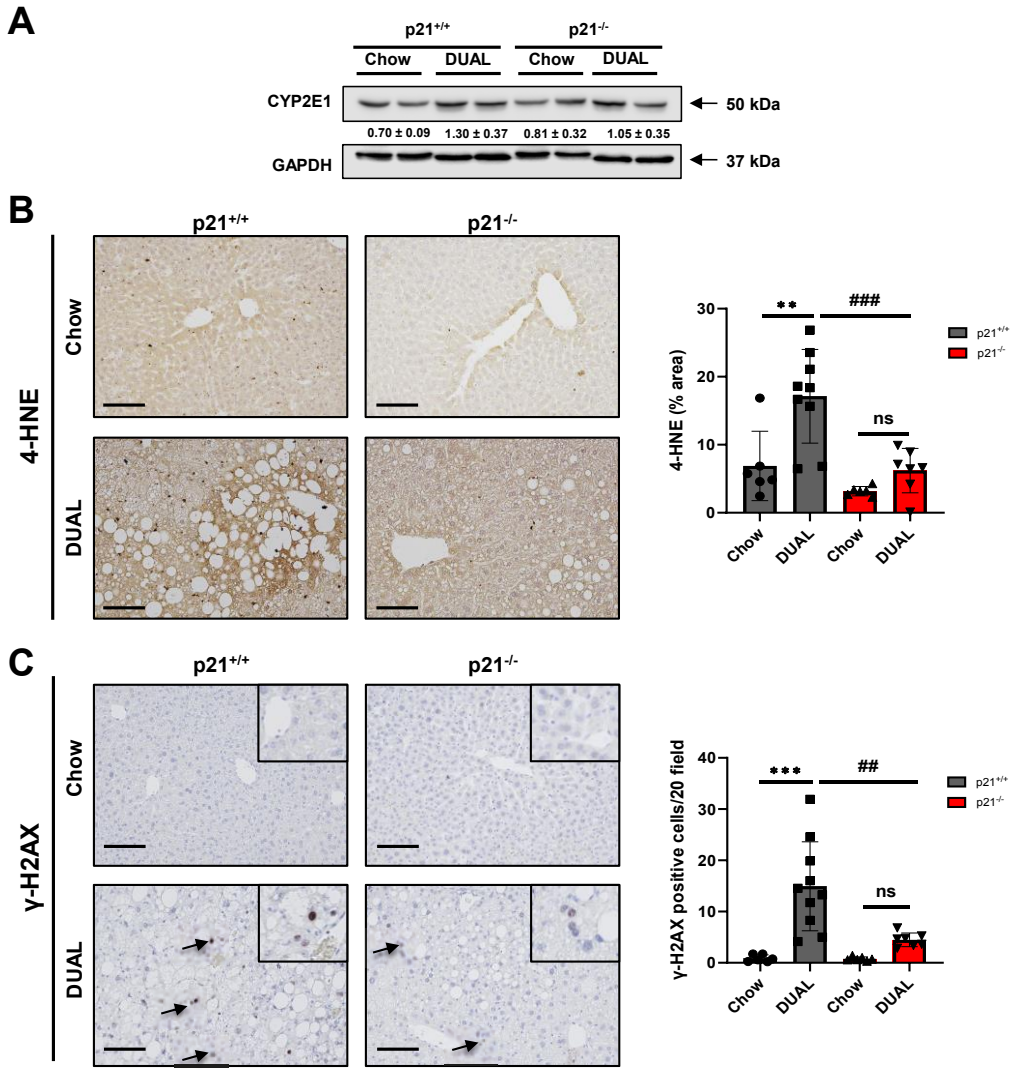

Figure 16. Oxidative stress and DNA damage after DUAL treatment. (**A**) CYP2E1 (50 kDa) immunoblotting assay using GAPDH (37 kDa) as loading control. Ratio between CYP2E1 and GAPDH was calculated. (**B**) Representative liver sections of $p21^{+/+}$ and $p21^{-/-}$ mice stained with 4-HNE and each quantification (% area). Scale bar = 100 μm. (n = 6-9). (**C**) Representative γ-H2AX-stained photographs of each group of mice after a DUAL diet and controls, and each quantification (positive cells/20 field). Scale bar = 100 μm. (n = 6-10). Data are expressed as the mean ± SD. Values with distinct superscripts are significantly different from each other assessed by one-way ANOVA, * shows intragroup differences and # intergroup differences (**P < 0.01, ***P < 0.001, ##P < 0.01, ###P < 0.001).

7.5 Hepatocyte cell death is reduced in p21$^{-/-}$ mice after DUAL diet treatment

Since oxidative stress contributes to liver damage and leads to hepatocyte cell death, we next examined cell death in both p21$^{+/+}$ and p21$^{-/-}$ animals, including cleaved caspase (CC)-3 and -8; phosphorylated receptor-interacting serine/threonine-protein kinase 1 (pRIPK1) and 3 (pRIPK3); and mixed linage kinase domain-like protein (pMLKL). A DUAL diet induced overexpression of CC-3 and -8, pRIPK1/3 and pMLKL in p21$^{+/+}$ mice. However, p21$^{-/-}$ animals were protected against necroptotic cell death (**Figure 17A**). Moreover, TUNEL staining in p21$^{-/-}$ mice was significantly reduced after a DUAL diet in contrast to p21$^{+/+}$ mice (**Figure 17B**). Altogether, these findings suggested that absence of p21 leads to reduced hepatic cell death.

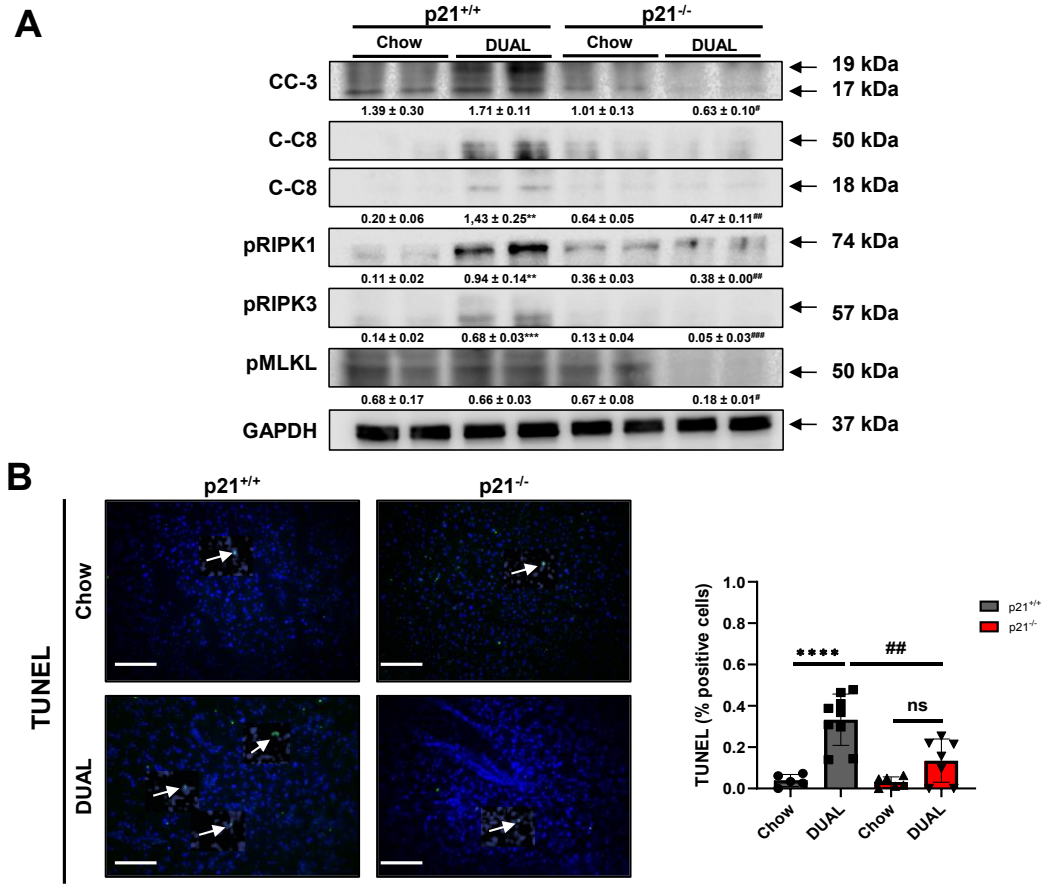

Figure 17. Hepatic cell death after a DUAL diet. (**A**) Total liver protein (two individuals' samples from each group are shown as a representative of the group) were isolated from DUAL diet-fed p21$^{+/+}$ and p21$^{-/-}$ mice and analyzed for CC-3 (19, 17 kDa), CC-8 (50, 18 kDa), pRIPK1 (74 kDa), pPRIPK3 (57 kDa) and pMLKL (50 kDa). The protein expression levels were normalized to the levels of total GAPDH (37 kDa). Ratio between CC-3, CC-8, pRIPK1, pRIPK3 and pMLKL and GAPDH was calculated. (**B**) TUNEL staining was performed in liver cryosections. Quantification of TUNEL positive cells (%) was done and

graphed (n = 5-10). Data are expressed as the mean ± SD. Values with distinct superscripts are significantly different from each other assessed by one-way ANOVA, * shows intragroup differences and # intergroup differences (**P < 0.01, ***P < 0.001, #P < 0.05, ##P < 0.01, ###P < 0.001).

Death of hepatocytes may trigger compensatory proliferation to maintain tissue homeostasis. Ki67 antibody recognizes a nuclear antigen present in G1, S, G2 and M phase of the cell cycle; whereas G0, quiescent cells do not express this antigen [94], for this reason Ki67 is a marker of cell proliferation. Consistently, Ki67 immunohistochemistry staining of liver sections revealed that cell proliferation was statistically reduced in $p21^{-/-}$ mice compared with $p21^{+/+}$ mice (**Figure 18A**). Due to the role of p21 in the progression of the cell cycle in the G1 phase as an inhibitor [95], we evaluated the mRNA transcripts of cell cycle mediators controlling the late G1 and S-phase progression. *CyclinD1* and *CyclinA2* expression were significantly reduced after a DUAL diet in $p21^{-/-}$ mice, compared with $p21^{+/+}$ animals, whilst *CyclinE1* expression was elevated in both genotypes of mice after the DUAL diet feeding (**Figure 18B**). Thus, $p21^{+/+}$ mice exhibit higher cell proliferation levels.

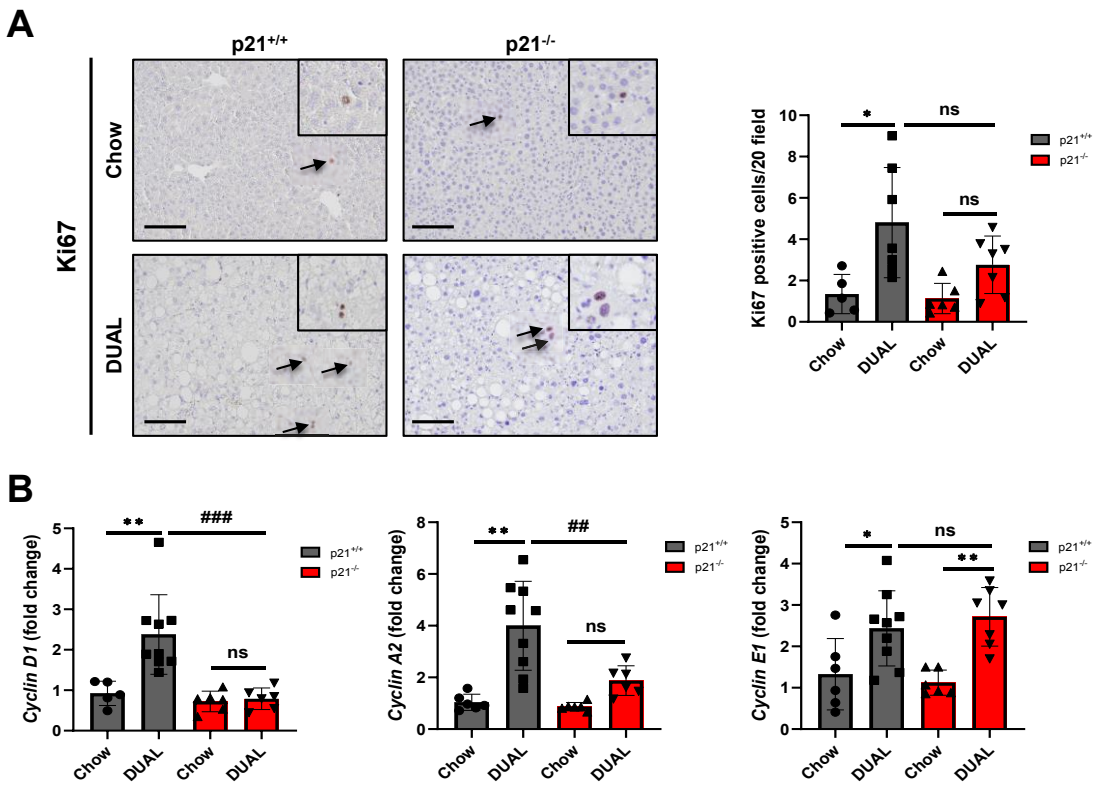

Figure 18. Compensatory cell proliferation increased in wild type mice after a DUAL diet. (**A**) Illustrative Ki67-stained liver sections from each group after feeding and Ki67 quantification. Scale bar = 100 µm. (n = 6-10). (**B**) Hepatic mRNA expression levels of *CyclinD1*, *CylincA2* and *CyclinE1* in liver of mice of each group relative to *Gapdh*. (n = 6-10). Data are expressed as the mean ± SD. Values with distinct superscripts are significantly different from each other assessed by one-way ANOVA, * shows intragroup differences and # intergroup differences (*P < 0.05, **P < 0.01, ##P < 0.01, ###P < 0.001).

7.6 Hepatic inflammation and fibrogenesis are reduced in p21-deleted mice after a DUAL diet

Fat accumulation and cell death in the liver further caused immune cell infiltration and hepatic inflammation [96]. p21 knockout animals showed a significant reduction in the accumulation of leukocytes ($CD45^+$ cells) and infiltrated cells ($CD11b^+$ cells) in contrast to $p21^{+/+}$ mice, checked by immunofluorescence staining (**Figure 19A, B**). Additionally, decreased levels of mRNA transcripts for *IL-6* and *Tnf-α* – proinflammatory cytokines – were found in $p21^{-/-}$ DUAL-fed mice (**Figure 19C**).

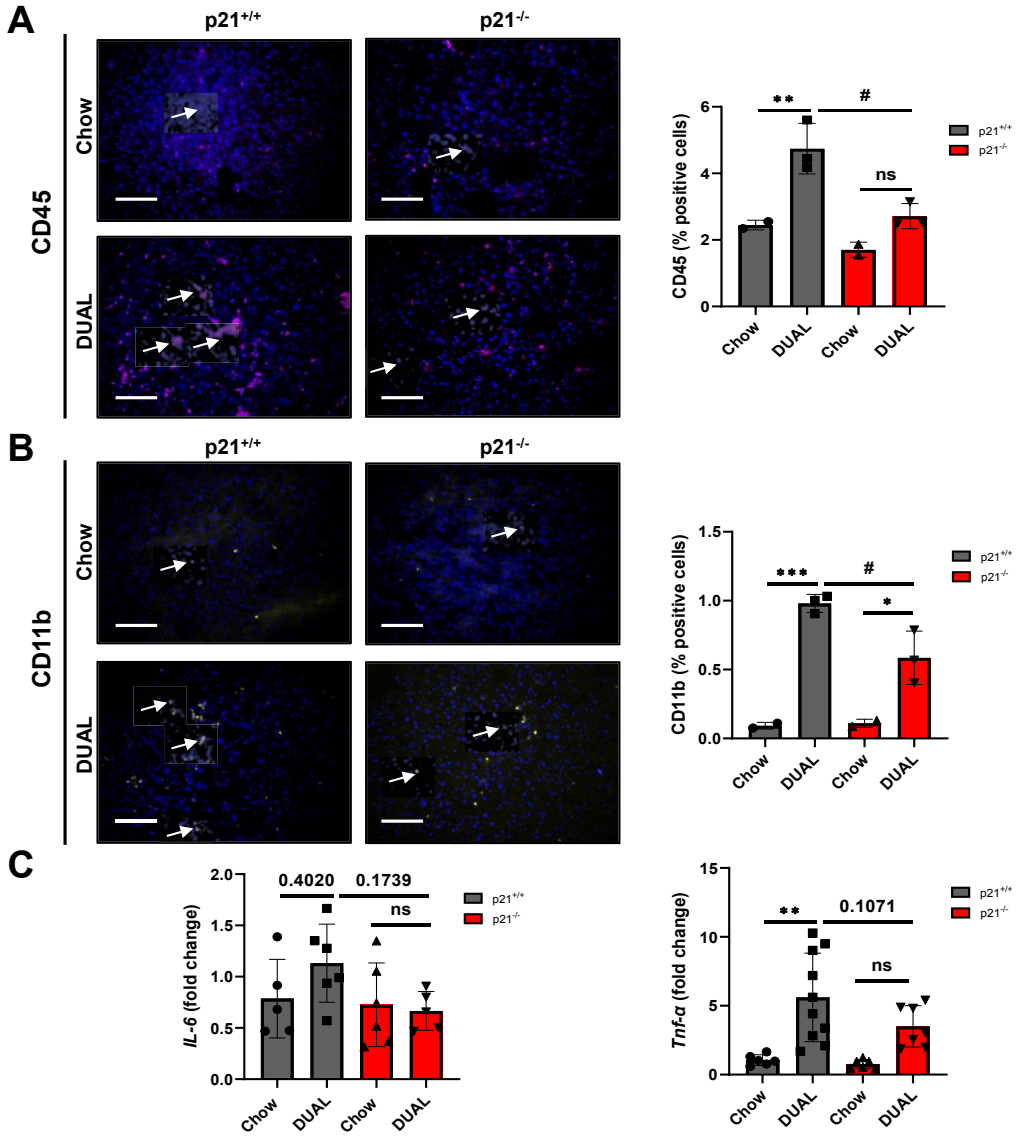

Figure 19. Immune cell infiltration in livers of DUAL-fed mice is increased in wild type (p21$^{+/+}$) mice compared to p21 knockout (p21$^{-/-}$) mice. (**A**) CD45^{+} and (**B**) CD11b^{+} cells immunofluorescence staining and each quantification using ImageJ© software (n = 2-3). (**C**) *IL-6* and *Tnf-α* mRNA relative expression to *Gapdh* in p21$^{+/+}$ and p21$^{-/-}$ mice after a DUAL diet (n = 6-10). Data are expressed as the mean ± SD. Values with distinct superscripts are significantly different from each other assessed by one-way ANOVA, * shows intragroup differences and # intergroup differences (*P < 0.05, **P < 0.01, ***P<0.001, #P < 0.05).

In fact, TNF-α overproduction induces the activation of hepatic stellate cells (HSCs) in the liver [97, 98]. During liver injury, quiescent HSCs differentiate into myofibroblast-like cells and become into an activated state, expressing alpha-smooth muscle actin (α-SMA) [97, 98]. We found a significantly underexpression of α-SMA in the liver of p21$^{-/-}$ mice compared with p21$^{+/+}$ animals after a DUAL diet (**Figure 20A**).

Moreover, quantitative chain reaction revealed that the DUAL diet in p21$^{-/-}$ did not upregulate pro-fibrogenetic genes such as *α-Sma* and *Collagen-1α1* (**Figure 20B, C**).

Activated HSCs are the major source of extracellular matrix (ECM) during fibrosis progression [98, 99]. Accordingly, SR and vimentin staining, clearly revealed that a DUAL diet induces less severe ECM deposition in p21$^{-/-}$ mice (**Figure 20D, E**).

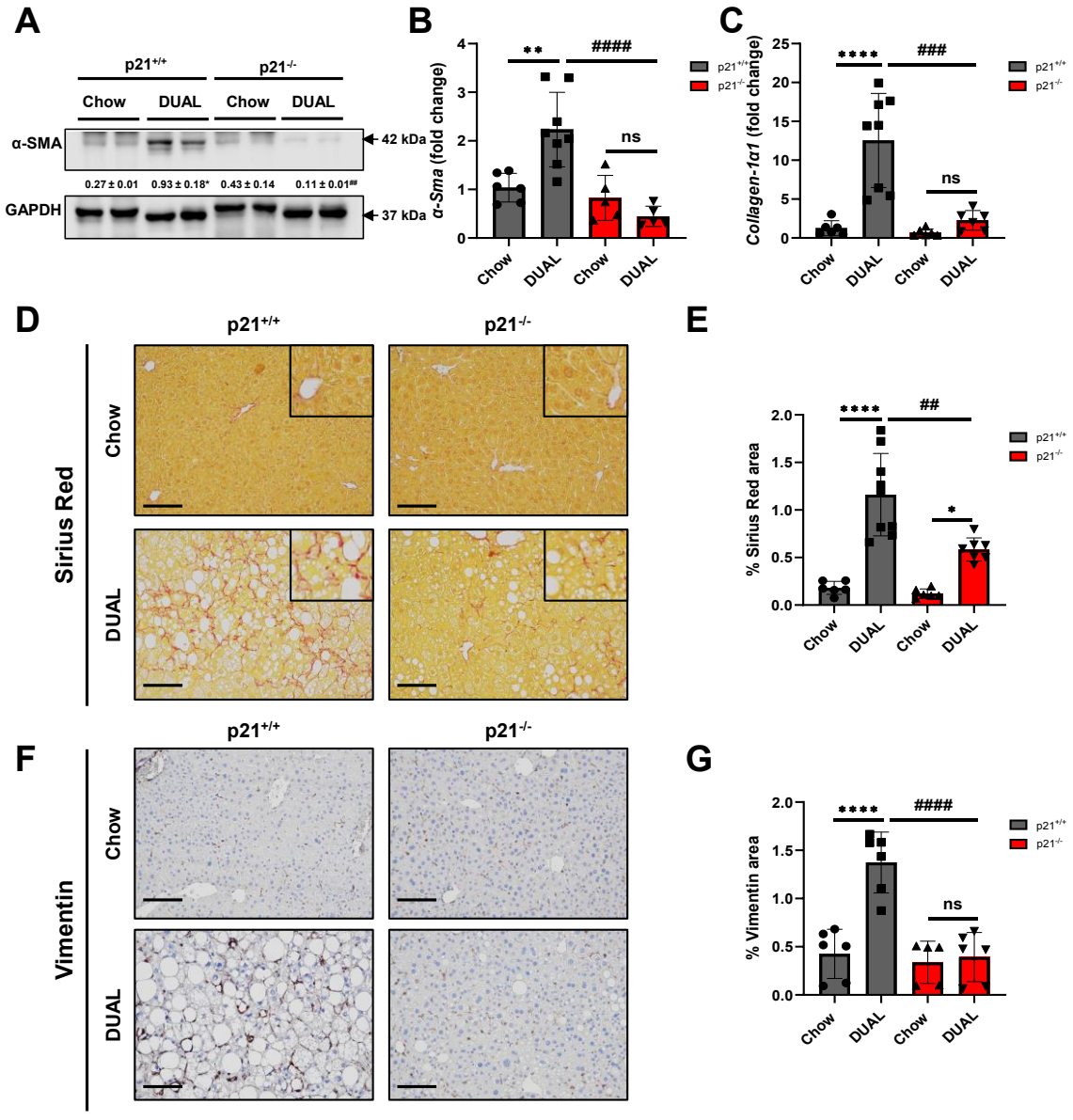

Figure 20. Liver fibrosis is reduced in p21$^{-/-}$ DUAL-fed mice. (**A**) Representative immunoblotting analysis of α-SMA (42 kDa) expression in liver samples of p21$^{+/+}$ and p21$^{-/-}$ mice after a DUAL diet and controls relative to GAPDH (37 kDa). Ratio between α-SMA and GAPDH was calculated. Two individuals' samples from each group are shown as a representative of the group. (n = 4). (**B**) *α-Sma* and (**C**) *Collagen-1α1* mRNA relative

expression in liver determined by qRT-PCR and normalized to *Gapdh* (n = 6-10). (**D**) Paraffin liver sections stained with SR and each quantification. Scale bar = 100 μm. (**E**) Immunohistochemistry of vimentin expressed at 20x magnification in liver samples from $p21^{+/+}$ and $p21^{-/-}$ mice after a DUAL treatment/controls and each quantification. Scale bar = 100 μm. Data are expressed as the mean ± SD. Values with distinct superscripts are significantly different from each other assessed by one-way ANOVA, * shows intragroup differences and # intergroup differences (*P < 0.05, **P < 0.01, ****P<0.0001, ##P < 0.01, ###P < 0.001, ####P < 0.0001).

Altogether, these results show that the absence of p21 in mice exerts a protection in liver in a preclinical model of NAFLD with ALD background (the DUAL diet) in terms of liver injury, steatosis, cell death, inflammation and fibrosis.

7.7 Preclinical ablation of p21 protects against non-alcoholic fatty liver disease (NAFLD)

Since the DUAL preclinical model, that represents the combined synergistic effect of both a WD and persistent alcohol intake, we next examined the role of p21 in each of the factors alone. Thus, a WD was performed during 14 weeks in $p21^{+/+}$ and $p21^{-/-}$ mice (**Figure 6**). Interestingly, macroscopic pictures of the liver and LW, BW and LW/BW ratio showed a significant reduction in $p21^{-/-}$ mice. (**Figure 21A**). Moreover, serum markers of liver damage, such as ALT and AST, were also significantly reduced in $p21^{-/-}$ WD-fed mice compared to $p21^{+/+}$ treated mice (**Figure 21B**). Thus, $p21^{-/-}$ mice display a protection against liver injury in a NAFLD murine model.

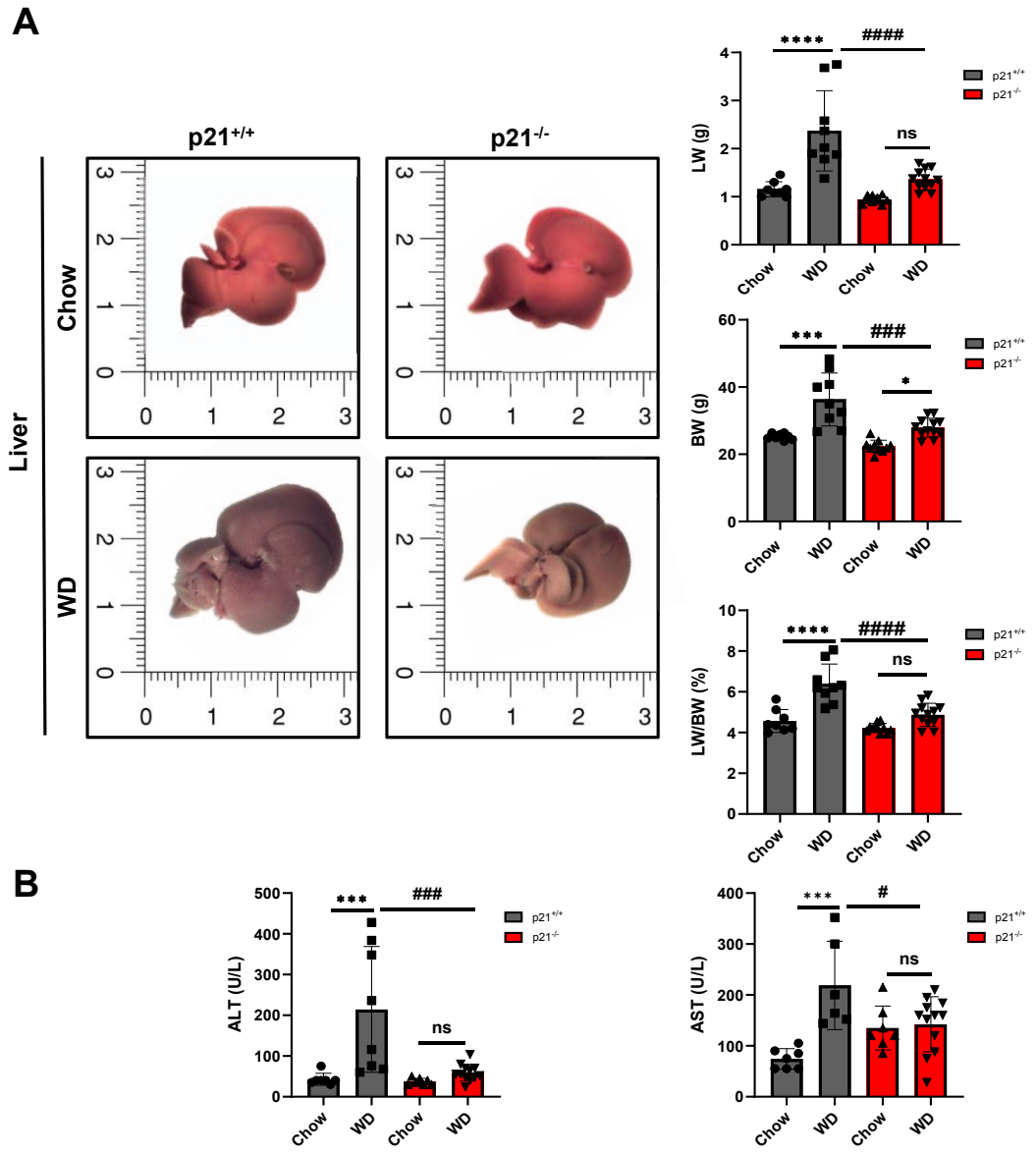

Figure 21. Liver injury was reduced in p21 knockout mice after a WD. (**A**) Macroscopic pictures of livers of $p21^{+/+}$ and $p21^{-/-}$ after a WD and controls. Scale bar was represented in cm (n = 6-10). LW (g), BW (g) and LW/BW ratio (%) (n = 8-12). (**B**) ALT and AST measurement in serum (U/L) of $p21^{+/+}$ and $p21^{-/-}$ WD-fed mice and controls. (n = 7-11). Data are expressed as the mean ± SD. Values with distinct superscripts are significantly different from each other assessed by one-way ANOVA, * shows intragroup differences and # intergroup differences (*P < 0.05, ***P < 0.001, #P < 0.05, ###P < 0.001, ####P <0.0001).

In terms of lipid accumulation in the liver, as we previously described in DUAL-fed mice, a significant reduction in steatosis (**Figure 22A**), TG content (**Figure 22B**) and ORO staining (**Figure 22C**) was observed in $p21^{-/-}$ mice compared to $p21^{+/+}$ mice after a WD treatment.

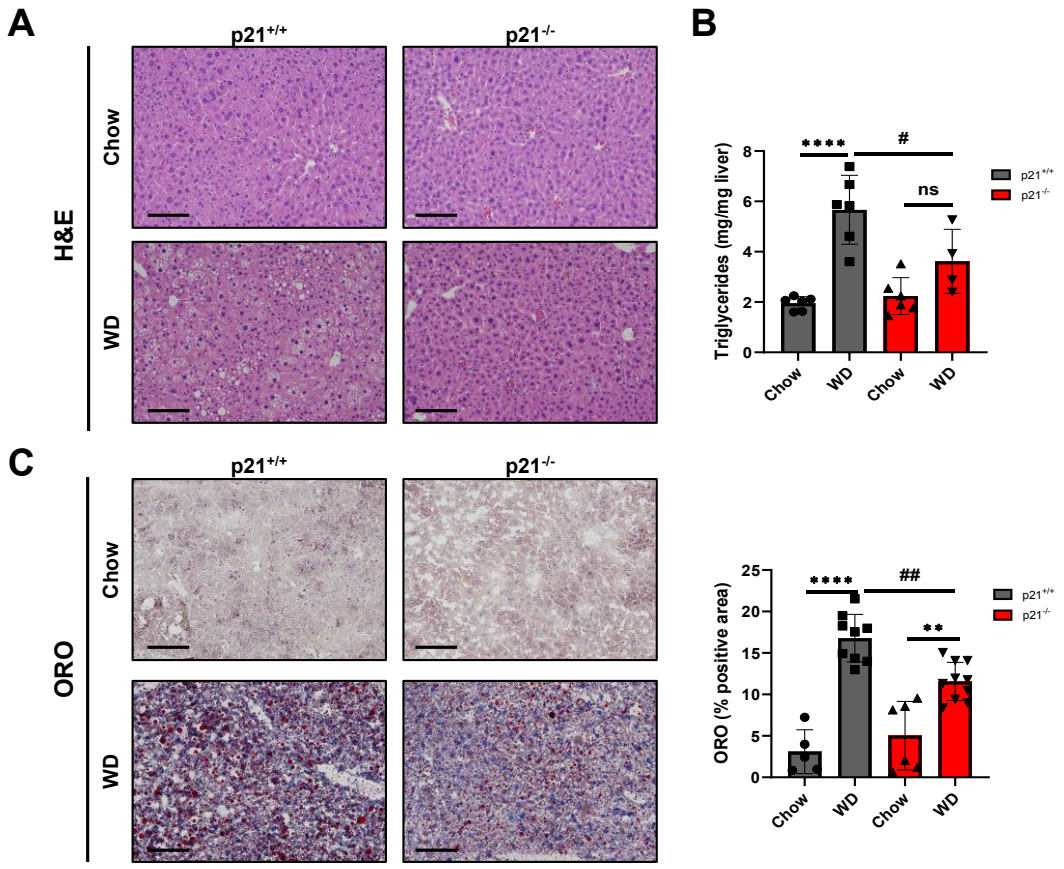

Figure 22. Lipid accumulation in liver after a WD is reduced in $p21^{-/-}$ mice. (**A**) H&E representative images in liver of $p21^{+/+}$ and $p21^{-/-}$ mice after a WD. Scale bar = 100 μm. (n = 5-6). (**B**) Quantification of hepatic triglycerides was done and graphed (n = 5-6). (**C**) Illustrative ORO-stained liver sections from each group. Scale bar = 100 μm. (n = 5-10). Quantification of ORO-stained area (n = 5-10). Data are expressed as the mean ± SD. Values with distinct superscripts are significantly different from each other assessed by one-way ANOVA, * shows intragroup differences and # intergroup differences (**P < 0.01, ****P<0.0001, #P < 0.05, ##P < 0.01).

Moreover, we assess insulin resistance, one of the main characteristics of metabolic syndrome (MetS), using the glucose tolerance test (GTT) in mice after a WD. GTT results in $p21^{+/+}$ animals showed a delay in the glucose uptake after a WD, but no differences were found in $p21^{-/-}$ mice (**Figure 23A**). To note, basal levels of glucose measured in blood were significantly lower in $p21^{-/-}$ mice after a chow diet (**Figure 23B**), indicating that metabolism might be deregulated in this mouse strain.

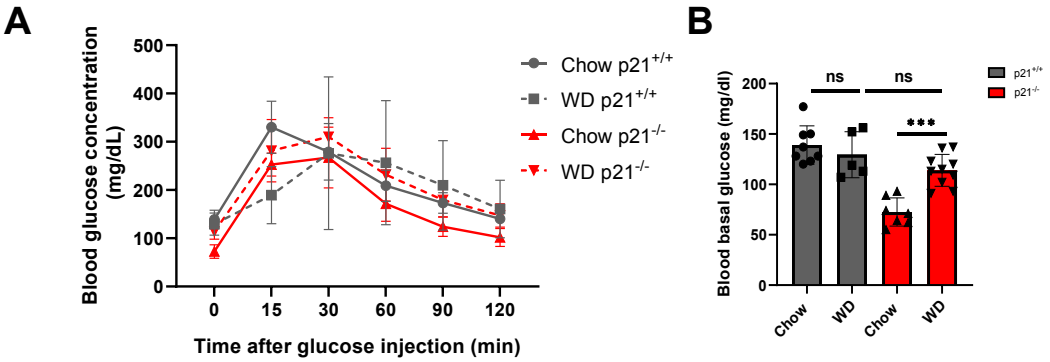

Figure 23. Glucose levels measured in $p21^{+/+}$ and $p21^{-/-}$ mice after a WD and controls. (**A**) GTT test. (**B**) Basal glucose levels in blood after 6h fasting. Data are expressed as the mean ± SD. Values with distinct superscripts are significantly different from each other assessed by one-way ANOVA, (n = 5-10, ***P<0.001).

According to the progression of the liver disease, we evaluated cell death in the liver after a WD. $p21^{-/-}$ mice displayed protection against cell death and a significant reduction in infiltrated cells compared with $p21^{+/+}$ mice after a WD, checked by TUNEL (**Figure 24A**) and CD11b IF (**Figure 24B**) staining, respectively. However, no differences were observed in compensatory proliferation (Ki67) and collagen deposition (SR) after a WD between both genotypes of mice (**Figure 24C, D**).

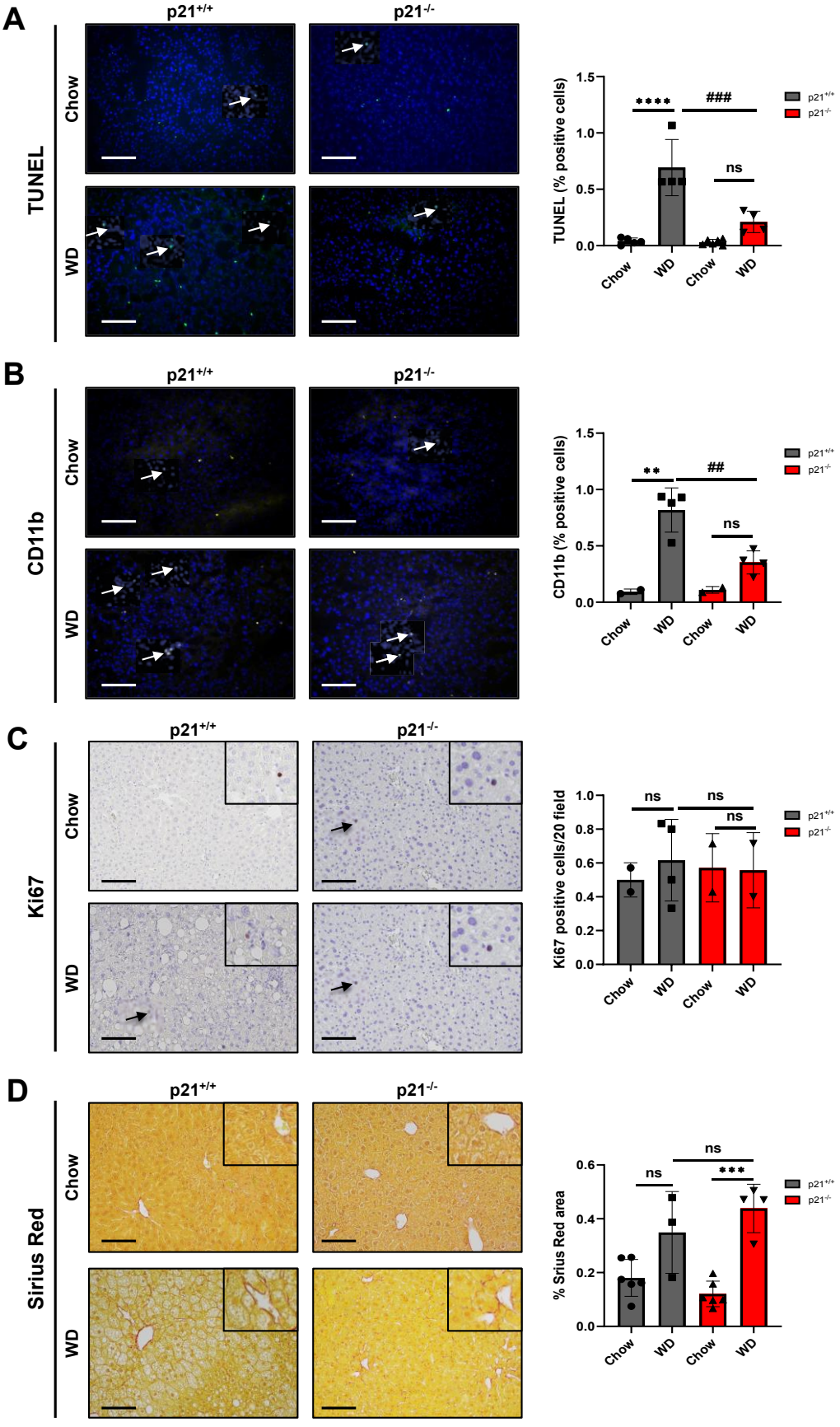
A
p21+/+
p21-/-
Chow
WD
TUNEL
TUNEL (% positive cells)
****
###
ns
p21+/+
p21-/-
Chow
WD
Chow
WD
B
p21+/+
p21-/-
Chow
WD
CD11b
CD11b (% positive cells)
**
##
ns
p21+/+
p21-/-
Chow
WD
Chow
WD
C
p21+/+
p21-/-
Chow
WD
Ki67
Ki67 positive cells/20 field
ns
ns
ns
p21+/+
p21-/-
Chow
WD
Chow
WD
D
p21+/+
p21-/-
Chow
WD
Sirius Red
% Sirius Red area
ns
ns
***
p21+/+
p21-/-
Chow
WD
Chow
WD

Figure 24. Changes in cell death, hepatic proliferation and fibrosis after a WD. (**A**) TUNEL staining was performed in liver cryosections of $p21^{+/+}$ and $p21^{-/-}$ mice and each quantification. Scale bar = 100 µm. (n= 4-6). (**B**) $CD11b^{+}$ cells analyzed using the Image J© software (n = 2-4). (**C**) Representative IHC staining of Ki67 after a WD and controls. Scale bar = 100 µm. Quantification of Ki67 positive cells. (n = 2-4). (**D**) Representative liver images stained with SR. Scale bar = 100 µm. Quantification of positive SR-stained area (%) (n = 3-6). Data are expressed as the mean ± SD. Values with distinct superscripts are significantly different from each other assessed by one-way ANOVA, * shows intragroup differences and # intergroup differences (**P<0.01, ***P<0.001, ****P<0.0001, ##P < 0.01, ###P < 0.001).

Altogether these results from a representative group of mice treated with a WD suggest that the deletion of p21 exhibits a protective effect against the deleterious effect of a diet rich in fat and cholesterol in terms of liver injury, hepatic steatosis, cell death and inflammation.

7.8 p21 knockout mice are not protected against murine alcohol-related liver disease (ALD)

To further explore the relevance of p21 in ALD, we performed an acute-on-chronic Lieber-DeCarli (LdC) diet plus multiple EtOH binges, a modification of the NIAA model [82] (**Figure 7**). No differences were observed between $p21^{+/+}$ and $p21^{-/-}$ mice, showed by macroscopic pictures and LW/BW ratio (**Figure 25A, B**). Furthermore, serum markers of liver damage, such as ALT and AST were increased after EtOH diet in $p21^{+/+}$ and $p21^{-/-}$ mice compared to controls, but no significantly differences were observed between both genotypes of mice (**Figure 25C**).

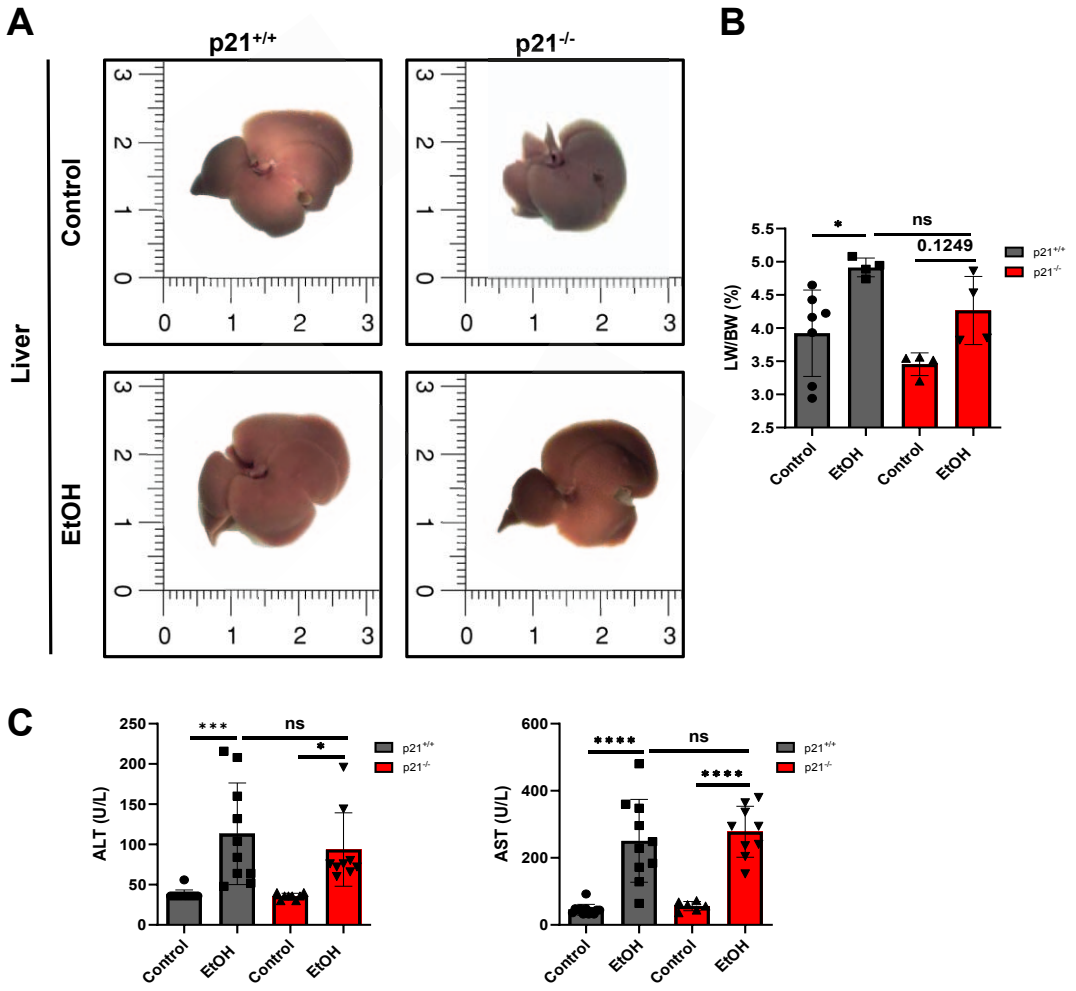

Figure 25. Chronic EtOH diet causes liver injury in p21$^{+/+}$ and p21$^{-/-}$ mice. (**A**) Liver pictures of p21$^{+/+}$ and p21$^{-/-}$ mice after LdC EtOH and control diet. (**B**) Liver weight-to-Body-weight (LW/BW) ratio (%) (n = 4-7). (**C**) ALT and AST measurement in serum (U/L) (n = 7-13). Data are expressed as the mean ± SD. Values with distinct superscripts are significantly different from each other assessed by one-way ANOVA, * shows intragroup differences and # intergroup differences (*P < 0.05, ***P<0.001, ****P<0.0001).

EtOH is metabolized in the liver in the hepatocytes by the cytochrome P450 2E1 (CYP2E1), this upregulation was shown in both genotypes of mice after chronic EOH feeding (**Figure 26A**). CYP2E1 plays a major role in EtOH-induced fatty liver and oxidant stress [100]. Histological analysis of H&E in liver revealed micro and macrosteatosis after EtOH diet in all the groups (**Figure 26B**), as well as significantly increase in hepatic triglycerides (**Figure 26C**) and lipid accumulation tested by ORO staining (**Figure 26D**), but no differences between p21$^{+/+}$ and p21$^{-/-}$ mice were found (**Figure 26B-D**).

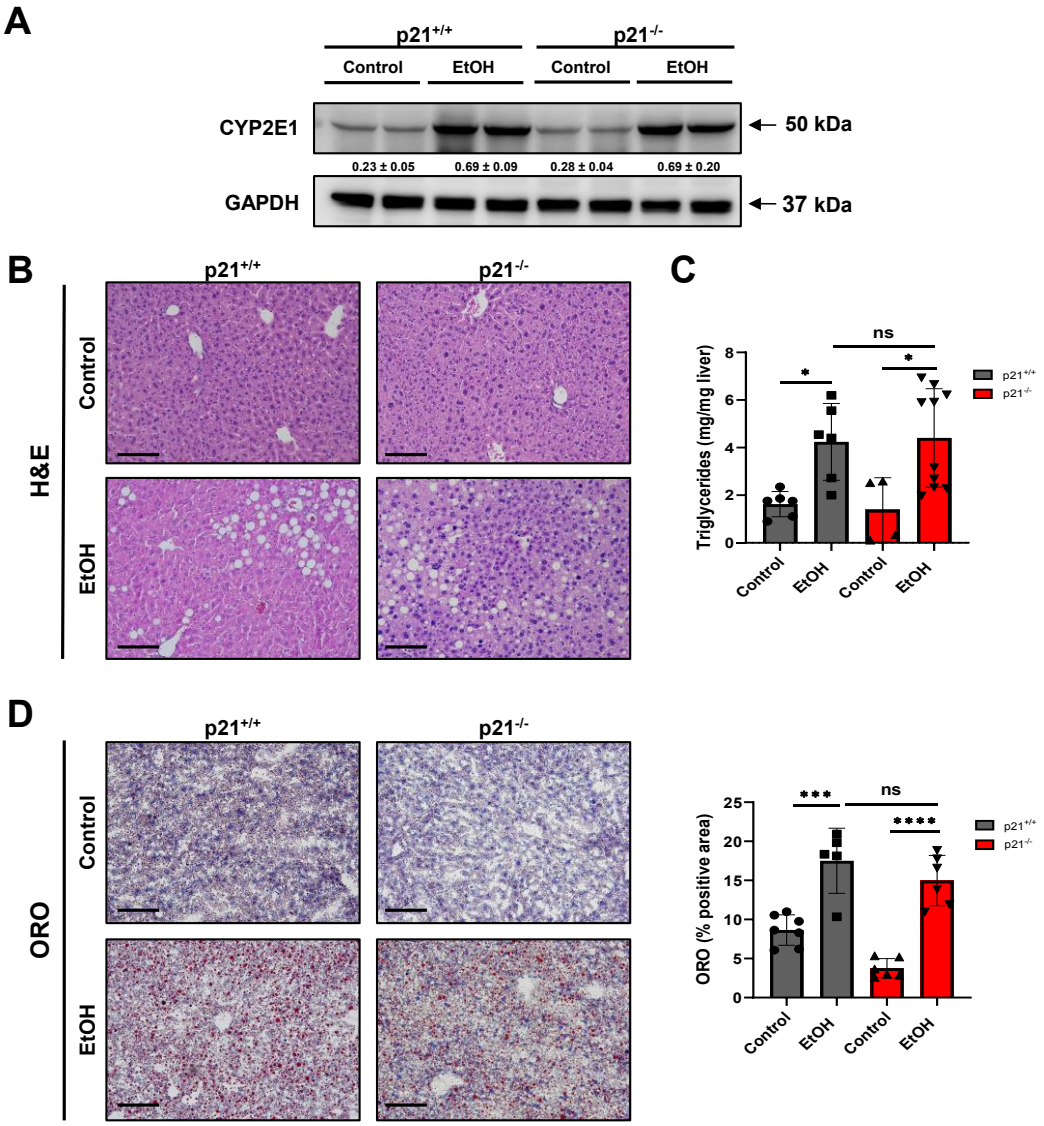

Figure 26. Loss of p21 does not exert a protective effect in liver after a chronic EtOH treatment. (**A**) CYP2E1 immunoblotting assay, GAPDH was used as a loading control. Ratio between CYP2E1 (50 kDa) and GAPDH (37 kDa) was calculated. Two individuals' samples from each group are shown as a representative of the group. (n = 4). (**B**) H&E staining in $p21^{+/+}$ and $p21^{-/-}$ mice after a LdC EtOH/control diet performed in paraffin sections. Scale bar = 100 µm. (n = 8-9). (**C**) Hepatic triglycerides levels expressed as mg/mg liver (n = 4-10). (**D**) ORO staining performed in liver cryosections of $p21^{+/+}$ and $p21^{-/-}$ mice after LdC EtOH and control diet. Scale bar = 100 µm. Quantification of lipid droplets by ORO positive area (%) was done and graphed. Data are expressed as the mean ± SD. Values with distinct superscripts are significantly different from each other assessed by one-way ANOVA, * shows intragroup differences and # intergroup differences. (n = 5-7, *P < 0.05, ***P<0.001, ****P<0.0001).

Alcohol triggers hepatocyte cell death; after chronic EtOH diet, the percentage of TUNEL-positive cells were significantly increased in all the groups and no protection was observed in p21$^{-/-}$ mice (**Figure 27A**). Nevertheless, compensatory proliferation showed by the number of Ki67 positive cells did not change (**Figure 27B**).

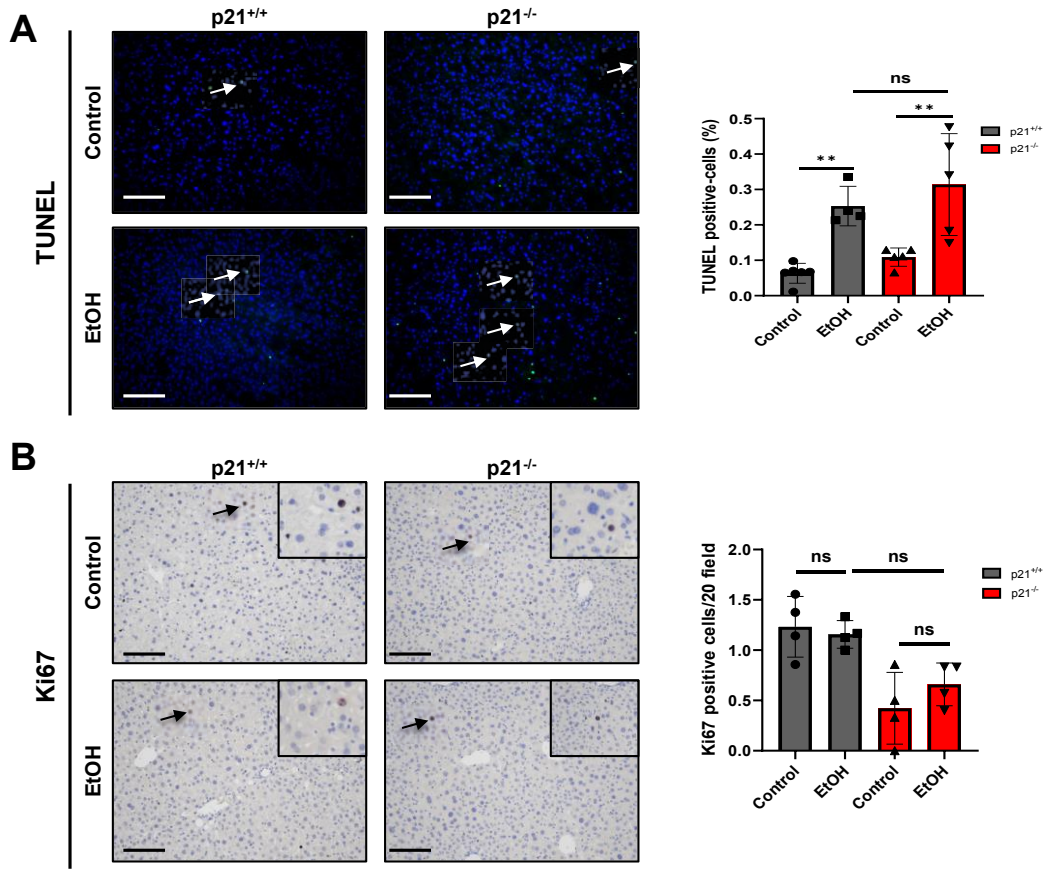

Figure 27. Chronic EtOH consumption causes changes in cell death. (**A**) TUNEL staining was performed in liver cryosections. Quantification of TUNEL-positive cells was done and graphed. Scale bar = 100 μm. (n = 4-7). (**B**) Representative Ki67-stained liver images in p21$^{+/+}$ and p21$^{-/-}$ after a LdC EtOH/control diet and each quantification. Scale bar = 100 μm. (n = 4-6). Data are expressed as the mean ± SD. Values with distinct superscripts are significantly different from each other, assessed by one-way ANOVA (**P < 0.01).

Since immune infiltration and inflammation are characteristic of alcohol induced liver injury, quantification of immunofluorescence staining of CD45^{+} and CD11b^{+} cells (%) showed an increase in p21$^{+/+}$ and p21$^{-/-}$ mice after chronic EtOH exposure (**Figure 28A, B**). Moreover, evaluation of collagen deposition determined an augment in the SR area (%) after treatment in p21$^{+/+}$ and p21$^{-/-}$ mice, while no significant changes were shown between both genotypes of mice (**Figure 28C**).

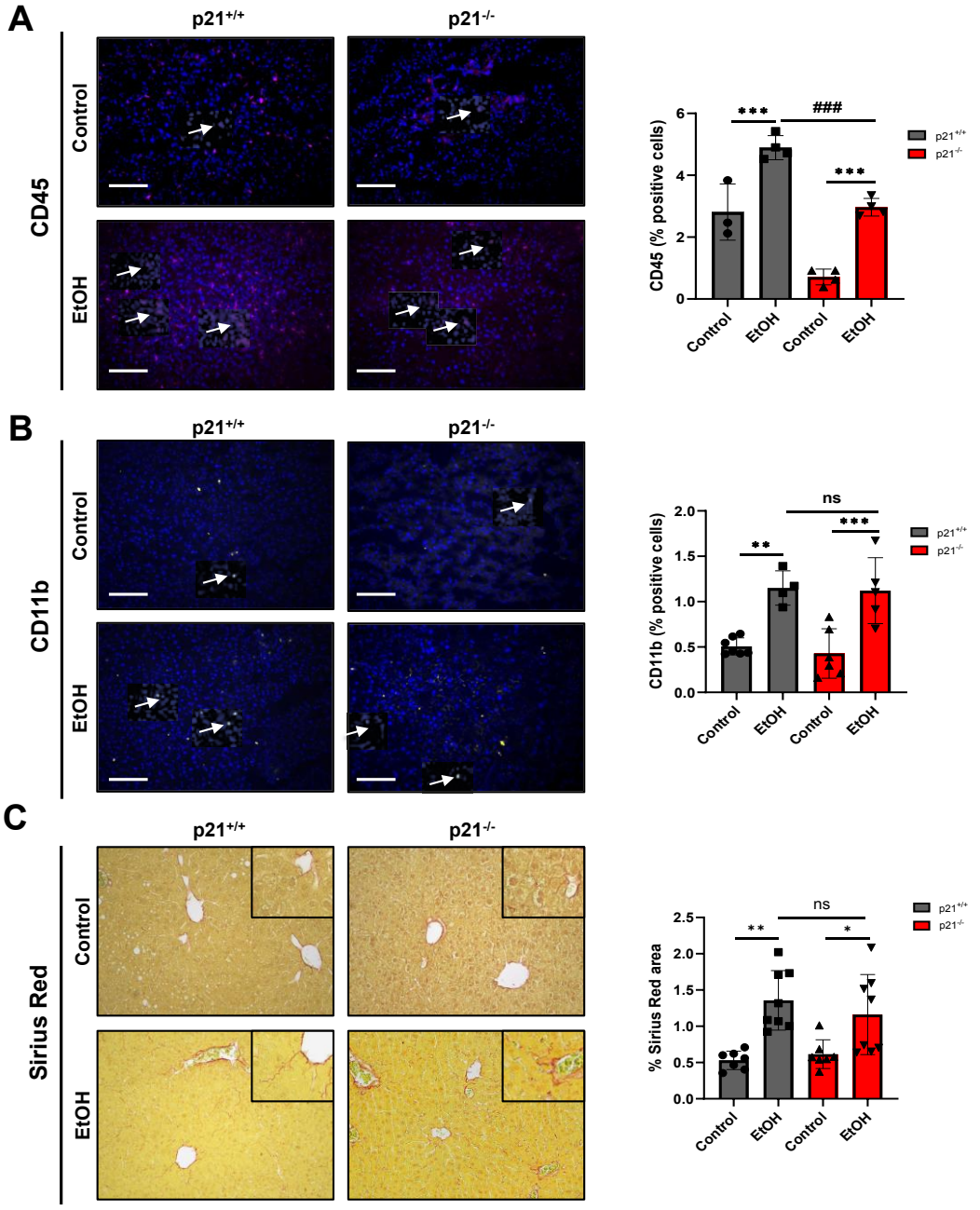

Figure 28. Changes in inflammation and fibrosis after the LdC diet plus multiple binges. Immunofluorescence staining performed in cryosections and quantification of % of $CD45^+$ (**A**) and $CD11b^+$ (**B**) cells analyzed using Image J© software (n =3-5). (**C**) SR staining. Scale bar = 100 µm. Quantification of positive SR-stained area (%). (n = 7-8). Data are expressed as the mean ± SD. Values with distinct superscripts are significantly different from each other assessed by one-way ANOVA, * shows intragroup differences and # intergroup differences (*P < 0.05, **P < 0.01, ***P < 0.001, ###P < 0.001).

In summary, our data indicate that p21 do not play a protective effect in preclinical ALD, tested in a murine model of acute-on-chronic EtOH consumption: the LdC diet plus multiple EtOH binges.

7.9 Lipid balance is deregulated in p21$^{-/-}$ hepatocytes

Additionally, to further investigate the specific cell type involved in the process, primary hepatocytes were isolated from C57BL6/J and silenced p21 expression by siRNA. *P21* mRNA expression and protein levels were tested by qRT-PCR and immunoblotting assays, respectively (**Figure 29A, B**).

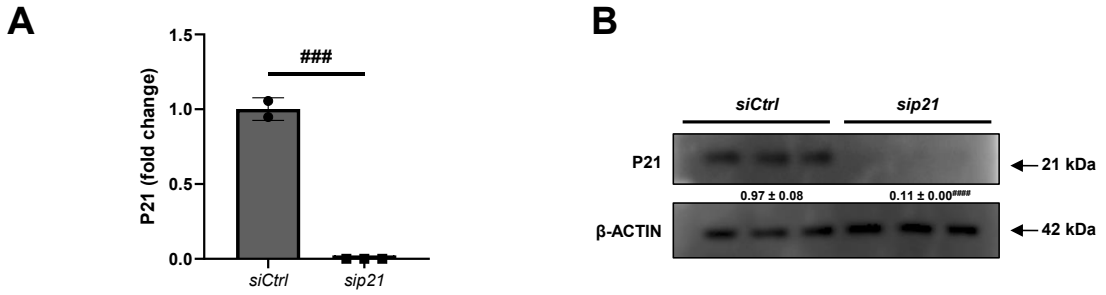

Figure 29. (**A**) *P21* mRNA relative expression to *Gapdh* in *siCtrl* and *sip21* hepatocytes (n = 3). (**B**) Comparative protein expression of P21 (21 kDa) in *siCtrl* and *sip21* hepatocytes by immunoblotting analysis. β-ACTIN (42 kDa) was used as a loading control. Ratio between P21 and β-ACTIN was calculated. (n = 3). Data are expressed as the mean ± SD. Values with distinct superscripts are significantly different from each other assessed by t-test (###P<0.001, ####P < 0.0001).

To initially assess glucose modulation of DNL following alterations in p21, we quantified incorporation of glucose carbons radioactively labeled into lipid fractions of wild type (*siCtrl*) hepatocytes and silenced p21 (*sip21*) hepatocytes, in presence or absence of insulin (in feed and fasting conditions, respectively). Compared with *siCtrl* hepatocytes, the contribution of glucose to DNL was significantly decreased in *sip21* hepatocytes, especially after insulin stimulation (**Figure 30A**).

Hepatic lipogenesis is substantially regulated at the transcriptional level by two transcription factors: the sterol regulatory element-binding protein-1c (SREBP1c) and the carbohydrate response element binding protein (ChREBP), which have an overlapping target genes and mediate the input from insulin and glucose, respectively [101-106]. Thus, we performed measurements in hepatocytes in response to glucose without insulin stimulation. As expected, a substantial decrease in the mRNA abundance of the lipogenic genes, *Srebp1c* and *Chrebp1*, was observed in *sip21* hepatocytes (**Figure 30B, C**). Otherwise, fatty acid oxidation assay performed with ^{14}C palmitate in *siCtrl* and *sip21* hepatocytes revealed an increase in *p21* silenced hepatocytes compared with *siCtrl* hepatocytes, but no significant differences were observed (**Figure 30D**). Besides, ORO

staining pictures of primary hepatocytes isolated from $p21^{+/+}$ and $p2^{-/-}$ mice showed a reduction in the accumulation of lipid droplets in p21 knockout mice compared to wild type mice (**Figure 30E**).

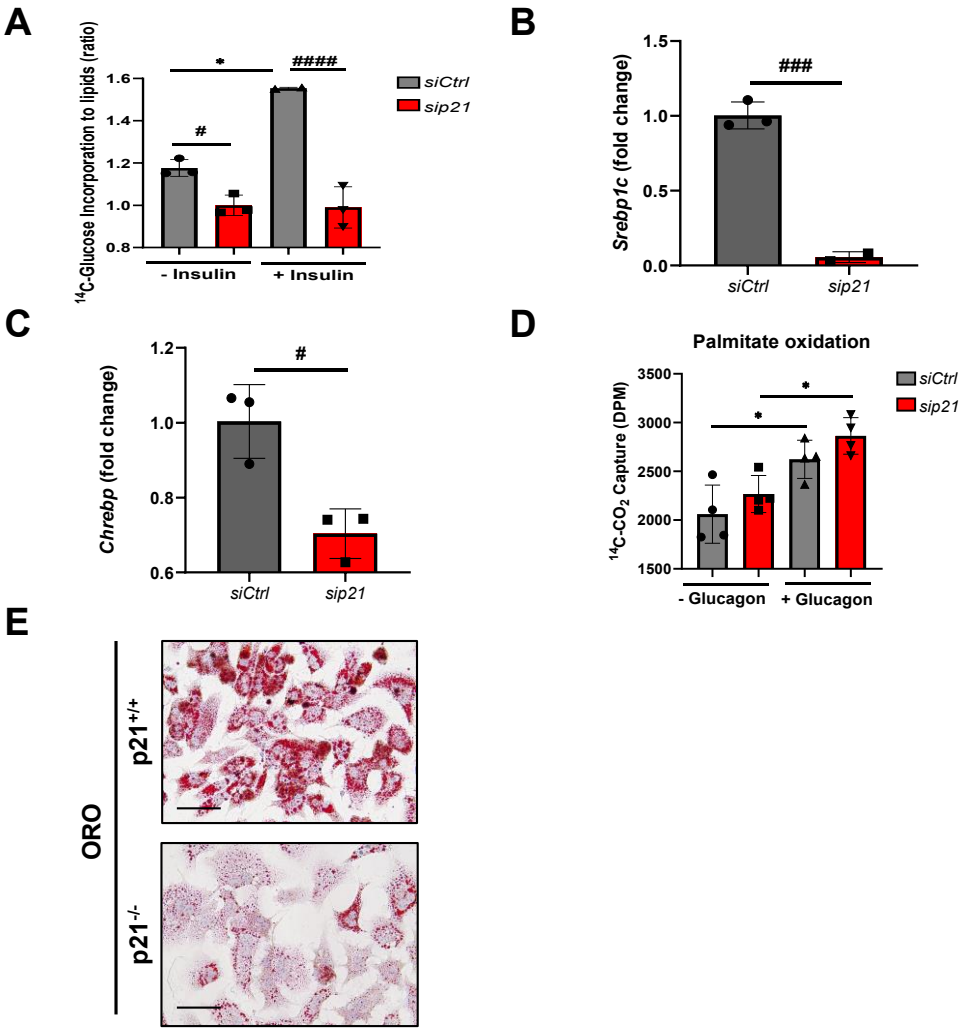

Figure 30. The deletion of p21 in hepatocytes diminished the lipogenesis. (**A**) Incorporation of glucose into lipid fractions of *siCtrl* and *sip21* hepatocytes treated with 0.25 uCi of D-[^{14}C(U)] glucose overnight. Data are presented as ratio of labeled glucose incorporation to lipids (n = 2-3). (**B**) *Srebp1c* and (**C**) *Chrebp1* mRNA relative expression to *Gapdh* in *siCtrl* and *sip21* hepatocytes. (**D**) Palmitate oxidation was quantified by measuring $^{14}CO_2$ production. (n = 4). (**E**) ORO staining performed in primary hepatocytes isolated from $p21^{+/+}$ and $p21^{-/-}$ mice. Scale bar = 50 µm. (n = 3). Data are expressed as the mean ± SD. Values with distinct superscripts are significantly different from each other assessed by one-way ANOVA or t-test, * represents intragroup differences and # shows intergroup differences (*P < 0.05, ***P<0.001, #P < 0.05, ####P < 0.0001).

Additionally, to answer if p21 is also involved in the glucose metabolism in the hepatocyte, we performed a ^{14}C lactate oxidation assay (**Figure 31A**) and a qRT-PCR of mitochondrial phosphoenolpyruvate carboxykinase 1 (mPck1), a relevant enzyme that regulates gluconeogenesis, and results revealed no significant differences between *siCtrl* and *sip21* hepatocytes (**Figure 31B**).

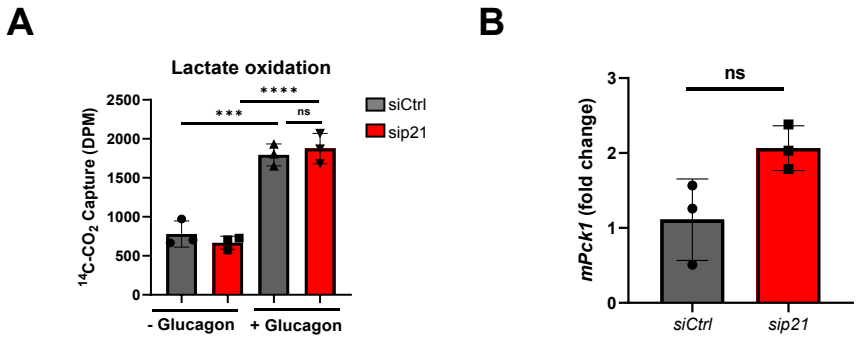

Figure 31. p21 has no effect on glucose metabolism. (**A**) Lactate oxidation was quantified by measuring $^{14}CO_2$ production. (n = 3). (**B**) *mPck1* mRNA relative expression to *Gapdh* in *siCtrl* and *sip21* hepatocytes (n = 3). Data are expressed as the mean ± SD. Values with distinct superscripts are significantly different from each other, assessed by one-way ANOVA or t-test (***P < 0.001, ****P < 0.0001).

7.10 Loss of p21 exacerbates the tumorigenesis progression in mouse livers

Hepatocellular carcinoma (HCC) is the end-stage of chronic liver disease. Therefore, we investigated the role of p21 in tumor initiation and progression using a mouse model of low latency HCC, the Alb-*Myc*^{tg} mice. We generated the double mutant Alb-*Myc*^{tg}/p21$^{-/-}$ mice and followed the progression of CLD and HCC development (**Figure 8**). To select the correct genotype of mice for the study, we performed an electrophoresis in agarose gel of the DNA extracted from the tail. The *P21*$^{+}$ allele was detected in agarose gel electrophoresis as a 208 bp DNA fragment, whereas the *P21*$^{-}$ allele was shown as 317 bp DNA fragment. Expression of Alb-*Myc*^{tg} transgene was observed as a 350 bp (**Figure 32A**). Moreover, *P21* mRNA expression was tested in liver of both mouse strains (**Figure 32B**).

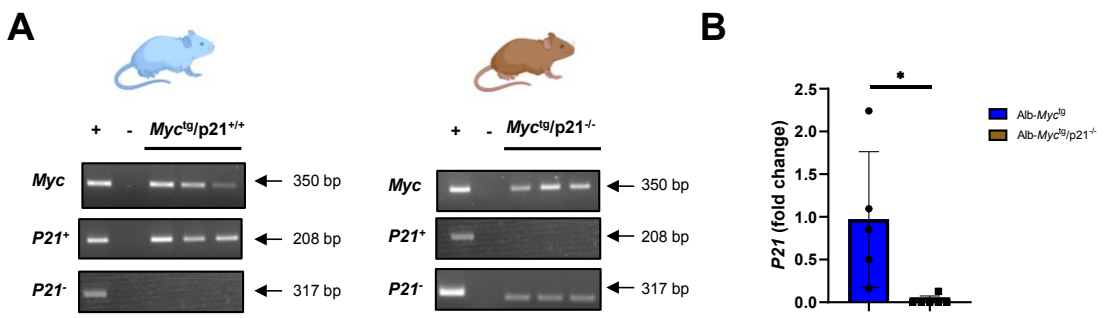

Figure 32. Confirmation of *Myc* overexpression and *P21* deletion in mice. 2% agarose gel showing the genotyping PCR result from mice tails of Alb-*Myc*^{tg} and Alb-*Myc*^{tg}/p21$^{-/-}$ mice. *Myc*^{tg} appears in 350 bp, *P21*$^{+}$ band in 208 bp and *P21*$^{-}$ is shown at 317 bp. Positive and negative controls were included in the gel. (**B**) *P21* mRNA expression measured in liver of p21$^{+/+}$ and p21$^{-/-}$ mice relative to *Gapdh*. Data are expressed as the mean ± SD. Values with distinct superscripts are significantly different from each other, assessed by t-test (n = 5-6, *P < 0.05).

At 1 year of age, livers of Alb-*Myc*^{tg}/p21$^{-/-}$ mice became enlarged and nodules were observed in the surface of the liver. As expected, LW/BW ratio was significantly increased in Alb-*Myc*^{tg}/p21$^{-/-}$ mice compared to Alb-*Myc*^{tg} mice (**Figure 33A**). According to serum transaminases, there is a significant increase in the levels of ALT and there is a tendency to increase in AST levels (**Figure 33B**). H&E and SR staining exhibited hepatocytes atypia and extensive collagen deposition in Alb-*Myc*^{tg}/p21$^{-/-}$ mice (**Figure 33C**).

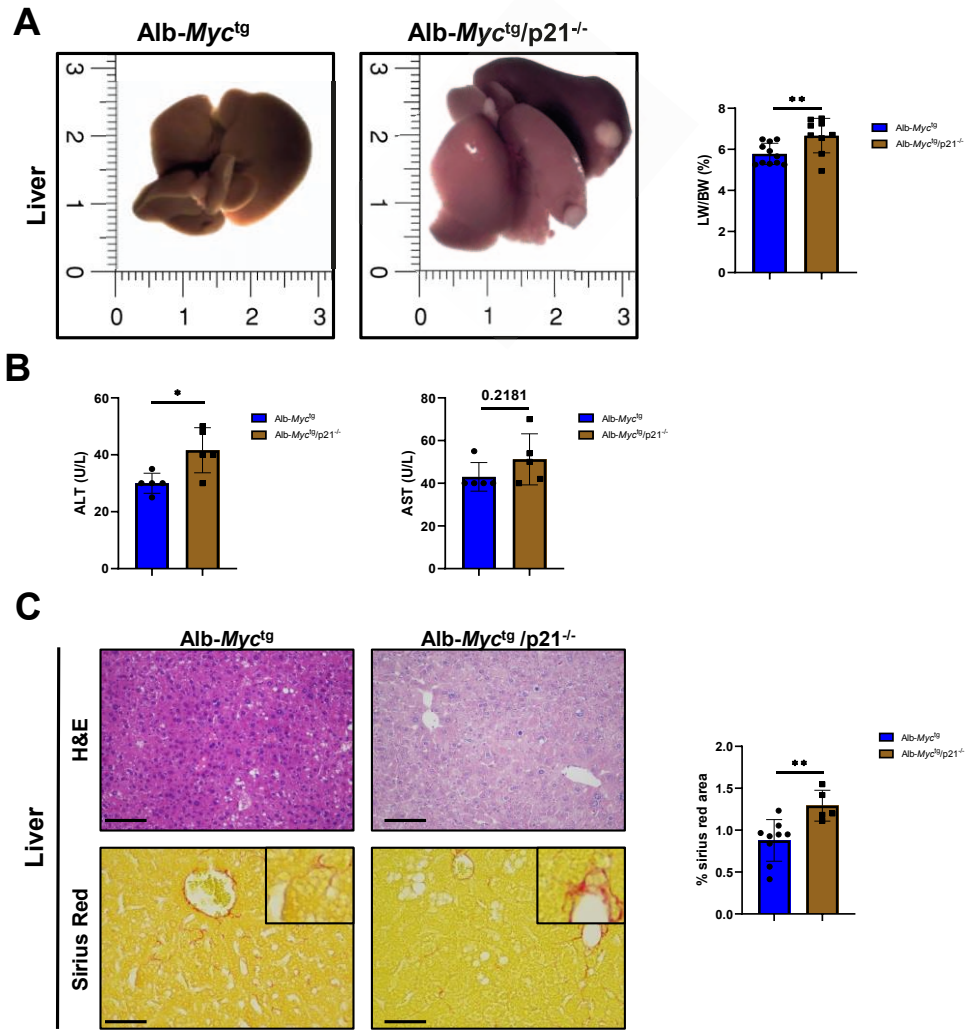

Figure 33. Loss of p21 exacerbates the phenotype in a liver cancer mouse model. (**A**) Macroscopic liver of Alb-*Myc*^{tg} and Alb-*Myc*^{tg} /p21$^{-/-}$ 52 weeks old mice. Scale bar in cm. Liver weight-to-body weight (LW/BW) ratio (%). (n= 9-11). (**B**) ALT and AST levels (U/L) (n = 6-7). (**C**) Representative liver images stained with H&E and SR. Scale bar = 100 µm. Quantification of positive SR-stained area (%) (n = 6-10). Data are expressed as the mean ± SD. Values with distinct superscripts are significantly different from each other, assessed by t-test (*P < 0.05, **P < 0.01).

Notably, we detected glutamine synthetase (GS) and cytokeratin 19 (CK19) positive staining liver of Alb-*Myc*^{tg}/p21$^{-/-}$ mice, a broadly used marker of HCC, also showing a pretumor area indicated by arrows. Besides, mRNA expression of *Ck19* has a tendency to increases in 52 weeks old Alb-Myc^{tg}/p21$^{-/-}$ animals (**Figure 34A**). Livers exhibit no differences in TUNEL staining and Ki67 positive cells between both groups of mice (**Figure 34B**). Consistently, *P53* mRNA expression was augmented in the liver

tissue of double mutant Alb-*Myc*^{tg}/p21$^{-/-}$ mice, a well-known tumor suppressor that regulates p21 (**Figure 34C**).

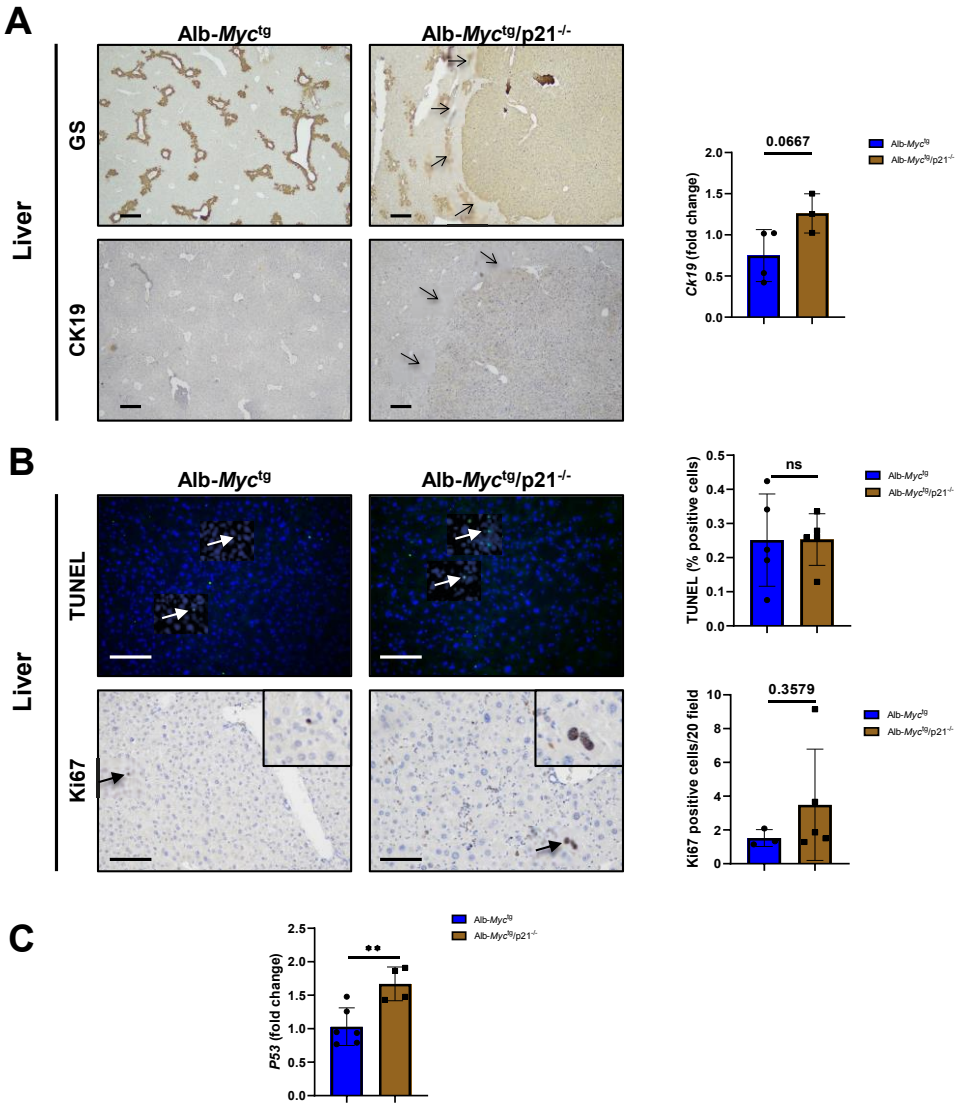

Figure 34. p21 deletion accentuates liver cancer. (**A**) GS and CK19 (IHC) staining of 52 weeks old Alb-*Myc*^{tg} and Alb-*Myc*^{tg}/p21$^{-/-}$ mice livers. Scale bar = 100 µm. (n = 6-7). *Ck19* mRNA expression determined by qRT-PCR and normalized to the amount of *Gapdh* in liver (n = 6). (**B**) TUNEL (IF) and Ki67 (IHC) staining performed in liver of Alb-*Myc*^{tg} and Alb-*Myc*^{tg}/p21$^{-/-}$ mice after 52 weeks old and each quantification. Scale bar = 100 µm. (n = 3-6). (**C**) *P53* mRNA expression determined by qRT-PCR and normalized to the amount of *Gapdh* in liver (n = 6). Data are expressed as the mean ± SD. Values with distinct superscripts are significantly different from each other, assessed by t-test (**P < 0.01).

These results indicated that loss of p21 exacerbates liver tumorigenesis, since one year old Alb-*Myc*^{tg}/p21$^{-/-}$ mice exhibit an increase in liver damage, cell proliferation, fibrosis and HCC markers.

DISCUSSION

8. Discussion

The increasing prevalence of chronic liver disease has been noted in recent times, being NAFLD [107, 108] and ALD two of the chief etiologies [109, 110]. According to the World Health Organization (WHO), in 2018, more than 3 million deaths every year are attributed to alcohol consumption [111]. Excessive alcohol consumption used to be a leading cause of CLD and accounts up to 60-80% of liver-related mortality in Europe [112]. Data from the WHO indicated that, in Spain, the average of pure alcohol consumption per capita in people over 15 years of age was 10 L between 2015 and 2017. However, this data was reduced 0.5 L compared to the period of 2009-2011, whereas in the last decade the pattern of binge drinking has increased threefold [113, 114].

Nowadays, a predominant sedentary lifestyle particularly in developing countries with low levels of physical activity and dietary habits based on the excess calorie intake contributes to increase the prevalence of NAFLD. Additionally, the current global epidemic of obesity and type 2 diabetes (T2DM) accentuate the present problem, causing a major health and burden of disease to the society [115, 116]. Studies indicated that in 2016 there were about 52 million people diagnosed with NAFLD in France, Germany, Italy and UK [117]. In Spain, as in most of Europe, NAFLD is highly prevalent with an approximate rate of 25.8 % in people between 15-85 years of age [118]. Notably, a modelling study forecasted calculated that this prevalence would increase by 21% from 2016 to 2030 and the NASH prevalence would increase by 49 % in the same period [119, 120].

Furthermore, it is frequent the coexistence of obesity, T2DM and alcohol consumption in the same individual, and nowadays, these individuals are underdiagnosed. Epidemiological studies in a large cohort of patients determined that obese patients with alcoholism have 2-3 times higher risk of developing steatohepatitis and progression to fibrosis or cirrhosis [121-124]. Thus, obesity and alcohol have a synergistic effect increasing the risk of incident HCC [125, 126].

Several genetic studies in mice confirmed the ability of p21 to delay tumor development in liver. However, lately it has become clear that p21 functions are far more complex than initially thought. Data from The Cancer Genome Atlas (TCGA) database revealed a significant reduction in *P21* transcripts in primary tumors of HCC patients compared to healthy tissue. *In vivo* models of acute and chronic liver injury showed that

p21 can regulate hepatocyte proliferation, controlling the rate of progression through G1 phase of the cell cycle in the regenerating liver [127-129]. A study in rats chronically fed with EtOH exhibited an inhibition in liver regeneration after partial hepatectomy, that correlated with upregulation of p21 and p27 in liver cell nuclei [130]. Moreover, patients diagnosed with AH revealed increased expression of p21 and arrest of cell cycle progression [131].

Recently, several studies demonstrated that there is a close association between increased expression of p21 and NAFLD, showed in animal models of obesity [132, 133] and in NAFLD patients [95, 134, 135], as a marker for prediction of adverse liver-related outcome [135]. Concomitant, our studies in wild type mice showed an increased in the mRNA transcripts and protein levels of p21 in a model of NAFLD alone (WD) and in combination with alcohol consumption (DUAL diet) [80]. Additionally, clinical results in obese patients, NAS ≤ 2 score, from the Spanish cohort from the Arrixaca University Hospital (Murcia, Spain) determined a trend towards increased expression of *P21*.

Therefore, p21 could be a target for drug development and therapy of CLD. Nevertheless, up to now, the role of p21 in the context of the CLD has been poorly addressed, and essential questions are still open. In the present study, we explored the role of p21 in CLD, specifically in NAFLD and NAFLD with ALD background.

The prominent proximal event of NAFLD is the accumulation FFAs in the liver. The liver gets FFAs primarily from three sources: FFA uptake from the circulation, DNL and dietary lipids that constitute around 15% of TG in the liver [136]. $p21^{-/-}$ mice do not exhibit a reduction of triglycerides in serum, as well as do not evidence an increase in the transcription of lipogenic enzyme genes, such as *Fas* after a DUAL diet. Evidence in H&E and ORO staining of reduced lipid accumulation in the liver of $p21^{-/-}$ mice were observed, supported by the triglycerides content in liver and *Pparγ* and *Cd36* gene expression related to FA uptake after. Clinical trials indicated that patients with NAFLD/NASH treated with PPARγ agonists manifested a liver response apart from the one in adipose tissue, reducing hepatic steatosis [59]. Moreover, β-oxidation evinced by the gene expression of *Pparα*, which is a mechanism for FFA disposal in the liver [60], is not reduced in $p21^{-/-}$ mice after the DUAL diet. This phenomenon was associated with the expression of FXRs. FXR signaling has several pleiotropic functions on various metabolic pathways, including the reduction of FFA enhancing the β-oxidation via PPARα [137, 138] as we demonstrated in our results with the mRNA expression of *Fxr1*. It is well accepted that NAFLD patients exhibit an elevated lipolysis and high circulating

FFA levels [139]. Therefore, our results were in consistence with the lipotoxic effect of p21 on free fatty acid-induced steatosis tested in L02 cells [140].

When FFA disposal mechanisms are overwhelmed, ROS are generated triggering lipotoxicity. One of the main intracellular sources of ROS is the cytochrome P450 metabolism [141], which is augmented after a DUAL diet. ROS also interacts with polyunsaturated FAs (PUFAs) resulting in lipid peroxidation and formation of 4-HNE [141], leading to DNA damage and H2AX phosphorylation [93]. Previous studies determined that 4-HNE can increase p21 in CYP2A5 knockout mice [142]. In concordance, our results revealed that 4-HNE levels in $p21^{-/-}$ animals are reduced. Endogenous intracellular sources of ROS contribute to disease progression in NAFLD [141]. This is consistent with an *in vitro* study that demonstrates that incubating hepatocytes with FFA increases their ROS formation [143]. Additionally, several animal models of NAFLD have provided persuasive evidence that ROS-mediated lipid peroxidation occurs [144, 145].

Oxidative stress contributes to the progression of NAFLD by inducing hepatic inflammatory cytokines. ROS along with products of lipid peroxidation result in increased release of numerous cytokines, such as TNF-α, which plays a key role in cell death, inflammation and fibrosis. *In vitro* and *in vivo* experiments have demonstrated the key role of liver cell death in NAFLD. Liver cell damage, liver cell death, inflammation and oxidative stress, the principal pathogenic features of NAFLD, are interrelated [146, 147]. Moreover, our data evidence a reduction in cell death in $p21^{-/-}$ mice after a DUAL diet, showing a reduction in TUNEL-positive cells and a downregulation of apoptotic (CC-3 and CC-8) and necroptotic (pRIPK1, pRIPK3 and pMLKL) markers. Studies have determined that using RIAP-56, a potent inhibitor of RIPK1, improves the histological characteristics of NAFLD in HFD mice through MLKL, reducing liver inflammation, fibrosis and liver lipid accumulation. Its mechanism may involve ameliorating mitochondrial dysfunction and promoting β-oxidation [148]. Additionally, Saeed *et al.* found that patients with NAFLD exhibited increased MLKL levels compared to the non-NAFLD group and that $MLKL^{-/-}$ mice induced with a high-fat diet showed decreased transferase levels, triglycerides, NAFLD activity scores, steatosis score, inflammation, balloon degeneration, and expression of DNL genes in the liver [149]. Proliferation in $p21^{-/-}$ mice after a DUAL diet is not augmented as expected. These results are in contraposition to previous studies that revealed a significant increase in liver proliferation when p21 is not present in HepG2 cells [150]. However, this discrepancy could be

explained by the compensatory upregulation of other CDKs inhibitors to the loss of p21, such as p16 [151].

CyclinD1 is involved in activating hepatocyte proliferation, restoring liver mass after partial hepatectomy [152]. According to the levels of *CyclinD1* in $p21^{-/-}$ mice and this assumption, liver proliferation measured by Ki67 staining was not activated in $p21^{-/-}$ mice after a DUAL diet. Moreover, recent data suggest that p21 may also exhibit oncogenic properties and induce proliferation of cancer cells by promoting the assembly of D-cyclins or by inhibiting apoptosis and inducing growth and prosurvival signals [153, 154].

In relation with the progression of NAFLD, HSCs play a crucial role. Activation of HSCs involve upregulation of various genes, including *α-Sma* and *Collagen-1α*. In our study, α-SMA levels and collagen deposition are reduced in $p21^{-/-}$ mice after the DUAL diet. Remarkably, recent studies with a big cohort of alcoholic patients showed the striking relationship between increased hepatocyte p21 expression and both fibrosis stage and liver outcome [155].

To further investigate the relevance of p21 in NAFLD, we treated mice with a WD for 14 weeks. $p21^{-/-}$ mice after a WD also displayed a protective effect against liver damage markers (ALT and AST), LW/BW ratio, lipid accumulation (ORO staining and hepatic triglycerides) and cell death (TUNEL staining). Additionally, $p21^{-/-}$ mice do not exhibit alterations in the glucose levels in blood after a WD checked by GTT. In patients diagnosed with NASH, the hepatic expression level of p21 is significantly higher than in patients with simple steatosis, moreover p21 expression in hepatocytes predicted adverse liver-related outcome [29, 30], and impaired hepatocyte replication by p21 expression correlates with insulin resistance and inflammatory activity [95, 134]. Hence, our findings provide a link between p21 and NAFLD in mice.

However, chronic EtOH feeding in mice does not increase the expression of p21. Our findings are in sharp contrast with Aravintan and colleagues' observations in two cohorts of ALD patients related the hepatocyte p21 expression with both, fibrosis stage and an adverse liver-related outcome [155]. However, this controversy between mouse models and patients could be explained by the exclusion of alcohol consumption in NAFLD patients. Regarding this problem, experts proposed a new term metabolic-associated fatty liver disease (MAFLD) that shifts the focus towards inclusive diagnostic criteria, the presence of metabolic abnormalities, rather than the absence of excessive alcohol intake. It also avoids competition between a diagnosis of ALD and NAFLD,

recognizing their synergistic effects on the liver [141]. The Lieber-DeCarli diet plus multiple EtOH binges performed in $p21^{+/+}$ and $p21^{-/-}$ mouse lines revealed that the lack of p21 does not exert a protective effect against ALD in mouse livers. p21 knockout mice showed liver damage (ALT, AST), increased levels of lipids in liver (ORO, liver triglycerides), cell death (TUNEL staining), inflammation (CD45 and CD11b positive cells) and liver fibrosis (SR) after a chronic EtOH diet, as well as it was observed in $p21^{+/+}$ mice.

To further investigate our findings, we focused on deciphering the cell type involved in the p21 protection against NAFLD. Ow and collages determinate that mice in which hepatocytes lack CDK1 develop metabolic disease [156]. Additionally, studies in L02 cells treated with free fatty acids revealed that p21 plays a role in lipid metabolism in hepatocytes [140]. So far, we isolated primary hepatocytes from mice (wild type and mutants) and functional assays were performed with *sip21*. ^{14}C assays results and *Srebp1c and Chrebp* mRNA expression in *sip21* primary hepatocytes indicate that the deletion of p21 in the hepatocyte has an effect in the reduction of lipogenesis and a tendency to increase in fatty acid oxidation, whereas glucose metabolism was not affected. Moreover, lipid accumulation measured by ORO staining in $p21^{-/-}$ primary hepatocytes were diminished compared to $p21^{+/+}$ primary hepatocytes.

Hence, for the first time, our findings provide a link between p21 and lipogenesis in hepatocytes. Our results are consistent with previous studies in primary hepatocytes of rat and AML12 mouse hepatocytes cells siRNA-mediated knockdown of *CylincD1*, where *de novo* lipogenesis was repressed as well as lipid catabolism; indicating that CyclinD1 is necessary and sufficient to promote accumulation of lipid droplets in proliferating hepatocytes [157].

Moreover, human studies determined that p21 is up-regulated during inflammation and fibrosis in CLD, and high p21 expression is linked with hepatocellular carcinoma (HCC) in chronic patients [158]. p21 expression associated with fibrosis stage and an adverse liver-related outcome in ALD patients [155].

Our results showed that the deletion of p21 in a cancer murine model exacerbates HCC. Alb-Myc^{tg}/$p21^{-/-}$ mice after 52 weeks old evidence liver damage (ALT), fibrosis (SR staining), such as a pretumor area that is not evident in Alb-Myc^{tg} mice (GS and CK19 staining). Moreover, the mRNA expression of the tumor suppressor *p53* is augmented in double mutant animals. Therefore, lack of p21 may exacerbates HCC. Our results are in

concordance with Ehedego *et al.* studies. They observed a protective effect of p21 against DNA damage, an acceleration of hepatocarcinogenesis and cholestasis in NEMO$^{\Delta hepa}$ animals, as well as an upregulation of p53 in NEMO$^{\Delta hepa}$/p21$^{-/-}$ mice [90].

A great plethora of literature determined that p21 is often deregulated in human cancers. First, it was firmly believed that p21 opposed to liver tumor development [90, 127, 129, 159, 160]. Recently, it has become clear that p21 has more complex functions than initially thought. Abbas and Dutta [39, 40, 161] described that p21 promotes or inhibits tumorigenesis depending on the cellular context, being a tumor suppressor or an oncogene [39, 40, 161].

In summary, in the present work, we show that p21 plays a crucial role in CLD, especially in NAFLD and NAFLD with ALD background. p21 deletion exerts a protective effect against liver damage in a DUAL diet and a WD mouse models. Whereas, the lack of p21 do not exert a protective effect in mice after a chronic EtOH diet (the Lieber-DeCarli diet plus multiple EtOH binges model). Moreover, we assumed that p21 may play a role in lipid metabolism in the hepatocyte. According to this hypothesis, a critically downregulated expression of p21 decreases lipogenesis in the hepatocyte. Mirroring this, our study demonstrated that p21$^{-/-}$ mouse line has less lipid vacuoles, decreases TG content, decreases expression of lipogenesis genes and consequently a diminution in liver damage, cell death and progression to fibrosis after a DUAL diet. We postulate that p21 affects lipid metabolism in the hepatocyte, mainly the lipogenesis. Related to HCC, the lack of p21 has a deleterious effect (52 weeks old Alb-*Myc*^{tg}p21$^{-/-}$ mouse model). (**Figure 35**). With these findings, our study proposes that p21 activity in hepatocytes can be a contributor to hepatic pathology and supports the concept that drugs targeting p21/CDKN1A cell cycle inhibitor are potentially viable therapeutic options for treating liver metabolic diseases.

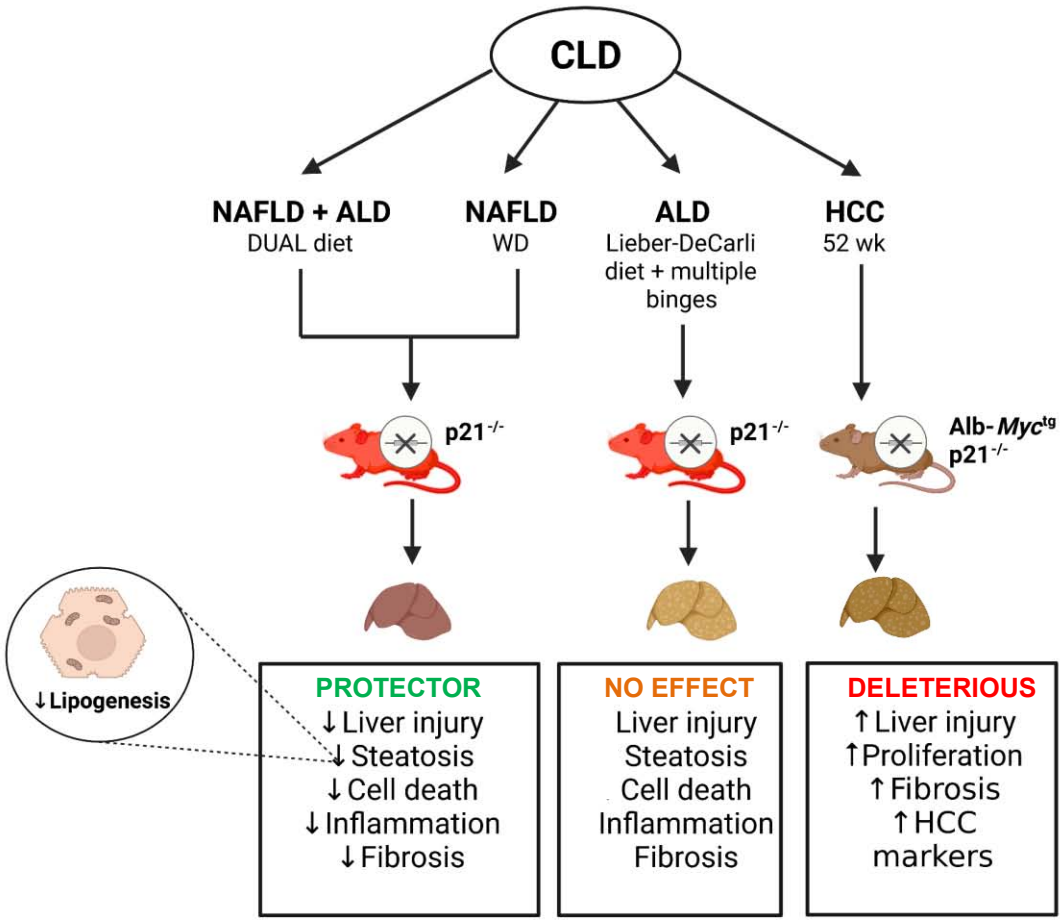

Figure 35. Role of p21 in CLD and specific function in the hepatocyte. Absence of p21 is protective against NAFLD plus ALD and NAFLD alone: decreased liver injury, steatosis, cell death, inflammation and fibrosis after a DUAL diet and a WD. In contrast, p21 has no relevance in a model of ALD, the LdC diet model plus multiple EtOH binges and exacerbates liver tumorigenesis in an HCC mouse model (Alb-*Myc*^{tg}/p21$^{-/-}$ mouse strain) after 52 weeks old. Hepatic lipid balance in p21 knockout mice is altered after a DUAL diet and a WD. Primary hepatocyte isolated from wild type mice and transfected with *sip21* and isolated from p21$^{+/+}$ and p21$^{-/-}$ mice revealed that the absence of p21 diminishes the lipogenesis in the hepatocyte.

CONCLUSIONS

9. Conclusions

1. *P21* expression is altered in primary tumors from patients with hepatocellular carcinoma (HCC) and in clinical and preclinical non-alcoholic fatty liver disease (NAFLD).

2. Absence of p21 exerts a protective effect against non-alcoholic fatty liver disease (NAFLD) and NAFLD with alcohol-related liver disease (ALD) background in mice, in terms of liver injury, steatosis, cell death, inflammation and fibrosis.

3. The absence of p21 does not have a specific effect in alcohol-related liver disease (ALD) in mice.

4. In absence of p21, lipid metabolism is deregulated in hepatocytes in terms of lipogenesis.

5. In terms of hepatocellular carcinoma (HCC), the absence of p21 exacerbates carcinogenesis in mice.

REFERENCES

10. References

1. Kruepunga, N., et al., *Anatomy of rodent and human livers: What are the differences?* Biochim Biophys Acta Mol Basis Dis, 2019. **1865**(5): p. 869-878.
2. Kalra A, Y.E., Wehrle CJ, et al. , *Physiology, Liver.* StatPearls, 2021.
3. Lindor, T.B.K., *Zakim and Boyer's Hepatology 7th Edition.* Elsevier, 2017. **1072**.
4. Tortora GJ, D.B., *Tortora's Principles of Anatomy and Physiology.* 2018.
5. Trefts, E., M. Gannon, and D.H. Wasserman, *The liver.* Curr Biol, 2017. **27**(21): p. R1147-R1151.
6. Sanz-García, C.F.-I., A.; Gracia-Sancho, J.; Arráez-Aybar, L.A.; Nevzorova, Y.A.; Cubero, F.J., *The Space of Disse: The Liver Hub in Health and Disease.* Livers, 2021. **1(1):3-26**.
7. Berasain, C. and M.A. Avila, *Regulation of hepatocyte identity and quiescence.* Cell Mol Life Sci, 2015. **72**(20): p. 3831-51.
8. Banales, J.M., J. Prieto, and J.F. Medina, *Cholangiocyte anion exchange and biliary bicarbonate excretion.* World J Gastroenterol, 2006. **12**(22): p. 3496-511.
9. Banales, J.M., et al., *Cholangiocyte pathobiology.* Nat Rev Gastroenterol Hepatol, 2019. **16**(5): p. 269-281.
10. Boyer, J.L., *Bile formation and secretion.* Compr Physiol, 2013. **3**(3): p. 1035-78.
11. Han, Y., et al., *Recent advances in the morphological and functional heterogeneity of the biliary epithelium.* Exp Biol Med (Maywood), 2013. **238**(5): p. 549-65.
12. Alpini, G., et al., *Large but not small intrahepatic bile ducts are involved in secretin-regulated ductal bile secretion.* Am J Physiol, 1997. **272**(5 Pt 1): p. G1064-74.
13. Alpini, G., et al., *Morphological, molecular, and functional heterogeneity of cholangiocytes from normal rat liver.* Gastroenterology, 1996. **110**(5): p. 1636-43.
14. Ishii, M., B. Vroman, and N.F. LaRusso, *Isolation and morphologic characterization of bile duct epithelial cells from normal rat liver.* Gastroenterology, 1989. **97**(5): p. 1236-47.
15. Kanno, N., et al., *Functional heterogeneity of the intrahepatic biliary epithelium.* Hepatology, 2000. **31**(3): p. 555-61.
16. Tabibian, J.H., et al., *Physiology of cholangiocytes.* Compr Physiol, 2013. **3**(1): p. 541-65.

17. Ludwig, J., et al., *Anatomy of the human biliary system studied by quantitative computer-aided three-dimensional imaging techniques.* Hepatology, 1998. **27**(4): p. 893-9.
18. Vroman, B. and N.F. LaRusso, *Development and characterization of polarized primary cultures of rat intrahepatic bile duct epithelial cells.* Lab Invest, 1996. **74**(1): p. 303-13.
19. De La Iglesia, F.A. and E.A. Porta, *Ciliated biliary epithelial cells in the livers of non-human primates.* Experientia, 1967. **23**(1): p. 49-51.
20. Wake, K., *"Sternzellen" in the liver: perisinusoidal cells with special reference to storage of vitamin A.* Am J Anat, 1971. **132**(4): p. 429-62.
21. Hendriks, H.F., et al., *Perisinusoidal fat-storing cells are the main vitamin A storage sites in rat liver.* Exp Cell Res, 1985. **160**(1): p. 138-49.
22. Hellerbrand, C., *Hepatic stellate cells--the pericytes in the liver.* Pflugers Arch, 2013. **465**(6): p. 775-8.
23. Senoo, H., et al., *Hepatic stellate cell (vitamin A-storing cell) and its relative--past, present and future.* Cell Biol Int, 2010. **34**(12): p. 1247-72.
24. Nguyen-Lefebvre, A.T. and A. Horuzsko, *Kupffer Cell Metabolism and Function.* J Enzymol Metab, 2015. **1**(1).
25. Bouwens, L., *Structural and functional aspects of Kupffer cells.* Revis Biol Celular, 1988. **16**: p. 69-94.
26. Naito, M., et al., *Differentiation and function of Kupffer cells.* Med Electron Microsc, 2004. **37**(1): p. 16-28.
27. Wisse, E., *Ultrastructure and function of Kupffer cells and other sinusoidal cells in the liver.* Med Chir Dig, 1977. **6**(7): p. 409-18.
28. Poisson, J., et al., *Liver sinusoidal endothelial cells: Physiology and role in liver diseases.* J Hepatol, 2017. **66**(1): p. 212-227.
29. Racanelli, V. and B. Rehermann, *The liver as an immunological organ.* Hepatology, 2006. **43**(2 Suppl 1): p. S54-62.
30. Leal-Esteban, L.C. and L. Fajas, *Cell cycle regulators in cancer cell metabolism.* Biochim Biophys Acta Mol Basis Dis, 2020. **1866**(5): p. 165715.
31. Norbury, C. and P. Nurse, *Animal cell cycles and their control.* Annu Rev Biochem, 1992. **61**: p. 441-70.
32. Lim, S. and P. Kaldis, *Cdks, cyclins and CKIs: roles beyond cell cycle regulation.* Development, 2013. **140**(15): p. 3079-93.
33. Harbour, J.W., et al., *Cdk phosphorylation triggers sequential intramolecular interactions that progressively block Rb functions as cells move through G1.* Cell, 1999. **98**(6): p. 859-69.

34. Julian, L.M. and A. Blais, *Transcriptional control of stem cell fate by E2Fs and pocket proteins.* Front Genet, 2015. **6**: p. 161.
35. Alimbetov, D., et al., *Pharmacological Targeting of Cell Cycle, Apoptotic and Cell Adhesion Signaling Pathways Implicated in Chemoresistance of Cancer Cells.* Int J Mol Sci, 2018. **19**(6).
36. Connell-Crowley, L., J.W. Harper, and D.W. Goodrich, *Cyclin D1/Cdk4 regulates retinoblastoma protein-mediated cell cycle arrest by site-specific phosphorylation.* Mol Biol Cell, 1997. **8**(2): p. 287-301.
37. Malumbres, M. and M. Barbacid, *To cycle or not to cycle: a critical decision in cancer.* Nat Rev Cancer, 2001. **1**(3): p. 222-31.
38. Sherr, C.J. and J.M. Roberts, *CDK inhibitors: positive and negative regulators of G1-phase progression.* Genes Dev, 1999. **13**(12): p. 1501-12.
39. Kreis, N.N., F. Louwen, and J. Yuan, *The Multifaceted p21 (Cip1/Waf1/CDKN1A) in Cell Differentiation, Migration and Cancer Therapy.* Cancers (Basel), 2019. **11**(9).
40. Abbas, T. and A. Dutta, *p21 in cancer: intricate networks and multiple activities.* Nat Rev Cancer, 2009. **9**(6): p. 400-14.
41. Waga, S., et al., *The p21 inhibitor of cyclin-dependent kinases controls DNA replication by interaction with PCNA.* Nature, 1994. **369**(6481): p. 574-8.
42. Engeland, K., *Cell cycle arrest through indirect transcriptional repression by p53: I have a DREAM.* Cell Death Differ, 2018. **25**(1): p. 114-132.
43. Chang, B.D., et al., *Effects of p21Waf1/Cip1/Sdi1 on cellular gene expression: implications for carcinogenesis, senescence, and age-related diseases.* Proc Natl Acad Sci U S A, 2000. **97**(8): p. 4291-6.
44. d'Adda di Fagagna, F., *Living on a break: cellular senescence as a DNA-damage response.* Nat Rev Cancer, 2008. **8**(7): p. 512-22.
45. Brugarolas, J., et al., *Radiation-induced cell cycle arrest compromised by p21 deficiency.* Nature, 1995. **377**(6549): p. 552-7.
46. Mitchell, K.O. and W.S. El-Deiry, *Overexpression of c-Myc inhibits p21WAF1/CIP1 expression and induces S-phase entry in 12-O-tetradecanoylphorbol-13-acetate (TPA)-sensitive human cancer cells.* Cell Growth Differ, 1999. **10**(4): p. 223-30.
47. Kitaura, H., et al., *Reciprocal regulation via protein-protein interaction between c-Myc and p21(cip1/waf1/sdi1) in DNA replication and transcription.* J Biol Chem, 2000. **275**(14): p. 10477-83.
48. Asrani, S.K., et al., *Burden of liver diseases in the world.* J Hepatol, 2019. **70**(1): p. 151-171.

49. Younossi, Z. and L. Henry, *Contribution of Alcoholic and Nonalcoholic Fatty Liver Disease to the Burden of Liver-Related Morbidity and Mortality.* Gastroenterology, 2016. **150**(8): p. 1778-85.
50. Marcellin, P. and B.K. Kutala, *Liver diseases: A major, neglected global public health problem requiring urgent actions and large-scale screening.* Liver Int, 2018. **38 Suppl 1**: p. 2-6.
51. European Association for the Study of the Liver. Electronic address, e.e.e. and L. European Association for the Study of the, *EASL Clinical Practice Guidelines: Management of hepatocellular carcinoma.* J Hepatol, 2018. **69**(1): p. 182-236.
52. Marrero, J.A., et al., *Diagnosis, Staging, and Management of Hepatocellular Carcinoma: 2018 Practice Guidance by the American Association for the Study of Liver Diseases.* Hepatology, 2018. **68**(2): p. 723-750.
53. Trinchet, J.C., et al., *Complications and competing risks of death in compensated viral cirrhosis (ANRS CO12 CirVir prospective cohort).* Hepatology, 2015. **62**(3): p. 737-50.
54. Loomba, R. and A.J. Sanyal, *The global NAFLD epidemic.* Nat Rev Gastroenterol Hepatol, 2013. **10**(11): p. 686-90.
55. European Association for the Study of the, L., D. European Association for the Study of, and O. European Association for the Study of, *EASL-EASD-EASO Clinical Practice Guidelines for the Management of Non-Alcoholic Fatty Liver Disease.* Obes Facts, 2016. **9**(2): p. 65-90.
56. Finelli, C. and G. Tarantino, *Is visceral fat reduction necessary to favour metabolic changes in the liver?* J Gastrointestin Liver Dis, 2012. **21**(2): p. 205-8.
57. Katsiki, N., D.P. Mikhailidis, and C.S. Mantzoros, *Non-alcoholic fatty liver disease and dyslipidemia: An update.* Metabolism, 2016. **65**(8): p. 1109-23.
58. Du, T., et al., *Lipid phenotypes in patients with nonalcoholic fatty liver disease.* Metabolism, 2016. **65**(9): p. 1391-8.
59. Ryoo, J.H., et al., *Clinical association between serum gamma-glutamyltransferase levels and the development of insulin resistance in Korean men: a 5-year follow-up study.* Diabet Med, 2014. **31**(4): p. 455-61.
60. Tomic, D., W.W. Kemp, and S.K. Roberts, *Nonalcoholic fatty liver disease: current concepts, epidemiology and management strategies.* Eur J Gastroenterol Hepatol, 2018. **30**(10): p. 1103-1115.
61. Lonardo, A., et al., *Hypertension, diabetes, atherosclerosis and NASH: Cause or consequence?* J Hepatol, 2018. **68**(2): p. 335-352.
62. Kim, D., A. Touros, and W.R. Kim, *Nonalcoholic Fatty Liver Disease and Metabolic Syndrome.* Clin Liver Dis, 2018. **22**(1): p. 133-140.

63. Bobrus-Chociej, A., et al., *Estimation of gamma-glutamyl transferase as a suitable simple biomarker of the cardiovascular risk in children with non-alcoholic fatty liver disease.* Acta Biochim Pol, 2018. **65**(4): p. 539-544.
64. Peverill, W., L.W. Powell, and R. Skoien, *Evolving concepts in the pathogenesis of NASH: beyond steatosis and inflammation.* Int J Mol Sci, 2014. **15**(5): p. 8591-638.
65. Giorgio, V., et al., *Pediatric non alcoholic fatty liver disease: old and new concepts on development, progression, metabolic insight and potential treatment targets.* BMC Pediatr, 2013. **13**: p. 40.
66. Buzzetti, E., M. Pinzani, and E.A. Tsochatzis, *The multiple-hit pathogenesis of non-alcoholic fatty liver disease (NAFLD).* Metabolism, 2016. **65**(8): p. 1038-48.
67. Dulai, P.S., et al., *Increased risk of mortality by fibrosis stage in nonalcoholic fatty liver disease: Systematic review and meta-analysis.* Hepatology, 2017. **65**(5): p. 1557-1565.
68. Marra, F. and G. Svegliati-Baroni, *Lipotoxicity and the gut-liver axis in NASH pathogenesis.* J Hepatol, 2018. **68**(2): p. 280-295.
69. Nevzorova, Y.A., et al., *Animal models for liver disease - A practical approach for translational research.* J Hepatol, 2020. **73**(2): p. 423-440.
70. Peacock, A., et al., *Global statistics on alcohol, tobacco and illicit drug use: 2017 status report.* Addiction, 2018. **113**(10): p. 1905-1926.
71. Ntandja Wandji, L.C., et al., *Combined alcoholic and non-alcoholic steatohepatitis.* JHEP Rep, 2020. **2**(3): p. 100101.
72. Teli, M.R., et al., *Determinants of progression to cirrhosis or fibrosis in pure alcoholic fatty liver.* Lancet, 1995. **346**(8981): p. 987-90.
73. European Association for the Study of the Liver. Electronic address, e.e.e., et al., *EASL Clinical Practical Guidelines on the management of acute (fulminant) liver failure.* J Hepatol, 2017. **66**(5): p. 1047-1081.
74. Rehm, J., et al., *Alcohol as a risk factor for liver cirrhosis: a systematic review and meta-analysis.* Drug Alcohol Rev, 2010. **29**(4): p. 437-45.
75. Cederbaum, A.I., *Alcohol metabolism.* Clin Liver Dis, 2012. **16**(4): p. 667-85.
76. Ceni, E., T. Mello, and A. Galli, *Pathogenesis of alcoholic liver disease: role of oxidative metabolism.* World J Gastroenterol, 2014. **20**(47): p. 17756-72.
77. Dumortier, J., et al., *Recurrent alcoholic cirrhosis in severe alcoholic relapse after liver transplantation: a frequent and serious complication.* Am J Gastroenterol, 2015. **110**(8): p. 1160-6; quiz 1167.

78. Gudowska, M., et al., *The Distribution of Liver Steatosis, Fibrosis, Steatohepatitis and Inflammation Activity in Alcoholics According to FibroMax Test.* Adv Clin Exp Med, 2015. **24**(5): p. 823-7.
79. Murakami, H., et al., *Transgenic mouse model for synergistic effects of nuclear oncogenes and growth factors in tumorigenesis: interaction of c-myc and transforming growth factor alpha in hepatic oncogenesis.* Cancer Res, 1993. **53**(8): p. 1719-23.
80. Benede-Ubieto, R., et al., *An Experimental DUAL Model of Advanced Liver Damage.* Hepatol Commun, 2021. **5**(6): p. 1051-1068.
81. Estevez-Vazquez, O., et al., *Fat: Quality, or Quantity? What Matters Most for the Progression of Metabolic Associated Fatty Liver Disease (MAFLD).* Biomedicines, 2021. **9**(10).
82. Lamas-Paz, A., et al., *Alcoholic liver disease: Utility of animal models.* World J Gastroenterol, 2018. **24**(45): p. 5063-5075.
83. Guo, F., et al., *The Lieber-DeCarli Diet-A Flagship Model for Experimental Alcoholic Liver Disease.* Alcohol Clin Exp Res, 2018. **42**(10): p. 1828-1840.
84. Nevzorova, Y.A., et al., *Overexpression of c-myc in hepatocytes promotes activation of hepatic stellate cells and facilitates the onset of liver fibrosis.* Biochim Biophys Acta, 2013. **1832**(10): p. 1765-75.
85. Benede-Ubieto, R., et al., *Guidelines and Considerations for Metabolic Tolerance Tests in Mice.* Diabetes Metab Syndr Obes, 2020. **13**: p. 439-450.
86. Charni-Natan, M. and I. Goldstein, *Protocol for Primary Mouse Hepatocyte Isolation.* STAR Protoc, 2020. **1**(2): p. 100086.
87. Kleiner, D.E., et al., *Design and validation of a histological scoring system for nonalcoholic fatty liver disease.* Hepatology, 2005. **41**(6): p. 1313-21.
88. Kurien, B.T. and R.H. Scofield, *Western blotting.* Methods, 2006. **38**(4): p. 283-93.
89. Gerhart-Hines, Z., et al., *Metabolic control of muscle mitochondrial function and fatty acid oxidation through SIRT1/PGC-1alpha.* EMBO J, 2007. **26**(7): p. 1913-23.
90. Ehedego, H., et al., *p21 ablation in liver enhances DNA damage, cholestasis, and carcinogenesis.* Cancer Res, 2015. **75**(6): p. 1144-55.
91. Parker, R., S.J. Kim, and B. Gao, *Alcohol, adipose tissue and liver disease: mechanistic links and clinical considerations.* Nat Rev Gastroenterol Hepatol, 2018. **15**(1): p. 50-59.

92. Mantena, S.K., et al., *Mitochondrial dysfunction and oxidative stress in the pathogenesis of alcohol- and obesity-induced fatty liver diseases.* Free Radic Biol Med, 2008. **44**(7): p. 1259-72.
93. Sharma, A., K. Singh, and A. Almasan, *Histone H2AX phosphorylation: a marker for DNA damage.* Methods Mol Biol, 2012. **920**: p. 613-26.
94. Wei, W., et al., *Rodent models and imaging techniques to study liver regeneration.* Eur Surg Res, 2015. **54**(3-4): p. 97-113.
95. Tomita, K., et al., *p53/p66Shc-mediated signaling contributes to the progression of non-alcoholic steatohepatitis in humans and mice.* J Hepatol, 2012. **57**(4): p. 837-43.
96. Wang, K., *Molecular mechanisms of hepatic apoptosis.* Cell Death Dis, 2014. **5**: p. e996.
97. Yang, Y.M. and E. Seki, *TNFalpha in liver fibrosis.* Curr Pathobiol Rep, 2015. **3**(4): p. 253-261.
98. Breuer, D.A., et al., *CD8(+) T cells regulate liver injury in obesity-related nonalcoholic fatty liver disease.* Am J Physiol Gastrointest Liver Physiol, 2020. **318**(2): p. G211-G224.
99. Mederacke, I., et al., *Fate tracing reveals hepatic stellate cells as dominant contributors to liver fibrosis independent of its aetiology.* Nat Commun, 2013. **4**: p. 2823.
100. Cederbaum, A.I., *Role of CYP2E1 in ethanol-induced oxidant stress, fatty liver and hepatotoxicity.* Dig Dis, 2010. **28**(6): p. 802-11.
101. Dentin, R., J. Girard, and C. Postic, *Carbohydrate responsive element binding protein (ChREBP) and sterol regulatory element binding protein-1c (SREBP-1c): two key regulators of glucose metabolism and lipid synthesis in liver.* Biochimie, 2005. **87**(1): p. 81-6.
102. Lane, E.A., et al., *HCF-1 Regulates De Novo Lipogenesis through a Nutrient-Sensitive Complex with ChREBP.* Mol Cell, 2019. **75**(2): p. 357-371 e7.
103. Abdul-Wahed, A., S. Guilmeau, and C. Postic, *Sweet Sixteenth for ChREBP: Established Roles and Future Goals.* Cell Metab, 2017. **26**(2): p. 324-341.
104. Uyeda, K. and J.J. Repa, *Carbohydrate response element binding protein, ChREBP, a transcription factor coupling hepatic glucose utilization and lipid synthesis.* Cell Metab, 2006. **4**(2): p. 107-10.
105. Wang, Y., et al., *Transcriptional regulation of hepatic lipogenesis.* Nat Rev Mol Cell Biol, 2015. **16**(11): p. 678-89.

106. Yecies, J.L., et al., *Akt stimulates hepatic SREBP1c and lipogenesis through parallel mTORC1-dependent and independent pathways.* Cell Metab, 2011. **14**(1): p. 21-32.
107. Eslam, M., et al., *A new definition for metabolic dysfunction-associated fatty liver disease: An international expert consensus statement.* J Hepatol, 2020. **73**(1): p. 202-209.
108. Eslam, M., et al., *MAFLD: A Consensus-Driven Proposed Nomenclature for Metabolic Associated Fatty Liver Disease.* Gastroenterology, 2020. **158**(7): p. 1999-2014 e1.
109. Heidelbaugh, J.J. and M. Bruderly, *Cirrhosis and chronic liver failure: part I. Diagnosis and evaluation.* Am Fam Physician, 2006. **74**(5): p. 756-62.
110. Paik, J.M., et al., *Nonalcoholic Fatty Liver Disease and Alcoholic Liver Disease are Major Drivers of Liver Mortality in the United States.* Hepatol Commun, 2020. **4**(6): p. 890-903.
111. Poznyak, V., et al., *The world health organization's global monitoring system on alcohol and health.* Alcohol Res, 2013. **35**(2): p. 244-9.
112. Pimpin, L., et al., *Burden of liver disease in Europe: Epidemiology and analysis of risk factors to identify prevention policies.* J Hepatol, 2018. **69**(3): p. 718-735.
113. Galan, I., M.J. Gonzalez, and J.L. Valencia-Martin, *[Alcohol drinking patterns in Spain: a country in transition].* Rev Esp Salud Publica, 2014. **88**(4): p. 529-40.
114. Bataller, R., et al., *Alcohol-related liver disease. Clinical practice guidelines. Consensus document sponsored by AEEH.* Gastroenterol Hepatol, 2019. **42**(10): p. 657-676.
115. Targher, G., C.D. Byrne, and H. Tilg, *NAFLD and increased risk of cardiovascular disease: clinical associations, pathophysiological mechanisms and pharmacological implications.* Gut, 2020. **69**(9): p. 1691-1705.
116. Inoue, Y., et al., *Epidemiology of Obesity in Adults: Latest Trends.* Curr Obes Rep, 2018. **7**(4): p. 276-288.
117. Paik, J.M., et al., *Changes in the Global Burden of Chronic Liver Diseases From 2012 to 2017: The Growing Impact of NAFLD.* Hepatology, 2020. **72**(5): p. 1605-1616.
118. Aller, R., et al., *Consensus document. Management of non-alcoholic fatty liver disease (NAFLD). Clinical practice guideline.* Gastroenterol Hepatol, 2018. **41**(5): p. 328-349.
119. Estes, C., et al., *Modeling NAFLD disease burden in China, France, Germany, Italy, Japan, Spain, United Kingdom, and United States for the period 2016-2030.* J Hepatol, 2018. **69**(4): p. 896-904.

120. Crespo, J., P. Iruzubieta, and J.V. Lazarus, *Can NAFLD overwhelm the Spanish healthcare system in the years to come?* Rev Esp Enferm Dig, 2022. **114**(1): p. 5-9.
121. Naveau, S., et al., *Harmful effect of adipose tissue on liver lesions in patients with alcoholic liver disease.* J Hepatol, 2010. **52**(6): p. 895-902.
122. Hart, C.L., et al., *Effect of body mass index and alcohol consumption on liver disease: analysis of data from two prospective cohort studies.* BMJ, 2010. **340**: p. c1240.
123. Chang, Y., et al., *Nonheavy Drinking and Worsening of Noninvasive Fibrosis Markers in Nonalcoholic Fatty Liver Disease: A Cohort Study.* Hepatology, 2019. **69**(1): p. 64-75.
124. Bedogni, G., et al., *Incidence and natural course of fatty liver in the general population: the Dionysos study.* Hepatology, 2007. **46**(5): p. 1387-91.
125. Loomba, R., et al., *Synergism between obesity and alcohol in increasing the risk of hepatocellular carcinoma: a prospective cohort study.* Am J Epidemiol, 2013. **177**(4): p. 333-42.
126. Sharma A, N.S., *Chronic Liver Disease.* StatPearls, 2021.
127. Lehmann, K., et al., *Liver failure after extended hepatectomy in mice is mediated by a p21-dependent barrier to liver regeneration.* Gastroenterology, 2012. **143**(6): p. 1609-1619 e4.
128. Marhenke, S., et al., *p21 promotes sustained liver regeneration and hepatocarcinogenesis in chronic cholestatic liver injury.* Gut, 2014. **63**(9): p. 1501-12.
129. Albrecht, J.H., et al., *Involvement of p21 and p27 in the regulation of CDK activity and cell cycle progression in the regenerating liver.* Oncogene, 1998. **16**(16): p. 2141-50.
130. Koteish, A., et al., *Ethanol induces redox-sensitive cell-cycle inhibitors and inhibits liver regeneration after partial hepatectomy.* Alcohol Clin Exp Res, 2002. **26**(11): p. 1710-8.
131. Lunz, J.G., 3rd, et al., *An inhibitor of cyclin-dependent kinase, stress-induced p21Waf-1/Cip-1, mediates hepatocyte mito-inhibition during the evolution of cirrhosis.* Hepatology, 2005. **41**(6): p. 1262-71.
132. Torbenson, M., et al., *STAT-3 overexpression and p21 up-regulation accompany impaired regeneration of fatty livers.* Am J Pathol, 2002. **161**(1): p. 155-61.
133. Zhang, X., et al., *Hepatic cellular senescence pathway genes are induced through histone modifications in a diet-induced obese rat model.* Am J Physiol Gastrointest Liver Physiol, 2012. **302**(5): p. G558-64.

134. Richardson, M.M., et al., *Progressive fibrosis in nonalcoholic steatohepatitis: association with altered regeneration and a ductular reaction.* Gastroenterology, 2007. **133**(1): p. 80-90.
135. Aravinthan, A., et al., *Hepatocyte senescence predicts progression in non-alcohol-related fatty liver disease.* J Hepatol, 2013. **58**(3): p. 549-56.
136. Donnelly, K.L., et al., *Sources of fatty acids stored in liver and secreted via lipoproteins in patients with nonalcoholic fatty liver disease.* J Clin Invest, 2005. **115**(5): p. 1343-51.
137. Ma, K., et al., *Farnesoid X receptor is essential for normal glucose homeostasis.* J Clin Invest, 2006. **116**(4): p. 1102-9.
138. Zhang, Y., et al., *Activation of the nuclear receptor FXR improves hyperglycemia and hyperlipidemia in diabetic mice.* Proc Natl Acad Sci U S A, 2006. **103**(4): p. 1006-11.
139. Marra, F., et al., *Molecular basis and mechanisms of progression of non-alcoholic steatohepatitis.* Trends Mol Med, 2008. **14**(2): p. 72-81.
140. Wang, J.W., et al., *Lipotoxic effect of p21 on free fatty acid-induced steatosis in L02 cells.* PLoS One, 2014. **9**(4): p. e96124.
141. Kuchay, M.S., N.S. Choudhary, and S.K. Mishra, *Pathophysiological mechanisms underlying MAFLD.* Diabetes Metab Syndr, 2020. **14**(6): p. 1875-1887.
142. Chen, X., et al., *Suppressed hepatocyte proliferation via a ROS-HNE-P21 pathway is associated with nicotine- and cotinine-enhanced alcoholic fatty liver in mice.* Biochem Biophys Res Commun, 2019. **512**(1): p. 119-124.
143. Cortez-Pinto, H., et al., *Lipids up-regulate uncoupling protein 2 expression in rat hepatocytes.* Gastroenterology, 1999. **116**(5): p. 1184-93.
144. Leclercq, I.A., et al., *CYP2E1 and CYP4A as microsomal catalysts of lipid peroxides in murine nonalcoholic steatohepatitis.* J Clin Invest, 2000. **105**(8): p. 1067-75.
145. Letteron, P., et al., *Acute and chronic hepatic steatosis lead to in vivo lipid peroxidation in mice.* J Hepatol, 1996. **24**(2): p. 200-8.
146. Zhao, J., Y. Hu, and J. Peng, *Targeting programmed cell death in metabolic dysfunction-associated fatty liver disease (MAFLD): a promising new therapy.* Cell Mol Biol Lett, 2021. **26**(1): p. 17.
147. Choi, M.E., et al., *Necroptosis: a crucial pathogenic mediator of human disease.* JCI Insight, 2019. **4**(15).
148. Majdi, A., et al., *Inhibition of receptor-interacting protein kinase 1 improves experimental non-alcoholic fatty liver disease.* J Hepatol, 2020. **72**(4): p. 627-635.

149. Saeed, W.K., et al., *Decrease in fat de novo synthesis and chemokine ligand expression in non-alcoholic fatty liver disease caused by inhibition of mixed lineage kinase domain-like pseudokinase.* J Gastroenterol Hepatol, 2019. **34**(12): p. 2206-2218.
150. Wang, T., et al., *Effects of knockout of lincRNA-p21 on the proliferation, migration and invasion ability of HepG2 liver cancer cells.* Oncol Lett, 2019. **17**(6): p. 5103-5107.
151. Merched, A.J. and L. Chan, *Absence of p21Waf1/Cip1/Sdi1 modulates macrophage differentiation and inflammatory response and protects against atherosclerosis.* Circulation, 2004. **110**(25): p. 3830-41.
152. Nunez, K.G., et al., *Cyclin D1 in the Liver: Role of Noncanonical Signaling in Liver Steatosis and Hormone Regulation.* Ochsner J, 2017. **17**(1): p. 56-65.
153. Roninson, I.B., *Oncogenic functions of tumour suppressor p21(Waf1/Cip1/Sdi1): association with cell senescence and tumour-promoting activities of stromal fibroblasts.* Cancer Lett, 2002. **179**(1): p. 1-14.
154. Liu, Y., et al., *Somatic cell type specific gene transfer reveals a tumor-promoting function for p21(Waf1/Cip1).* EMBO J, 2007. **26**(22): p. 4683-93.
155. Aravinthan, A., et al., *Hepatocyte expression of the senescence marker p21 is linked to fibrosis and an adverse liver-related outcome in alcohol-related liver disease.* PLoS One, 2013. **8**(9): p. e72904.
156. Ow, J.R., et al., *Remodeling of whole-body lipid metabolism and a diabetic-like phenotype caused by loss of CDK1 and hepatocyte division.* Elife, 2020. **9**.
157. Wu, H., et al., *Evidence for a Novel Regulatory Interaction Involving Cyclin D1, Lipid Droplets, Lipolysis, and Cell Cycle Progression in Hepatocytes.* Hepatol Commun, 2019. **3**(3): p. 406-422.
158. Shiraki, K. and H. Wagayama, *Cytoplasmic p21(WAF1/CIP1) expression in human hepatocellular carcinomas.* Liver Int, 2006. **26**(8): p. 1018-9.
159. Hui, L., et al., *Proliferation of human HCC cells and chemically induced mouse liver cancers requires JNK1-dependent p21 downregulation.* J Clin Invest, 2008. **118**(12): p. 3943-53.
160. Willenbring, H., et al., *Loss of p21 permits carcinogenesis from chronically damaged liver and kidney epithelial cells despite unchecked apoptosis.* Cancer Cell, 2008. **14**(1): p. 59-67.
161. Xia, M., D. Knezevic, and L.T. Vassilev, *p21 does not protect cancer cells from apoptosis induced by nongenotoxic p53 activation.* Oncogene, 2011. **30**(3): p. 346-55.

APPENDIX

11. Appendix

11.1 Curriculum vitae

Arantza Lamas Paz

DNI: 35608082B

Date of birth: 15/06/1994

ORCID: https://orcid.org/0000-0001-5857-4320

Email address: arlamas@ucm.es / arlamaspaz@gmail.com

Mobil phone: (+34) 655338274

EDUCATION

Ph.D. in Biomedical Research, Complutense University of Madrid (UCM), Madrid (Spain). **2017-Present**

M.Sc. Immunology Research, Complutense University of Madrid (UCM), Madrid (Spain). Score 8.73 **2017**

B.Sc. Biology, University of Santiago de Compostela (USC), Galicia (Spain). Score 7.22 **2016**

SKILLS

Laboratory skills: animal experimentation (Functions A, B and C - rodents, lagomorphs and carnivores), gavage, IP injection, tail vein injection, vena cava inferior and retro orbital blood collection, gut permeability (FITC-dextran), dissection (liver, fat, gut, brain, brown adipose tissue, muscle), primary hepatocytes isolation, cell lines (Caco-2, HepG2, HepaRG), co-cultures, transfections, i*n vivo* and *in vitro* models (HCC, ALD, NAFLD), PCR, qPCR, Western blot, staining (IHC, IF), microscopy (optical and fluorescent), extracellular vesicles (EVs).

Technical skills: quantitative image analysis (Image J, ImageStudio), statistical analysis, data management and plotting (GraphPad), bibliography (EndNote, MEGA), illustration tools (Photoshop, BioRender), samples comparison (GEO2R), molecular visualization (PyMOL), Office software.

Interpersonal and collaboration skills: conflict resolution, team collaborations, scientific writing and communication (lay and specialized).

Languages: fluent in English, Spanish (native), Galician language (native), beginner in French and Portuguese.

PROFESIONAL EXPERIENCE

RESEARCH

Predoctoral UCM-Harvard Researcher **Apr 2018-Present**

PhD in Biomedical Research in the Immunology Department of the Complutense University of Madrid (UCM), Madrid (Spain). Scholarship call: Grants for pre-doctoral contracts for research personnel in training. 2017. Complutense University of Madrid, Harvard collaboration. Project: **Role of p21/CDKN1A in chronic liver disease (CLD)**. Directors: Francisco Javier Cubero Palero and Yulia Nevzorova. Group: Liver injury and inflammation.

Predoctoral Researcher Member in the imas12-Research Group **Nov 2016-Present**

Predoctoral Researcher Member of the Lymphocyte immunology group (imas12-associated), 12 de Octubre Hospital, Madrid (Spain).

Researcher visitor **Sept 2021-Dec 2022**

Researcher visitor of the Department of Cancer Biology (Longwood Center). Dana-Farber Cancer Institute, Boston, MA, USA. In collaboration with the "Real Colegio Complutense (RCC)" in Harvard. Harvard University. Supervisor: Pere Puigserver.

M.Sc. Researcher **Dec 2016-Sep 2017**

M.Sc. Researcher of the Immunology Department of the Complutense University of Madrid (UCM), Madrid (Spain). M.Sc. project: **Immunity in the gut-liver axis in alcoholism**. Director: Francisco Javier Cubero Palero. Group: Liver injury and inflammation.

B.Sc. Researcher **Sept 2015-Jul 2016**

B.Sc Researcher of the Biochemistry and Molecular Biology in the Biological Research Center of the Santiago de Compostela University (CIBUS), Galicia (Spain). B.Sc project: **Preliminary genetic characterization of *Spondylus limbatus* G. B. Sowerby II, 1847, from the Ecuadorian coast.** Director: Manuel Rey Mendez. Group: Molecular Systematics (SISMOL).

Researcher visitor **Feb 2016**

Researcher visitor of the Molecular Medicine and Chronic Disease Research Center (CIMUS) of the Santiago de Compostela University, Galicia (Spain). Project: **Learning and use of biochemical techniques of proteins and special treatment with prions**. Director: Jesús R. Requena. Group: Molecular Pathology of Rare Diseases.

Researcher visitor **Sept 2015**

Researcher visitor of the Biological Chemistry and Molecular Matters Research Center (CIQUS) of the Santiago de Compostela University, Galicia (Spain). Project: **Evaluation of polymeric micelles from dendrimers as a drug and protein delivery system**. Director: Eduardo Fernández Megía.

TEACHING

Teaching collaboration **Feb 2022- May 2022**

Teacher of the Laboratory Practices in the Immunology subject included in the Medicine Degree of the Complutense University of Madrid (UCM), Madrid (Spain). Course 2021-2022. Hours: 24.

Teaching collaboration **Feb 2021- May 2021**

Teacher of the Laboratory Practices in the Immunology subject included in the Medicine Degree of the Complutense University of Madrid (UCM), Madrid (Spain). Course 2020-2021. Hours: 12.

Teaching collaboration **May 2019**

Teaching collaboration in the program "Research and professional opportunities for Health Sciences. How to start to be a young investigator". Faculty of Medicine, Complutense University of Madrid (UCM), Madrid (Spain).

Teaching collaboration **Feb 2019- May 2019**

Teacher of the Laboratory Practices in the Immunology subject included in the Medicine Degree of the Complutense University of Madrid (UCM), Madrid (Spain). Course 2018-2019. Hours: 12.

Teaching collaboration **Nov 2018**

Laboratory Teacher of the "II Edition INMUNE WORLD" XVIII SCIENCE WEEK 2018". Faculty of Medicine, Complutense University of Madrid (UCM). Madrid (Spain).

Teaching collaboration **Nov 2017**

Laboratory Teacher of the "I Edition INMUNE WORLD" XVII SCIENCE WEEK 2018". Faculty of Medicine, Complutense University of Madrid (UCM). Madrid (Spain).

ARTICLE REVIEW

Ardaiz N, Gomar C, Vasquez M, et al. **Insulin Fused to Apolipoprotein A-I Reduces Body Weight and Steatosis in DB/DB Mice**. Front Pharmacol. **2021**;11:591293. Published 2021 Feb 19. doi:10.3389/fphar.2020.591293 **Dec 2020**

CONGRESS / CONFERENCE PARTICIPATION

(See section **11.2.1**)

PUBLICATIONS

(See section **11.2.2**)

COURSES

Radiation Safety Initial Training **Sept 2021**

DFCI EHS Radiation Safety Initial Training. Dana-Farber Cancer Institute. Boston, MA, (USA).

Human Intestinal Organoid Virtual Training **Jun 2021**

The Human Intestinal Organoid Virtual Training Course. STEMCELL. Online.

Western Blot Training **Jun 2021**

Master of Science in Blotting Course - Western Blotting University. Bio-Rad.Online.

Risks prevention training **Apr 2021**

Occupational risks prevention course. Complutense University of Madrid (UCM). Online.

Animal experimentation course **Feb 2019**

Functions A, B and C in animal experimentation (rodents, lagomorphs and carnivores). Approved by the Community of Madrid, Madrid (Spain). Complutense University of Madrid (UCM), Madrid (Spain).

Food Handler **Oct 2015**

Food Handler Course. Xunta de Galicia, Galicia (Spain).

English course **Jul 2011**

English language course and experience in a native family for 3 weeks in La Valeta (Malta). Educational First (EF) Organization.

English course **Jul 2010**

English language course and experience in a native family for 3 weeks in York (UK). Educational First (EF) Organization.

CONGRESS / CONFERENCE ATTENDANCE

X Jornada de la Sociedad de Inmunología de la Comunidad de Madrid (SICAM). Madrid (Spain). May 2022

Jornadas y Seminarios de Investigación IiSGM: **Animal models for fatty liver – a practical approach for translational research**. Yulia Nevzorova. Online.	Apr 2022
Biomedicine Seminars of the Complutense University of Madrid (UCM). **Inmunología del eje hígado-intestino.** Rubén Francés. Madrid (Spain).	Apr 2022
Conference Series on DILI: **Advancing in vitro models of drug-induced liver injury (DILI): key techniques for the study of the immunological features of idiosyncratic hepatotoxicity in cell cultures.** Daniel Di Ceo. Online.	Apr 2022
Liver Seminars: **Integrated multi-omics for the identification of novel therapies for alcoholic hepatitis.** Ramón Bataller. Online.	Apr 2022
The mentoring program organized by Women in ECUSA (MECUSA) and Career Development and Advisory (CDA) for Autonomous Community of Madrid PhD students interested in STEM career options in the USA. 4 mentoring sessions. Online.	Mar 2022
Conference Series on DILI: New insights: young investigator series. **Functional imaging of hepatotoxicity: Interruption of bile acid uptake by hepatocytes after acetaminophen overdose ameliorates hepatotoxicity.** Online.	Mar 2022
Conference Series on DILI: New insights: young investigator series. **Drug-induced cholestasis: models, biomarkers and industrial challenges**. Online.	Feb 2022
Conference Series on DILI: New insights: young investigator series. **Role of histopathology in the assessment of animal models in DILI prediction**. Online.	Jan 2022
Conference Series on DILI: New insights: young investigator series. **Generation of cell and gene iPSCs specific knockouts.** Online	Dec 2022
CONFERENCES ON THE INVESTIGATORY CAREER. SCIENTIFIC PUBLICATIONS AND COMMUNICATION OF SCIENCE. HOW TO WRITE A SCIENTIFIC ARTICLE: GUIDELINES AND KEYS. Online	Feb 2021
CONFERENCES ON THE INVESTIGATORY CAREER. STAGES OF THE INVESTIGATORY CAREER (PREDOCTORAL AND POSTDOCTORAL). Online.	Feb 2021
Week of Science Science and Cinema. Department of Immunology, Ophthalmolongia and ENT, Complutense University of Madrid (UCM), Madrid (Spain).	Nov 2019

AWARDS

Honor award **May 2012**

High School Honor Award. Scientific-Biosanitary Modality. Institute of Secondary Education Pino Manso, O Porriño (Pontevedra, Galicia, Spain). Score: 9.32.

(See section **11.3 Travel awards**)

VOLUNTEER

Volunteer 1st International NASH Day. Madrid (Spain). **Jun 2018**

11.2 Publications

11.2.1 Conference abstracts

Oral communication **May 2022**

Oral communication at the "47º Congreso Annual de la Asociación Española para el Estudio del Hígado (AEEH). Madrid (Spain). **Papel de p21/CDKN1A en la progresión de la enfermedad del hígado graso no alcohólico (EHGNA) / Role of p21 in the chronic liver disease (CLD) progression. Arantza Lamas-Paz**, Feifei Guo, Fengjie Hao, Olga Estévez-Vázquez, Raquel Benedé-Ubieto, Elena Vázquez-Ogando, Elena Blázquez- López, Iris Asensio, Javier Vaquero, Rafael Bañares, Carlos Sanz-García, Eduardo Martínez-Naves, Teresa C. Delgado, María Luz Martínez-Chantar, Pere Puigserver, Yulia A. Nevzorova, Francisco Javier Cubero.

Abstract submission **Mar 2022**

Abstract submission at the Joint Meeting of ISBRA and ESBRA 2nd World Congress on Alcohol and Alcoholism - "Alcohol and vesicle trafficking: role in pathogenesis and utility as biomarkers Symposium". Cracow (Poland). **Blood and fecal extracellular vesicles (EVs) as biomarkers of injury in the gut-liver axis during alcohol-induced liver disease. A. Lamas-Paz**, L. Morán, O. Estévez-Vázquez, R.l Benedé-Ubieto, B. Salinas, S. Sydor, R. Vilchez-Vargas, L. Moreno, M. Gómez del Moral, L. P. Bechmann, E. Martínez-Naves, J. Vaquero, R. Bañares, Y. A. Nevzorova, F. J. Cubero.

Oral communication **Oct 2021**

Oral communication at the Inauguration of the Academic Year of the Real Colegio Complutense (RCC) in Harvard. **Role of p21 in the chronic liver disease (CLD) progression. Arantza Lamas-Paz**

Oral communication **Oct 2021**

Oral communication at the "3º Reunión de hepatología traslacional. Enfermedad hepática metabólica del hígado graso a la cirrosis y sus complicaciones". Alicante (Spain). **Utilidad del sistema Keap1-Nrf2 como marcador de la progresión de la enfermedad hepática.** Laura Morán, Hui Ye, Olga Estévez, **Arantza Lamas-Paz**, Elena Vázquez, Elena Blázquez, Iris Asensio Nuria López-Alcántara, Pierluigi Ramadori, Christoph J. Wruck, Mohamed Ramadan Mohamed, Manolo Gómez del Moral, Javier Vaquero, Rafael Bañares, Yulia A. Nevzorova,1,2,3,7, Francisco Javier Cubero.

Poster communication **Oct 2021**

Poster communication at the "3º Reunión de hepatología traslacional. Enfermedad hepática metabólica del hígado graso a la cirrosis y sus complicaciones", Alicante (Spain). **Fat: Quality or Quantity? What matters most for the progression of Metabolic Associated Fatty Liver Disease (MAFLD).** Olga Estévez Vázquez, Raquel Benedé-Ubieto, Feifei Guo, Beatriz Gómez-Santos, Patricia Aspichueta, Johanna Reissing, Tony Bruns, Carlos Sanz-García, Svenja Sydor, Lars P. Bechmann, Eva Maranillo, José Ramón Sañudo, María Teresa Vázquez, **Arantza Lamas-Paz**, Laura Morán, Marina S. Mazariegos, Andreea Ciudin, Javier Vaquero, Eduardo Martínez-Naves, Christian Liedtke, José R. Regueiro, Christian Trautwein, Rafael Bañares, Francisco Javier Cubero, Yulia A. Nevzorova, Juan M Pericàs, María Isabel Peligros.

Poster communication **Feb 2021**

Poster communication at the Digital Liver Cancer Simmit. EASL (European Association for the Study of the Liver), online. **The combination of alcohol and metabolic syndrome is a fast track to hepatic tumorigenesis.** Benedé-Ubieto R; Chen C; Estévez-Vázquez O; Guo F; **Lamas-Paz A**; Morán L; Reißing J; Bruns T; Zheng K; Peligros MI; Vaquero J; Trautwein C; Liedtke C; Bañares R; Cubero FJ; Nevzorova YA

Poster communication **Sept 2019**

Poster communication at the EASL NAFLD SUMMIT, Sevilla (Spain). **Differential effects of palmitic acid on the development of NASH and related metabolic disorders.** Olga Estévez Vázquez, Raquel Benedé, Feifei Guo, **Arantza Lamas Paz**, Javier Vaquero, Rafael Bañares, Francisco Javier Cubero, Yulia Nevzorova.

Poster communication **Jul 2019**

Poster communication at the Paris NASH Meeting, Paris (France). **Differential effects of palmitic acid on the development of NASH and related metabolic disorders.** Estévez-Vázquez O, Benedé-Ubieto R, Guo F, **Lamas-Paz A**, Vaquero J, Bañares R, Cubero FJ, Nevzorova YA.

Poster communication **Feb 2019**

Poster communication at the "44º Congreso Anual de la Asociación Española para el Estudio del Hígado (AEEH)", Madrid (Spain). **Comunicación hígado-intestino a través de vesículas extracelulares (VEs) durante la intoxicación aguda alcohólica: Influencia del género y la edad. Arantza Lamas-Paz**, Laura Morán, Fengjie Hao, Laura Moreno, Manuel Gómez del Moral, Eduardo Martínez-Naves, Javier Vaquero, Rafael Bañares, Yulia A. Nevzorova, Francisco Javier Cubero.

Poster communication **Jun 2018**

Poster communication at the EASL Monothematic Conference: GUT-LIVER AXIS, Leuven (Belgium). **Age and gender disparity in binge drinking: A gut-liver axis story. Arantza Lamas Paz,** Yulia Nevzorova, Fengjie Hao, Manuel Gómez del Moral, Eduardo Martínez-Naves, Francisco Javier Cubero.

Poster communication **Jun 2018**

Poster communication at the "II Edición PhDay. Facultad de Medicina, Madrid (Spain). **Age and gender disparity in binge drinking: a gut-liver axis story. Arantza Lamas Paz**, Yulia Nevzorova, Fengjie Hao, Manuel Gómez del Moral, Eduardo Martínez-Naves, Francisco Javier Cubero.

11.2.2 Journal publications

Feifei Guo, Olga Estévez-Vázquez, Raquel Benedé-Ubieto, Douglas Maya-Miles, Kang Zheng, Rocío Gallego-Durán, Ángela Rojas, Javier Ampuero, Manuel Romero-Gómez, Kaye Philip, Isioma U. Egbuniwe, Chaobo Chen, Jorge Simon, Teresa C. Delgado, María Luz Martínez-Chantar, Jie Sun, Johanna Reissing, Tony Bruns, **Arantza Lamas-Paz**, Manuel Gómez del Moral, Marius Maximilian Woitok, Javier Vaquero, José R. Regueiro, Christian Liedtke, Christian Trautwein, Rafael Bañares, Francisco Javier Cubero and Yulia A. Nevzorova. **A Shortcut from Metabolic-Associated Fatty Liver Disease (MAFLD) to Hepatocellular Carcinoma (HCC): c-MYC a Promising Target for Preventative Strategies and Individualized Therapy**. Cancers (Basel). **2021**;14(1):192.

Olga Estévez-Vázquez , Raquel Benedé-Ubieto, Feifei Guo, Beatriz Gómez-Santos, Patricia Aspichueta, Johanna Reissing, Tony Bruns, Carlos Sanz-García, Svenja Sydor, Lars P Bechmann, Eva Maranillo, José Ramón Sañudo, María Teresa Vázquez, **Arantza Lamas-Paz,** Laura Morán, Marina S Mazariegos, Andreea Ciudin, Juan M Pericàs, María Isabel Peligros, Javier Vaquero, Eduardo Martínez-Naves, Christian Liedtke, José R Regueiro, Christian Trautwein, Rafael Bañares, Francisco Javier Cubero, Yulia A

Nevzorova. **Fat: Quality, or Quantity? What Matters Most for the Progression of Metabolic Associated Fatty Liver Disease (MAFLD)**. Biomedicines. **2021**;9(10):1289.

Raquel Benedé-Ubieto, Olga Estévez-Vázquez, Feifei Guo, Chaobo Chen, Youvika Singh, Helder I. Nakaya, Manuel Gómez del Moral, **Arantza Lamas-Paz**, Laura Morán, Nuria López-Alcántara, Johanna Reissing, Tony Bruns, Matías A. Avila, Eva Santamaría, Marina S. Mazariegos, Marius Maximilian Woitok, Ute Haas, Kang Zheng, Ignacio Juárez, José Manuel Martín-Villa, Iris Asensio, Javier Vaquero, Maria Isabel Peligros, Josepmaria Argemi, Ramón Bataller, Javier Ampuero, Manuel Romero Gómez, Christian Trautwein, Christian Liedtke, Rafael Bañares, Francisco Javier Cubero, Yulia A. Nevzorova. **An Experimental DUAL Model of Advanced Liver Damage**. Hepatol Commun. **2021**;5(6):1051-1068.

Arantza Lamas-Paz*, Laura Morán*, Jin Peng, Beatriz Salinas, Nuria López-Alcántara, Svenja Sydor, Ramiro Vilchez-Vargas, Iris Asensio, Fengjie Hao, Kang Zheng, Beatriz Martín-Adrados, Laura Moreno, Angel Cogolludo, Manuel Gómez Del Moral, Lars Bechmann, Eduardo Martínez-Naves, Javier Vaquero, Rafael Bañares, Yulia A Nevzorova, Francisco Javier Cubero. **Intestinal Epithelial Cell-Derived Extracellular Vesicles Modulate Hepatic Injury via the Gut-Liver Axis During Acute Alcohol Injury**. Front Pharmacol. **2020**;11:603771.

Arantza Lamas-Paz, Fengjie Hao, Leonard J Nelson, Maria Teresa Vázquez, Santiago Canals, Manuel Gómez del Moral, Eduardo Martínez-Naves, Yulia A Nevzorova, and Francisco Javier Cubero. **Alcoholic liver disease: Utility of animal models**. World J Gastroenterol. **2018**;24(45):5063-5075.

cancers

MDPI

Article

A Shortcut from Metabolic-Associated Fatty Liver Disease (MAFLD) to Hepatocellular Carcinoma (HCC): c-MYC a Promising Target for Preventative Strategies and Individualized Therapy

Feifei Guo [1,2,†], Olga Estévez-Vázquez [1,†], Raquel Benedé-Ubieto [1,3], Douglas Maya-Miles [4,5,6], Kang Zheng [1,7], Rocío Gallego-Durán [4,5,6], Ángela Rojas [4,5,6], Javier Ampuero [4,5,6], Manuel Romero-Gómez [4,5,6,8], Kaye Philip [9], Isioma U. Egbuniwe [9], Chaobo Chen [1,10,11], Jorge Simon [6,12], Teresa C. Delgado [12], María Luz Martínez-Chantar [6,12], Jie Sun [7], Johanna Reissing [13], Tony Bruns [13], Arantza Lamas-Paz [1], Manuel Gómez del Moral [14], Marius Maximilian Woitok [13], Javier Vaquero [6,15,16], José R. Regueiro [1], Christian Liedtke [13], Christian Trautwein [13], Rafael Bañares [1,6,15,16], Francisco Javier Cubero [1,6,16,‡] and Yulia A. Nevzorova [1,6,13,16,*,‡]

1 Department of Immunology, Ophthalmology and ENT, School of Medicine, Complutense University of Madrid, 12 de Octubre (imas12) Health Research Institute, 28040 Madrid, Spain; feiguo@ucm.es (F.G.); olgaeste@ucm.es (O.E.-V.); rabenede@ucm.es (R.B.-U.); kzheng@ucm.es (K.Z.); chaochen@ucm.es (C.C.); arlamas@ucm.es (A.L.-P.); regueiro@med.ucm.es (J.R.R.); Rafael.banares@salud.madrid.org (R.B.); fcubero@ucm.es (F.J.C.)
2 Department of Obstetrics and Gynaecology, The Affiliated Drum Tower Hospital of Nanjing University Medical School, Nanjing 210023, China
3 Department of Physiology, Genetics and Microbiology, Faculty of Biology, Complutense University Madrid, 28040 Madrid, Spain
4 Institute of Biomedicine of Seville (IBiS), SeLiver Group, Virgen del Rocío University Hospital/CSIC/University of Seville, 41013 Seville, Spain; dmaya-ibis@us.es (D.M.-M.); rgallego-ibis@us.es (R.G.-D.); marojas-ibis@us.es (Á.R.); jampuero-ibis@us.es (J.A.); mromerogomez@us.es (M.R.-G.)
5 UCM Digestive Diseases, Virgen del Rocío University Hospital, 41013 Seville, Spain
6 Centro de Investigación Biomédica en Red de Enfermedades Hepáticas y Digestivas (CIBEREHD), 28220 Madrid, Spain; jsimon.ciberehd@cicbiogune.es (J.S.); mlmartinez@cicbiogune.es (M.L.M.-C.); j.vaquero@iisgm.com (J.V.)
7 Department of Anesthesiology, Zhongda Hospital, School of Medicine, Southeast University, Nanjing 210009, China; sunjie@seu.edu.cn
8 Department of Medicine, University of Seville, 41009 Seville, Spain
9 Department of Pathology, Nottingham University Hospitals NHS Trust, Queen's Medical Centre Campus, Nottingham NG7 2UH, UK; Philip.Kaye@nuh.nhs.uk (K.P.); Isioma.Egbuniwe@nottingham.ac.uk (I.U.E.)
10 Department of General Surgery, Wuxi Xishan People's Hospital, Wuxi 214000, China
11 Department of Hepatic-Biliary-Pancreatic Surgery, The Affiliated Drum Tower Hospital of Nanjing University Medical School, Nanjing 210023, China
12 Liver Disease Laboratory, Center for Cooperative Research in Biosciences (CIC bioGUNE), Basque Research and Technology Alliance (BRTA), 48160 Derio, Spain; tcardoso@cicbiogune.es
13 Department of Internal Medicine III, University Hospital RWTH Aachen, 52074 Aachen, Germany; joreissing@ukaachen.de (J.R.); tbruns@ukaachen.de (T.B.); M.Woitok@eclevar.com (M.M.W.); cliedtke@ukaachen.de (C.L.); ctrautwein@ukaachen.de (C.T.)
14 Department of Cell Biology, Complutense University School of Medicine, 28040 Madrid, Spain; mgomezm@med.ucm.es
15 Servicio de Aparato Digestivo, Hospital General Universitario Gregorio Marañón, 28009 Madrid, Spain
16 Instituto de Investigación Sanitaria Gregorio Marañón (IiSGM), 28007 Madrid, Spain
* Correspondence: yulianev@ucm.es; Tel.: +49-(0)241-80-80662; Fax: +49-(0)241-80-82455
† These authors contributed equally to this work.
‡ These authors contributed equally to this work.

check for updates

Citation: Guo, F.; Estévez-Vázquez, O.; Benedé-Ubieto, R.; Maya-Miles, D.; Zheng, K.; Gallego-Durán, R.; Rojas, Á.; Ampuero, J.; Romero-Gómez, M.; Philip, K.; et al. A Shortcut from Metabolic-Associated Fatty Liver Disease (MAFLD) to Hepatocellular Carcinoma (HCC): c-MYC a Promising Target for Preventative Strategies and Individualized Therapy. *Cancers* **2022**, *14*, 192. https://doi.org/10.3390/cancers14010192

Academic Editor: George Papatheodoridis

Received: 11 November 2021
Accepted: 20 December 2021
Published: 31 December 2021

Publisher's Note: MDPI stays neutral with regard to jurisdictional claims in published maps and institutional affiliations.

Simple Summary: Metabolic-associated fatty liver disease (MAFLD) is a chronic liver disease associated with obesity, diabetes mellitus type 2 (DM2), and hyperlipidemia. It can also progress to end-stage hepatocellular carcinoma (HCC); the underlying mechanisms are still unknown, but endogenous (i.e., genetic) factors such as oncogenes have been suggested to play a role. We found

biomedicines

MDPI

Article

Fat: Quality, or Quantity? What Matters Most for the Progression of Metabolic Associated Fatty Liver Disease (MAFLD)

Olga Estévez-Vázquez [1,2], Raquel Benedé-Ubieto [1,2], Feifei Guo [2], Beatriz Gómez-Santos [3], Patricia Aspichueta [3,4,5], Johanna Reissing [6], Tony Bruns [6], Carlos Sanz-García [2], Svenja Sydor [7], Lars P. Bechmann [7], Eva Maranillo [8], José Ramón Sañudo [8], María Teresa Vázquez [8], Arantza Lamas-Paz [2], Laura Morán [2,9], Marina S. Mazariegos [2], Andreea Ciudin [10], Juan M. Pericàs [5,11], María Isabel Peligros [12], Javier Vaquero [5,9,13], Eduardo Martínez-Naves [2,14], Christian Liedtke [6], José R. Regueiro [2,14], Christian Trautwein [6], Rafael Bañares [2,5,9,13], Francisco Javier Cubero [2,5,9,†] and Yulia A. Nevzorova [2,5,6,9,*,†]

1 Department of Physiology, Genetics and Microbiology, Faculty of Biology, Complutense University of Madrid, 28040 Madrid, Spain; olgaeste@ucm.es (O.E.-V.); rabenede@ucm.es (R.B.-U.)
2 Department of Immunology, Ophthalmology and ENT, School of Medicine, Complutense University of Madrid, 28040 Madrid, Spain; feirguo@163.com (F.G.); csanz17@ucm.es (C.S.-G.); arlamas@ucm.es (A.L.-P.); lmoran@ucm.es (L.M.); mamazari@ucm.es (M.S.M.); emnaves@ucm.es (E.M.-N.); regueiro@ucm.es (J.R.R.); rbanares@ucm.es (R.B.); fcubero@ucm.es (F.J.C.)
3 Department of Physiology, Faculty of Medicine and Nursing, University of Basque Country UPV/EHU, 48940 Leioa, Spain; bgomezsantos@gmail.com (B.G.-S.); patricia.aspichueta@ehu.eus (P.A.)
4 Biocruces Health Research Institute, 48903 Barakaldo, Spain
5 Centro de Investigación Biomédica en Red de Enfermedades Hepáticas y Digestivas (CIBEREHD), Instituto de Salud Carlos III, 28220 Madrid, Spain; pericasjm@gmail.com (J.M.P.); javiervaq@hotmail.com (J.V.)
6 Department of Internal Medicine III, University Hospital RWTH Aachen, 52074 Aachen, Germany; joreissing@ukaachen.de (J.R.); tbruns@ukaachen.de (T.B.); cliedtke@ukaachen.de (C.L.); ctrautwein@ukaachen.de (C.T.)
7 Department of Internal Medicine, University Hospital Knappschaftskrankenhaus, Ruhr-University Bochum, 44801 Bochum, Germany; svenja.sydor@ruhr-uni-bochum.de (S.S.); lars.bechmann@rub.de (L.P.B.)
8 Department of Human Anatomy and Embryology, School of Medicine, Complutense University of Madrid, 28040 Madrid, Spain; evamaranillo@med.ucm.es (E.M.); jrsanudo@med.ucm.es (J.R.S.); tvazquez@med.ucm.es (M.T.V.)
9 Instituto de Investigación Sanitaria Gregorio Marañón (IiSGM), 28009 Madrid, Spain
10 Endocrinology Department, Vall d'Hebron University Hospital, Vall d'Hebron Institute for Research (VHIR), 08035 Barcelona, Spain; aciudin@vhebron.net
11 Liver Unit, Internal Medicine Department, Vall d'Hebron University Hospital, Vall d'Hebron Institute for Research (VHIR), 08035 Barcelona, Spain
12 Servicio de Anatomía Patológica, Hospital General Universitario Gregorio Marañón, 28007 Madrid, Spain; isabel.peligros@salud.madrid.org
13 Servicio de Aparato Digestivo, Hospital General Universitario Gregorio Marañón, 28007 Madrid, Spain
14 12 de Octubre Health Research Institute (imas12), 28041 Madrid, Spain
* Correspondence: yulianev@ucm.es; Tel.: +49-(0)241-80-80662; Fax: +49-(0)241-80-82455
† These authors contributed equally to this work.

check for updates

Citation: Estévez-Vázquez, O.; Benedé-Ubieto, R.; Guo, F.; Gómez-Santos, B.; Aspichueta, P.; Reissing, J.; Bruns, T.; Sanz-García, C.; Sydor, S.; Bechmann, L.P.; et al. Fat: Quality, or Quantity? What Matters Most for the Progression of Metabolic Associated Fatty Liver Disease (MAFLD). *Biomedicines* **2021**, *9*, 1289. https://doi.org/10.3390/biomedicines9101289

Academic Editor: Shaker A. Mousa

Received: 12 August 2021
Accepted: 19 September 2021
Published: 22 September 2021

Publisher's Note: MDPI stays neutral with regard to jurisdictional claims in published maps and institutional affiliations.

Abstract: Objectives: Lately, many countries have restricted or even banned transfat, and palm oil has become a preferred replacement for food manufacturers. Whether palm oil is potentially an unhealthy food mainly due to its high content of saturated Palmitic Acid (PA) is a matter of debate. The aim of this study was to test whether qualitative aspects of diet such as levels of PA and the fat source are risk factors for Metabolic Syndrome (MS) and Metabolic Associated Fatty Liver Disease (MAFLD). Methods: C57BL/6 male mice were fed for 14 weeks with three types of Western diet (WD): 1. LP-WD—low concentration of PA (main fat source—corn and soybean oils); 2. HP-WD—high concentration of PA (main fat source—palm oil); 3. HP-Trans-WD—high concentration of PA (mainly transfat). Results: All types of WD caused weight gain, adipocyte enlargement, hepatomegaly, lipid metabolism alterations, and steatohepatitis. Feeding with HP diets led to more prominent obesity, hypercholesterolemia, stronger hepatic injury, and fibrosis. Only the feeding with HP-Trans-WD resulted in glucose intolerance and elevation of serum transaminases. Brief withdrawal of WDs

An Experimental DUAL Model of Advanced Liver Damage

Raquel Benedé-Ubieto,[1,2] Olga Estévez-Vázquez,[1,2*] Feifei Guo,[2*] Chaobo Chen ,[2] Youvika Singh,[3] Helder I. Nakaya,[3,4] Manuel Gómez del Moral ,[5] Arantza Lamas-Paz,[2] Laura Morán,[2] Nuria López-Alcántara,[2,6] Johanna Reissing,[7] Tony Bruns,[7] Matías A. Avila ,[8-10] Eva Santamaría,[8,9] Marina S. Mazariegos,[2] Marius Maximilian Woitok,[7] Ute Haas,[7] Kang Zheng,[2,11,12] Ignacio Juárez,[2] José Manuel Martín-Villa,[2,13] Iris Asensio,[9,13,14] Javier Vaquero ,[9,13,14] Maria Isabel Peligros,[15] Josepmaria Argemi,[16-18] Ramón Bataller ,[16,19] Javier Ampuero,[9,20] Manuel Romero Gómez ,[9,20] Christian Trautwein,[7] Christian Liedtke ,[7] Rafael Bañares,[2,9,13,14] Francisco Javier Cubero ,[2,11**] and Yulia A. Nevzorova [2,7,11**]

Individuals exhibiting an intermediate alcohol drinking pattern in conjunction with signs of metabolic risk present clinical features of both alcohol-associated and metabolic-associated fatty liver diseases. However, such combination remains an unexplored area of great interest, given the increasing number of patients affected. In the present study, we aimed to develop a preclinical DUAL (alcohol-associated liver disease plus metabolic-associated fatty liver disease) model in mice. C57BL/6 mice received 10% vol/vol alcohol in sweetened drinking water in combination with a Western diet for 10, 23, and 52 weeks (DUAL model). Animals fed with DUAL diet elicited a significant increase in body mass index accompanied by a pronounced hypertrophy of adipocytes, hypercholesterolemia, and hyperglycemia. Significant liver damage was characterized by elevated plasma alanine aminotransferase and lactate dehydrogenase levels, extensive hepatomegaly, hepatocyte enlargement, ballooning, steatosis, hepatic cell death, and compensatory proliferation. Notably, DUAL animals developed lobular inflammation and advanced hepatic fibrosis. Sequentially, bridging cirrhotic changes were frequently observed after 12 months. Bulk RNA-sequencing analysis indicated that dysregulated molecular pathways in DUAL mice were similar to those of patients with steatohepatitis. *Conclusion:* Our DUAL model is characterized by obesity, glucose intolerance, liver damage, prominent steatohepatitis and fibrosis, as well as inflammation and fibrosis in white adipose tissue. Altogether, the DUAL model mimics all histological, metabolic, and transcriptomic gene signatures of human advanced steatohepatitis, and therefore serves as a preclinical tool for the development of therapeutic targets. (*Hepatology Communications* 2021;5:1051-1068).

Excessive alcohol drinking is a leading cause of chronic liver disease and accounts for up to 60%-80% of liver-related mortality in Europe.[1] These data become even more relevant considering that alcohol-associated liver disease (ALD) receives only about 5% of the attention in the field of hepatology.[2]

The principal fact that only about 6%-30% of heavy drinkers develop cirrhosis indicates that additional factors modulate the risk of ALD progression.[1] Clinical observations commonly suggest a wide individual susceptibility, and indicate several risk factors for ALD including drinking patterns, female gender, genetic background, cigarette smoking, occupational hazards, and hepatotropic viruses. Obesity and metabolic syndrome (MS) represent another important group of risk factors that accelerate fibrosis

Abbreviations: ALD, alcohol-associated liver disease; ALT, alanine aminotransferase; ANOVA, analysis of variance; AST, aspartate aminotransferase; Bcl2, B cell lymphoma 2; BMI, body mass index; BW, body weight; CPT-1c, carnitine palmitoyltransferase 1c; DEN, diethylnitrosamine; DUAL, ALD plus MAFLD; ECM, extracellular matrix; EtOH, ethanol; FFA, free fatty acid; H&E, hematoxylin and eosin; HSC, hepatic stellate cell; IF, immunofluorescence; IHC, immunohistochemistry; LDH, lactate dehydrogenase; MAFLD, metabolic associated fatty liver disease; mRNA, messenger RNA; MS, metabolic syndrome; NAFLD, nonalcoholic fatty liver disease; NF-κB, nuclear factor kappa B; ORO, Oil Red O; PCNA, proliferating cell nuclear antigen; Pi3K, phosphoinositide 3-kinase; RNA-seq, RNA sequencing; SR, sirius red; TEM, transmission electron microscopy; TG, triglycerides; TLR, toll-like receptor; TNF-α, tumor necrosis factor-α; WAT, white adipose tissue; WD, Western diet; α-SMA, α-smooth muscle actin.

Received November 3, 2020; accepted February 7, 2021.
Additional Supporting Information may be found at onlinelibrary.wiley.com/doi/10.1002/hep4.1698/suppinfo.
**These authors contributed equally to this work.*
***These authors contributed equally as senior authors.*
Supported by EXOHEP-CM (S2017/BMD-3727), Ramón y Cajal (RYC-2014-15242 and RYC-2015-17438), NanoLiver-CM (Y2018/NMT-4949), COST Action (CA17112), AMMF (2018/117), ERAB (EA 18/14), MINECO Retos (SAF2016-78711 and SAF2017-87919-R), and German Research Foundation (DFG NE 2128/2-1, SFB 1382-403224013/A02, and SFB/TRR57/P04). FJC is a Gilead Research Liver

frontiers in Pharmacology

ORIGINAL RESEARCH
published: 21 December 2020
doi: 10.3389/fphar.2020.603771

Intestinal Epithelial Cell-Derived Extracellular Vesicles Modulate Hepatic Injury via the Gut-Liver Axis During Acute Alcohol Injury

Arantza Lamas-Paz[1,2†], Laura Morán[1,3†], Jin Peng[4†], Beatriz Salinas[3,5,6,7], Nuria López-Alcántara[1], Svenja Sydor[8], Ramiro Vilchez-Vargas[9], Iris Asensio[3,10], Fengjie Hao[1,2,11], Kang Zheng[1,2,12], Beatriz Martín-Adrados[1,2], Laura Moreno[8,13], Angel Cogolludo[8,13], Manuel Gómez del Moral[2,14], Lars Bechmann[8], Eduardo Martínez-Naves[1,2], Javier Vaquero[3,10], Rafael Bañares[3,10], Yulia A. Nevzorova[1,2,15‡] and Francisco Javier Cubero[1,2‡]*

[1]Department of Immunology, Ophthalmology and ENT, Complutense University School of Medicine, Madrid, Spain, [2]12 de Octubre Health Research Institute (imas12), Madrid, Spain, [3]Servicio de Aparato Digestivo del Hospital General Universitario Gregorio Marañón, Instituto de Investigación Sanitaria Gregorio Marañón (IISGM), Madrid, Spain, [4]Department of Hepatobiliary Surgery, Nanjing Drum Tower Hospital, The Affiliated Hospital of Nanjing University Medical School, Nanjing, China, [5]Centro Nacional de Investigaciones Cardiovasculares Carlos III, Madrid, Spain, [6]Bioengineering and Aerospace Engineering Department, Universidad Carlos III de Madrid, Madrid, Spain, [7]Centro de Investigación Biomédico en Red de Salud Mental (CIBERSAM), Madrid, Spain, [8]Department of Internal Medicine, University Hospital Knappschaftskrankenhaus, Ruhr-University Bochum, Bochum, Germany, [9]Department of Gastroenterology, Hepatology, and Infectious Diseases, Otto von Guericke University Hospital Magdeburg, Magdeburg, Germany, [10]Centre for Biomedical Research, Network on Liver and Digestive Diseases (CIBEREHD), Madrid, Spain, [11]Department of General Surgery, Hepatobiliary Surgery, Ruijin Hospital, Shanghai Jiao Tong University School of Medicine, Shanghai, China, [12]Department of Anesthesiology, Zhongda Hospital, School of Medicine, Southeast University, Nanjing, China, [13]Department of Pharmacology and Toxicology, Complutense University School of Medicine and Centre for Biomedical Research, Network on Respiratory Diseases (CIBERES), Madrid, Spain, [14]Department of Cell Biology, Complutense University School of Medicine, Madrid, Spain, [15]Department of Internal Medicine III, University Hospital RWTH Aachen, Aachen, Germany

OPEN ACCESS

Edited by:
Ralf Weiskirchen,
RWTH Aachen University, Germany

Reviewed by:
Laura E. Nagy,
Cleveland Clinic, United States
Paramananda Saikia,
Cleveland Clinic, United States
Chaoxin Man,
Northeast Agricultural University, China

***Correspondence:**
Francisco Javier Cubero
fcubero@ucm.es

†These authors have contributed equally to this work and share first authorship
‡These authors have contributed equally to this work and share senior authorship

Specialty section:
This article was submitted to Gastrointestinal and Hepatic Pharmacology, a section of the journal Frontiers in Pharmacology

Received: *07 September 2020*
Accepted: *05 October 2020*
Published: *21 December 2020*

Citation:
Lamas-Paz A, Morán L, Peng J, Salinas B, López-Alcántara N, Sydor S, Vilchez-Vargas R, Asensio I, Hao F, Zheng K, Martín-Adrados B, Moreno L, Cogolludo A, Gómez del Moral M, Bechmann L, Martínez-Naves E, Vaquero J, Bañares R, Nevzorova YA and Cubero FJ (2020) Intestinal Epithelial Cell-Derived Extracellular Vesicles Modulate Hepatic Injury via the Gut-Liver Axis During Acute

Binge drinking, i.e., heavy episodic drinking in a short time, has recently become an alarming societal problem with negative health impact. However, the harmful effects of acute alcohol injury in the gut-liver axis remain elusive. Hence, we focused on the physiological and pathological changes and the underlying mechanisms of experimental binge drinking in the context of the gut-liver axis. Eight-week-old mice with a C57BL/6 background received a single dose (p.o.) of ethanol (EtOH) [6 g/kg b.w.] as a preclinical model of acute alcohol injury. Controls received a single dose of PBS. Mice were sacrificed 8 h later. In parallel, HepaRGs and Caco-2 cells, human cell lines of differentiated hepatocytes and intestinal epithelial cells intestinal epithelial cells (IECs), respectively, were challenged in the presence or absence of EtOH [0–100 mM]. Extracellular vesicles (EVs) isolated by ultracentrifugation from culture media of IECs were added to hepatocyte cell cultures. Increased intestinal permeability, loss of

Abbreviations: ADH, alcohol dehydrogenase; ALDH, aldehyde dehydrogenase; BAC, blood alcohol concentration; DLS, dynamic light scattering; EtOH, ethanol; EVs, extracellular vesicles; H&E, hematoxylin and eosin; IF, immunofluorescence; IECs, intestinal epithelial cells; IL-1β, interleukin-1β; KCs, Kupffer cells; LPS, lipopolysaccharides; LW/BW, liver weight vs. body weight; NTA, nanoparticle tracking analysis; ORO, oil red O; qRT-PCR, quantitative real-time PCR; Srebp-1, sterol regulatory binding protein-1; Tnf-α, tumor necrosis factor-alpha; TJs, tight junctions; Tlr-4, toll-like receptor-4; ZO-1, zone occludens-1.

World Journal of Gastroenterology

Submit a Manuscript: http://www.f6publishing.com

World J Gastroenterol 2018 December 7; 24(45): 5063-5075

DOI: 10.3748/wjg.v24.i45.5063

ISSN 1007-9327 (print) ISSN 2219-2840 (online)

REVIEW

Alcoholic liver disease: Utility of animal models

Arantza Lamas-Paz, Fengjie Hao, Leonard J Nelson, Maria Teresa Vázquez, Santiago Canals, Manuel Gómez del Moral, Eduardo Martínez-Naves, Yulia A Nevzorova, Francisco Javier Cubero

Arantza Lamas-Paz, Fengjie Hao, Eduardo Martínez-Naves, Francisco Javier Cubero, Department of Immunology, Ophthalmology and ORL, Complutense University School of Medicine, Madrid 28040, Spain

Arantza Lamas-Paz, Fengjie Hao, Eduardo Martínez-Naves, Yulia A Nevzovova, Francisco Javier Cubero, 12 de Octubre Health Research Institute (imas12), Madrid 28041, Spain

Leonard J Nelson, Institute for Bioengineering (IBioE), School of Engineering, Faraday Building, The University of Edinburgh, Edinburgh EH9 3 JL, Scotland, United Kingdom

Maria Teresa Vázquez, Department of Human Anatomy and Embryology, Complutense University School of Medicine, Madrid 28040, Spain

Santiago Canals, Instituto de Neurociencias, Consejo Superior de Investigaciones Científicas, Universidad Miguel Hernández, San Juan de Alicante 03550, Spain

Manuel Gómez del Moral, Department of Cell Biology, Complutense University School of Medicine, Madrid 28040, Spain

Yulia A Nevzorova, Department of Genetics, Physiology and Microbiology, Faculty of Biology, Universidad Complutense, Madrid 28040, Spain

Yulia A Nevzorova, Department of Internal Medicine III, University Hospital RWTH Aachen, Aachen 52062, Germany

ORCID number: Arantza Lamas-Paz (0000-0001-5857-4320); Fengjie Hao (0000-0002-6734-265X); Leonard J Nelson (0000-0002-4197-4843); Maria Teresa Vázquez (0000-0003-3537-0901); Santiago Canals (0000-0003-2175-8139); Manuel Gómez del Moral (0000-0002-0642-8142); Eduardo Martínez-Naves (0000-0001-8136-9042); Yulia A Nevzorova (0000-0003-1390-8002); Francisco Javier Cubero (0000-0003-1499-650X).

Author contributions: Lamas-Paz A and Hao F equally contributed to the manuscript writing and figure design; Nelson LJ, Vázquez MT, Canals S, Gómez del Moral M and Martínez-Naves E critiqued the manuscript, checked English language and provided fundamental guidance. Nevzorova YA and Cubero FJ outlined and corrected the review and provided guidance.

Supported by the MINECO Retos, No. SAF2016-78711 and SAF2017-87919R; EXOHEP-CM, No. S2017/BMD-3727; the AMMF Cholangiocarcinoma Charity, No. 2018/117; the COST Action, No. CA17112; Ramón y Cajal, No. RYC-2014-15242 and No. RYC-2015-17438; grant of ERAB, No. EA 14/18; Gilead Liver Research Scholar 2018, No. 44/2018; Ministerio de Sanidad, Servicios Sociales e Igualdad, No. 2017I065; and the UCM group "Lymphocyte Immunobiology", No. 920631 (imas12-associated, Ref. IBL-6). German Research Foundation (SFB/TRR57/P04 and DFG NE 2128/2-1); Interdisciplinary Center for Clinical Research from the Faculty of Medicine at RWTH Aachen University (IZKF/E8-2).

Conflict-of-interest statement: The authors declare that they have no conflict of interest.

Manuscript source: Invited manuscript

Correspondence author to: Francisco Javier Cubero, BSc, MSc, PhD, Assistant Professor, Department of Immunology, Ophthalmology and ORL, Complutense University School of Medicine, c/Doctor Severo Ochoa 9, Madrid 28040, Spain. fcubero@ucm.es
Telephone: +34-91-3941385
Fax: +34-91-394164

Received: October 19, 2018
Peer-review started: October 19, 2018
First decision: November 1, 2018
Revised: November 8, 2018
Accepted: November 9, 2018
Article in press: November 9, 2018
Published online: December 7, 2018

Abstract

Alcoholic liver disease (ALD) is a major cause of acute

11.3 Travel awards

Free registration **May 2022**

Free registration award of the AEEH “Inscripción Beca Asociación Española para el Estudio del Hígado (AEEH). 47º Congreso Anual de la AEEH”. Madrid (Spain).

Full bursary **Jun 2019**

Full bursary award of the EASL (European Association for the Study of the Liver), EASL Monothematic Conference: GUT-LIVER AXIS.Leuven (Belgium).

Free registration **Feb 2019**

Free registration award of the AEEH “Inscripción Beca Asociación Española para el Estudio del Hígado (AEEH). 44º Congreso Anual de la AEEH”. Madrid (Spain).

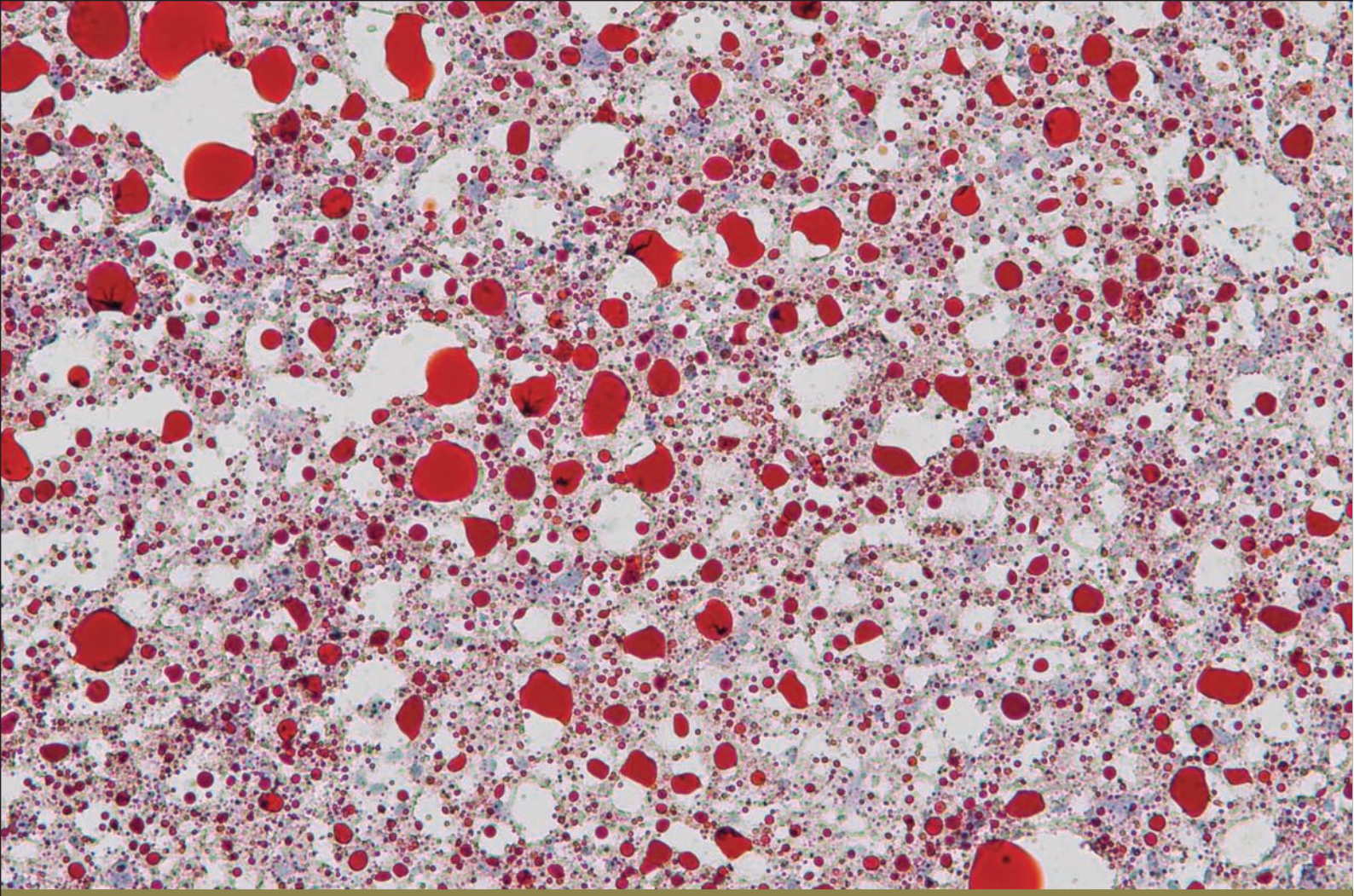

UNIVERSIDAD
COMPLUTENSE
MADRID